China Geology 7 (2024) 762−796

China Geology

Journal homepage: http://chinageology.cgs.cn
https://www.sciencedirect.com/journal/china-geology

Geology and mineralization of the Hongqiling large magmatic nickel-copper-cobalt deposit (22×10^4 t) in Jilin Province, China: A review

Cong Chen[a], Yu-chao Gu[a,*], Di Zhang[a,*], Tao-tao Wu[a, b], Ai Li[c], Yun-sheng Ren[d], Qing-qing Shang[e], Jian Zhang[a], Xiong-fei Bian[a], Fei Su[a], Jia-lin Yang[a], Qiu-shi Sun[a], Xiao-hai Li[a], Wan-zhen Liu[f], Zhen-ming Sun[g], Sen Zhang[h], Yu-hui Feng[i]

[a] *Shenyang Center of China Geological Survey*, *Shenyang* 110034, *China*
[b] *School of Earth Sciences and Resources*, *China University of Geosciences (Beijing)*, *Beijing* 100083, *China*
[c] *College of Computer Science & Technology*, *Qingdao University*, *Qingdao* 266071, *China*
[d] *Institute of Disaster Prevention*, *Langfang* 065200, *China*
[e] *College of Earth Sciences*, *Jilin university*, *Changchun* 130000, *China*
[f] *Geological Survey Institute of Jilin Province*, *Changchun* 130000, *China*
[g] *School of Surveying and Mapping Engineering*, *Changchun Institute of Technology*, *Changchun* 130000, *China*
[h] *Physical Geological Materials Center of Natural Resources*, *China Geological Survey*, *Langfang* 065200, *China*
[i] *Shenyang Normal University*, *Shenyang* 110034, *China*

ARTICLE INFO

Article history:
Received 13 September 2023
Received in revised form 16 May 2024
Accepted 24 May 2024
Available online 29 August 2024

Keywords:
Nickel-copper-cobalt deposit
Fractional crystallization
Crustal contamination
Magmatic
Mineralization
Re-Os isotopic age
Sulfur isotopic
Metallogenic mode
Prospecting model
Western Pacific's active continental margin
Mineral exploration engineering
Hongqiling
Jilin

ABSTRACT

The Hongqiling large nickel-copper-cobalt deposit (hereafter referred to as the Hongqiling deposit), a typical mafic-ultramafic copper-nickel deposit in China, boasts proven Ni (Ni) resources of approximately 22×10^4 t, associated copper resources of 2×10^4 t, and associated cobalt (Co) resources of 0.5×10^4 t, with Ni reserves ranking 10th among China's magmatic nickel deposits. Geotectonically, the Hongqiling deposit is situated in the superimposed zone between the Xing'an-Mongolian orogenic belt and the circum-Western Pacific's active continental margin belt. Its ore-bearing plutons occur within the metamorphic rocks of the Ordovician Hulan Group, with the emplacement of plutons and the locations of orebodies governed by the deep-seated Huifahe fault and its secondary NW-trending Fujia-Hejiagou-Beixinglong-Changsheng fault zone. In the deposit, the rock assemblages of ore-bearing plutons predominantly encompass gabbro - pyroxenite - olivine pyroxenite - pyroxene peridotite (pluton No. 1) and norite-orthopyroxenite-harzburgite (pluton No. 7), with ore-bearing lithofacies consisting primarily of olivine pyroxenite and pyroxenite facies. The Hongqiling deposit hosts stratoid, overhanging lentoid, veined, and pure-sulfide veined orebodies. Its ores principally contain metallic minerals including pyrrhotite, pentlandite, chalcopyrite, violarite, and pyrite. Despite unidentified magma sources of ore-bearing mafic-ultramafic rocks, it is roughly accepted that the magmatic evolution in the Hongqiling deposit primarily involved fractional crystallization and crustal contamination. The ore-forming materials were primarily derived from the upper mantle, mixed with minor crustal materials. The ore-bearing mafic-ultramafic rocks in the deposit, primarily emplaced during the Indosinian (208–239 Ma), were formed in an intense extension setting followed by the collisional orogeny between the North China Plate and the Songnen-Zhangguangcai Range Block during the Middle-Late Triassic. From the perspective of the metallogenic geological setting, surrounding rocks, ore-controlling structures, and rock assemblages, this study identified one favorable condition and seven significant indicators for prospecting for Hongqiling-type nickel deposits and developed a prospecting model of the Hongqiling deposit. These serve as valuable references for exploring similar nickel deposits in the region, as well as the deep parts and margins of the Hongqiling deposit.

First author: *E-mail address*: 1010674241@qq.com (Cong Chen).

* Corresponding author: *E-mail address*: guyi1224@126.com (Yu-chao Gu); 594139452@qq.com (Di Zhang).

Literary editor: Li-qiong Jia
doi:10.31035/cg2023106
2096-5192/© 2024 China Geology Editorial Office.

1. Introduction

Magmatic sulfide deposits associated with mafic-ultramafic complexes serve as the primary sources of Ni, copper, and platinum-group elements (PGEs; Naldrett AJ, 2010; Mudd GM and Jowitt SM, 2014). Numerous copper-nickel sulfide deposits have been discovered and investigated, including the Jinchuan nickel deposit in Eastern Kunlun, China (Zhao Y et al., 2022; Liu YG et al., 2019; Cai QS et al., 2023), the Mascot nickel-copper-PGE deposit in British Columbia (Manor MJ et al., 2016), the Noril'sk nickel-copper-PGE deposit in Russia (Naldrett AJ, 2004), and the Aguablanca nickel-copper-PGE deposit in southwestern Iberia (Piña R et al., 2010). These world-class nickel-copper sulfide deposits are primarily distributed along paleocratonic margins (e.g., the Noril'sk and Jinchuan deposits) and continental rifts (e.g., the Kambalda and Duluth deposits; Naldrett AJ, 2004; Ripley EM and Li C, 2013; Lightfoot PC and Evans-Lamswood D, 2015). Besides, many of them, such as the Mascot deposit in British Columbia (Manor MJ et al., 2016) and the Kalatongke (Qian et al., 2018; Kang Z, 2020) and Hongqiling (Wu FY et al., 2004) deposits in China, occur in orogenic belts.

The Hongqiling deposit once ranked as the second largest copper-nickel sulfide deposit in China (Wu FY et al., 2004). This deposit is situated in the superimposed zone between the Paleo-Asian Ocean plate and the Paleo-Pacific Plate, which experienced prolonged complex structural evolution and frequent tectono-magmatic activity. The extensive deep-seated fault structures and multistage mantle-derived magmatic activity provided favorable metallogenic conditions for magmatic copper-nickel deposits in this zone. The No. 1 ore-bearing pluton in the Hongqiling deposit was discovered by the No. 7 Exploration Team of Jilin Nonferrous Metal Geological Exploration Bureau (the current Team 607 of Jilin Nonferrous Metal Geological Exploration Bureau) in early 1959. Then, the Hongqiling deposit was officially uncovered in 1960, introducing new practices of prospecting for magmatic copper-nickel sulfide deposits in Jilin Province (Editorial Board of The Discovery History of Mineral Deposits of China, Jilin Volume, 1991). The discovery and exploration history of the Hongqiling deposit can be roughly divided into the first and second stages. In the first stage (1959–1965), the No. 7 Exploration Team of Jilin Nonferrous Metal Geological Exploration Bureau discovered the protolith outcrops of the No. 1 ore-bearing pluton (i.e., the Dalingdongshan pluton) through ore occurrence examination and route survey. Based on comprehensive geophysical and geochemical explorations, terrain and geological surveys, and drilling verification, this pluton was formally named the Hongqiling nickel deposit in 1960. In 1964, the Hongqiling mine was formally put into production. Subsequently, Team 102 of Liaoning Geological Exploration Company of Northeast Nonferrous Metal Bureau discovered the No. 7 pluton during the examination of magnetic anomalies at the periphery of the No. 1 pluton. In the second stage (1971–1983), the large-scale open-pit mine of the No. 7 pluton was put into operation in 1971, shifting from open-pit mining to underground mining in 1978 (Editorial Board of *Jilin Volume of The Discovery History of Mineral Deposits of China,* 1991). By the end of 2018, it was confirmed that the Hongqiling deposit had proven Ni resources over 20×10^4 t, along with medium-sized cobalt deposits and small copper deposits, with Ni reserves ranking 10th among China's magmatic nickel deposits (Sun T et al., 2019). However, over 50 years of exploration and exploitation have led to a severe shortage of Ni resources in the Hongqiling deposit, posing a high resource crisis of the mine (Sun T et al., 2019). In recent years, the implementation of national projects for exploring successive mineral resources in mines with resource crisis has contributed to significant breakthroughs in deep prospecting of the Hongqiling deposit (Yang XL, 2012; Xu ZH, 2020; Xu ZH et al., 2022), further corroborating the enormous potential for exploring magmatic copper-nickel deposits in deep part of the Hongqiling area (Xu ZH et al., 2022).

Extensive theoretical studies have been conducted on the geological characteristics, diagenetic and metallogenic epochs, tectonic setting, magma sources and their evolution, mineralization, and metallogenic mechanisms of the Hongqiling deposit (Xi AH et al., 2004; Wu FY et al., 2004; Zhang GL and Wu FY, 2005; Feng GY et al., 2011; Hao LB et al., 2012; Wei B et al., 2013; Wei QQ, 2015; Li A, 2019; Xue HR, 2020; Zhang LS, 2022; Dai M et al., 2023). Focusing on the prospecting for Hongqiling-type nickel deposits, some researchers explored the metallogenic regularity and prospecting prediction of these deposits (Zhi XJ, 2005; Yang XL, 2012; Sun LJ, 2013; Xu ZH, 2020). Based on the geological characteristics of the Hongqiling deposit, this study summarized and analyzed the diagenetic and metallogenic epochs, diagenesis, and mineralization of the Hongqiling deposit by systematically organizing previous research results. It determined the metallogenic model of the Hongqiling deposit by generalizing from a multi-dimensional comparison of similar deposits in orogenic belts. Accordingly, this study comprehensively summarized the favorable metallogenic conditions and prospecting indicators of the Hongqiling deposit. Finally, it established a prospecting model for Hongqiling-type deposits with a view to providing a significant reference for exploring similar nickel deposits in the region, as well as deep parts and margins of the Hongqiling area.

2. Regional geological setting

The Hongqiling deposit, located in the east of Panshi City, Jilin Province, China, is situated in the superimposed zone between the Xing'an-Mongolian orogenic belt and the circum-Western Pacific's active continental margin belt (Fig. 1a). From the Paleozoic to the Mesozoic, this zone successively experienced the evolution, superposition, and

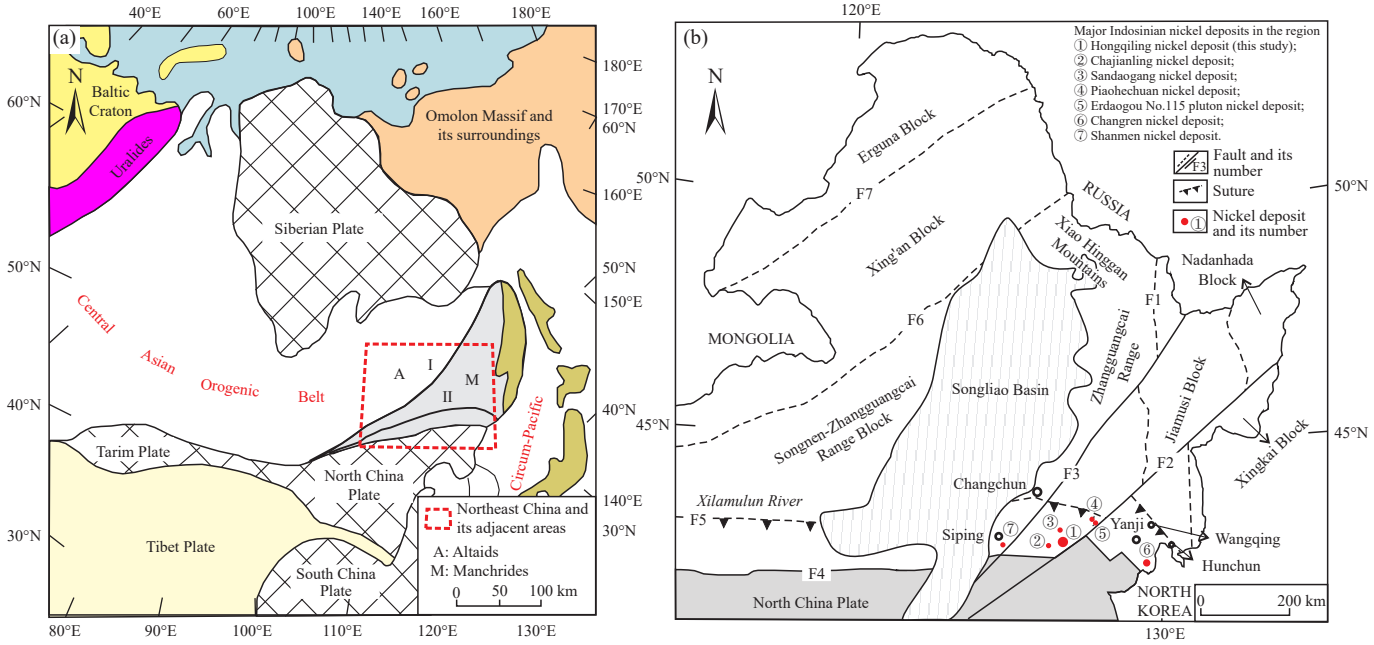

Fig. 1. Maps of the geotectonic location (a) and major deposit distribution of the study area (b; base maps modified from Wu FY et al., 2007; Xu ZG et al., 2008; Chen C, 2017). F1–Mudanjiang fault; F2–Dunhua-Mishan fault; F3–Yitong-Yilan fault; F4–Chifeng-Kaiyuan-Hailong-Fuerhe-Longjing Baijin fault; F5–Xilamulun-Changchun-Wangqing-Hunchun suture zone; F6–Hegenshan-Heihe fault; F7–Tayuan-Xiguitu fault; I–Tayuan-Xiguitu fault; II–Suolun-Xilamulun-Changchun-Wangqing-Hunchun suture zone.

transformation of the Paleo-Asian and Paleo-Pacific oceans. The resulting complex tectonic evolution and multistage tectono-magmatic activity created superior geological conditions and material basis for the multistage mineralization of endogenetic metals in this zone.

2.1. Regional strata

Paleozoic, Mesozoic, and Cenozoic strata are exposed in the Hongqiling area (Table 1), with the Paleozoic Ordovician, Carboniferous, and Permian strata being the most developed. For the ore-bearing mafic-ultramafic rocks of the Hongqiling deposit, their direct surrounding rocks prove to be the Xiaosangedingzi and Huangyingtun formations of the Paleozoic Ordovician Hulan Group. In contrast, the ore-bearing mafic-ultramafic rocks of the Chajianling nickel deposit were emplaced in the Upper Paleozoic Permian Shoushangou Formation (Fig. 2a).

2.2. Regional structures

Due to the superimposed evolution of the Paleo-Asian Ocean and the Circum-Pacific tectonic domains, the area experienced significant tectonism, leading to the formation of well-developed faults and folds. Besides the dominant deep-seated Huifahe fault, the study area also hosts many crustal faults, including the NW-trending Heishizhen-Yantongshan and Huadian-Shuanghezhen faults, the nearly-NS-trending Liuhe-Jilin fault, and the nearly EW-trending Liaoyuan-Panshi fault, as well as their secondary faults (Fig. 2b). These faults, in various directions and at different levels, constitute the tectonic framework of the area.

The Hongqiling area is primarily governed by the deep-seated Huifahe fault and the Heishizhen-Yantongshan fault zone (Fig. 2b). The nearly NE-trending Huifahe fault, recognized as a translithospheric fault, is a boundary fault between the North China Plate and the continental margin accretion zone in the north (Ma JX et al., 1998). This fault, featuring a considerable cutting depth and frequent inherited activity, and their derived NW- and NE-trending faults, also characterized by multistage activity, jointly determine the spatial distributions of metamorphic rock series of the Eopaleozoic Hulan Group, mafic-ultramafic plutons, and copper-nickel sulfide orebodies in the study area. The Heishizhen-Yantongshan fault is a NW-trending crustal fault, along which several valleys are found, dislocating Mesozoic and earlier geobodies. This fault is approximately 1–1.5 km wide, with compression zones, tectonic breccias, and tectonic lenses inside (Li ZT et al., 1994). This fault was once considered as a branch of the NE-trending Huifahe fault. However, Li ZT et al. (1994) proposed that the Heishizhen-Yantongshan fault was probably formed during the Eopaleozoic and experienced multistage activity, with the scale gradually increasing over the geological time.

Due to significant tectonic movements, strata such as the Huangyingtun Formation of the Hulan Group underwent compression, resulting in fold deformations, which are identified as tight linear complex folds composed of several alternating, parallel anticlines and synclines. Currently, these strata are mostly incomplete due to frequent, intense magmatic activity, with merely partial fold morphologies preserved (Ma JX et al., 1998).

2.3. Regional magmatic rocks

Intrusive rocks are well-developed in the Hongqiling area,

Table 1. Regional stratigraphic division of the study area (after Geology and Mineral Exploration and Development Bureau of Jilin Province, 1985; Regional Geology and Mineral Survey Institute of Jilin Province, 2016).

Chronostratigraphy			Lithostratigraphy				
Erathem	System	Series	Group/formation		Member	Code	Lithological description
Cenozoic	Quaternary	Holocene	Modern riverbeds, floodplains, and first-order terraces			Qh^{al}	Sandy conglomerates and loams
		Pleistocene	Second-order terraces			Qp^{3al}	Lower part: Sands gravel layer; upper part: loess
Mesozoic	Cretaceous	Lower	Heiwaizi Formation			K_1hw	Conglomerates and conglomeratic greywacke
	Jurassic	Lower-top	Nanloushan Formation			$J_{1-2}n$	Andesites, rhyolites, andesitic -rhyolitic tuff, and breccia-bearing tuff, interbedded with tuffaceous sandstones locally
Upper Paleozoic	Permian	Lower-top	Shoushangou Formation			$P_{1-2}s$	Lower part: Carbonaceous garnet-sericite schists and andalusite slates; upper part: interbeds consisting of carbonaceous slates and tuffaceous fine-grained sandstones
	Carboniferous-Permian	Lower-upper	Shizuizi Formation			CP_S	Upper part: medium- to fine- grained feldspar-quartz sandstones, fine-grained sandstones, siltstone slates, siltstones, and rhyolitic tuff, with biogenic limestones locally visible; lower part: Crystalline limestones interbedded with fine-grained sandstones
			Mopanshan Formation			CP_m	White thickly laminated marbles
Lower Paleozoic	Ordovician	Lower-upper	Hulan Group	Xiaosangedingzi Formation	2 Member	Ox^2	Marbles, siliceous banded marbles, and siliceous nodular marbles, interbedded with limestone marbles locally
					1 Member	Ox^1	Biotite-plagioclase leptynites, kyanite-garnet-staurolite-muscovite schist muscovite schist, biotite-diorite leptynites, and thickly laminated marbles
				Huangyingtun Formation	2 Member	Oh^2	Hornblende-plagioclase leptynites, biotite-plagioclase leptynites, siliceous banded marbles, and translucent-hornblende-plagioclase leptynites
					1 Member	Oh^1	Tourmaline- and garnet-bearing two-mica plagiogneisses

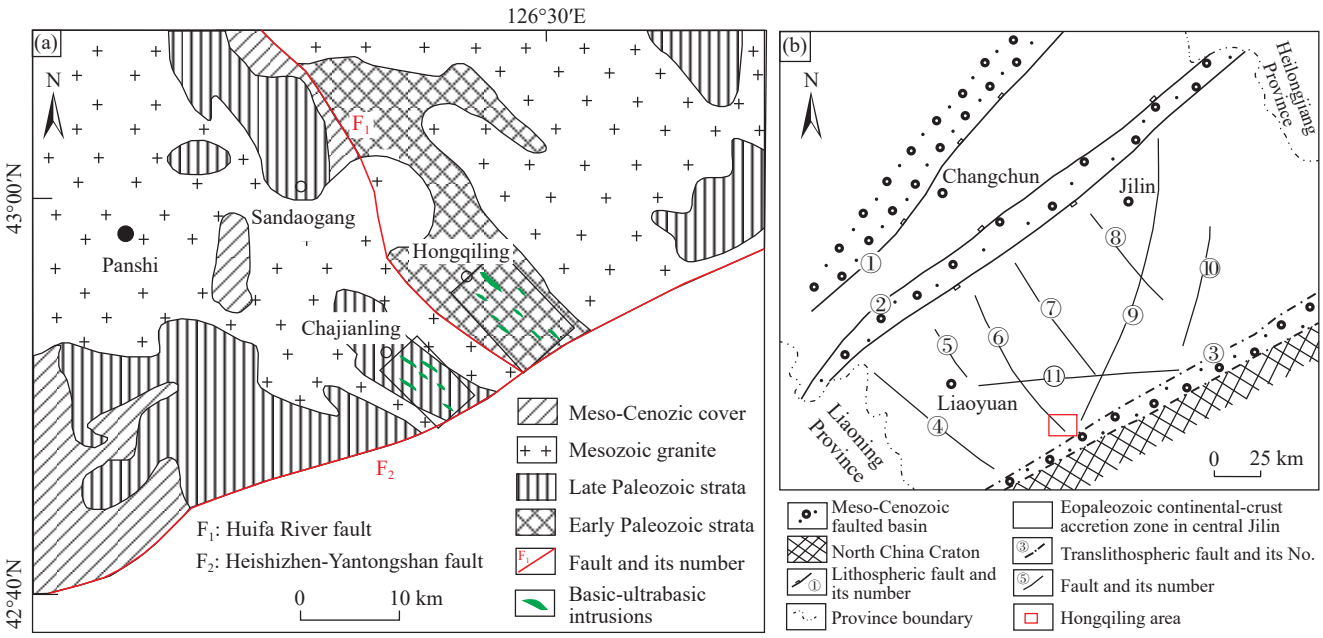

Fig. 2. Geolgical sketch map of the Hongqiling area (a; after Wu FY et al., 2004) and geological structure map of Hongqiling and its adjacent areas (b; after Ma JX et al., 1998). ①–Siping-Changchun fault; ②–Yilan-Yitong fault; ③–Huifahe fault; ④–Liaoyuan-Dongfeng fault; ⑤–Yitong-Huinan fault; ⑥–Yantongshan-Heishi fault; ⑦–Huadian-Shuanghezhen fault; ⑧–Fengman-Huashulinzi fault; ⑨–Liuhe-Jilin fault; ⑩–Hongtuya-Jiaohe fault; ⑪–Liaoyuan-Panshi fault zone.

including the Caledonian, Variscan, Indosinian, and Yanshanian intrusive rocks based on their intrusion epochs (Table 2). The Caledonian intrusive rocks primarily comprise metamorphic hornblendites and metamorphic pyroxenites, occurring mostly as veins. The Variscan intrusive rocks consist of mafic-ultramafic rocks and granites, with the former occurring as veins along NW-trending faults and the latter, with a gneissic structure due to the late-stage tectonic activity, occurring as batholiths. The Indosinian intrusive rocks, associated closely with the formation of copper-nickel

Table 2. Regional magmatic activity stages and magmatic rock formation sequence in the study area (after Geology and Mineral Exploration and Development Bureau of Jilin Province, 1985; Regional Geology and Mineral Survey Institute of Jilin Province, 2016).

Geological epoch	Tectonic period	Chronology /Ma	Intrusive rock	Representative pluton	Volcanic rock	Reference
Mesozoic	Yanshanian		Fine-grained alaskitic granite and graphic granite	Shangmingshui pluton	Andesite, rhyolite, Andesite rhyolite tuff	
			Biotite granite	Sifangdingzi pluton		
			Diorite	Laogualazi pluton		
			Pyroxenite and hornblende	No. 2 pluton in the Chajianling deposit		
	Indosinian	238±3	Diorite	No. 8 pluton in the Hongqiling deposit		Wei QQ, 2015
		212.2±2.6; 237.0±3.0	Diorite pegmatite	No. 2 pluton in the Hongqiling deposit		Wei QQ, 2015; Hao LB et al., 2012; Sun LJ, 2013
		239.6±2.6; 212.5±2.8; 216±5	Gabbro	No. 1 pluton in the Chajianling deposit, and Nos. 1, 2, and 3 plutons in the Hongqiling deposit		Hao LB et al., 2013; Hao LB et al., 2012; Zhang GL and Wu FY,
		220.6±2	Olivine pyroxenite	No. 1 pluton in the Hongqiling deposit		Feng GY et al., 2011
		228.2±3.0; 228.8±2.8	Hornblende pyroxenite and olivine-bearing hornblende pyroxenite	No. 3 pluton in the Hongqiling deposit and No. 1 pluton in the Chajianling deposit		Wei QQ, 2015; Liu JY et al., 2010
			Olivine	Nos. 1 and 31 plutons in the Hongqiling		
Paleozoic	Variscan	263.6±1.6	Biotite granitic mylonite	Beigou pluton		Song J et al., 2017
			Gneissic granite	Dongliuchuan pluton		
		258±3; 272±4	Gabbro	Nos. 5 and 6 plutons in the Hongqiling		Sun LJ, 2013; Wei QQ, 2015
			Pyroxenite	Rock belt II of the Hongqiling area		
			Hornblende peridotite and peridotite	No. 24 pluton in the Hongqiling deposit		
	Caledonian		Metamorphic pyroxenite	No. 4 pluton in the Hongqiling deposit		
			Metamorphic hornblendite	Nos. 14, 18, and 19 plutons in the Hongqiling deposit		

sulfide deposits in the study area, principally encompass peridotites, olivine pyroxenites, hornblende pyroxenites, olivine-bearing hornblende pyroxenites, norites, and gabbros. The Yanshanian intrusive magmatism occurred in two stages. The early-stage Yanshanian intrusive rocks were dominated by intermediate-mafic rocks, including pyroxenites, hornblendes, gabbros, and diorites. The late-stage Yanshanian intrusive rocks are dominated by granitoids, including medium- to fine-grained biotite granites, granites, alaskitic granites, and graphic granites, occurring as batholiths or stocks. The Yanshanian granites are intimately linked with gold (Au) and polymetallic mineralization in the study area. Additionally, vein rocks like granites, dioritic porphyrites, felsites, felsophyres, diorites, pegmatites, and granitic aplites are found along fault structures extending in different directions (Geology and Mineral Exploration and Development Bureau of Jilin Province, 1985).

2.4. Regional geophysical and geochemical characteristics

The Hongqiling area lies within the Guanma-Panshi-Hulan high Bouguer gravity high anomaly zone (scale: 1∶200000), with Bouguer gravity anomaly values ranging from -5×10^{-5} m/s^2 to -25×10^{-5} m/s^2. This Bouguer gravity high is attributed to the high-density rocks like the metamorphic rock series of the Paleozoic Ordovician Hulan Group (Xu ZH, 2020).

The regional 1∶200000 aeromagnetic anomaly survey shows that the Hongqiling area is situated within the Panshi-Hongqiling-Huadian zone with high aeromagnetic anomalies. The regional aeromagnetic field is generally NNE-directed and locally EW-directed, with anomaly values mostly varying between 10 nT and 260 nT. The high aeromagnetic anomalies are principally caused by the volcanic and sedimentary rock series dominated by marine volcanic clastics, terrigenous clastics, and carbonate rocks (Xu ZH, 2020).

As shown in the geochemical anomaly map of the Ni element from the regional 1∶200000 stream sediment survey, zones with high Ni background values are primarily distributed in the NE direction along both sides of the Dunhua-Mishan fault. Such distribution highly aligns with the spatial occurrence of magmatic copper-nickel deposits discovered in the study area, such as the large Hongqiling nickel deposit and the medium-sized Changren nickel deposit. Zones with low Ni background values are primarily

distributed along the Antu-Yanji-Helong areas, also found sporadically in Yitong and Hunchun. This distribution pattern is associated closely with intrusive rocks like Early Jurassic granodiorites and Late Cretaceous quartz diorites (Fig. 3).

2.5. Regional mineral deposits

The study area boasts abundant endogenetic metal deposits, including magmatic copper-nickel deposits, porphyry molybdenum deposits, skarn iron deposits, and magmatic-hydrothermal gold deposits. The magmatic copper-nickel deposits in this area include the large Hongqiling deposit and small Chajianling, Sandaogang, and Piaohechuan deposits (Fig. 1b), serving as a vital industrial base of Ni ores in China. The porphyry molybdenum deposit is represented by the super large Daheishan molybdenum deposit. The magmatic-hydrothermal gold deposit is typified by large Erdaodianzi gold deposit.

3. Geological characteristics of the Hongqiling deposit

3.1. Strata

The strata exposed within the Hongqiling deposit are dominated by the Lower Paleozoic Hulan Group, along with trace quantities of sandy conglomerates in the Cretaceous Heiwaizi Formation in the south (Fig. 4). The Hulan Group comprises garnet-two-mica plagiogneisses, biotite plagiogneisses, plagioclase amphibolites, and muscovite schists, all exhibiting significant ductile deformations (Xi AH et al., 2006). The ore-bearing mafic-ultramafic plutons principally intruded into the garnet-two-mica plagiogneisses and biotite plagiogneisses in the lower portion. The plutons generally have strikes ranging from 310° to 330°, consistent with those of surrounding rocks' gneissosity. Besides, the plutons are nearly in conformity with the surrounding rocks.

3.1.1. Hulan Group

The Hulan Group serves as a significant occurrence layer for minerals like Au, silver (Ag), Cu-Ni, lead (Pb)-zinc (Zn), and marbles in the region. This group is segmented into the Huangyingtun and Xiaosangedingzi formations from bottom to top.

For the Huangyingtun Formation, the metamorphic protoliths are composed of terrigenous clastics and carbonate rocks interbedded with mafic to intermediate-acid volcanic rocks, undergoing metamorphism of the amphibolite-greenschist facies. This formation is a set of metamorphic rocks comprising tourmaline- and garnet-bearing two-mica plagiogneisses, biotite-plagioclase leptynites, hornblende-plagioclase leptynites, and kyanite schists, interbedded with multi-layer siliceous banded marbles. Its top is in conformity with marbles or graphite-bearing marbles of the Xiaosangedingzi Formation.

The Xiaosangedingzi Formation is composed primarily of siliceous banded marbles, graphite-bearing marbles, and thickly laminated marbles, interbedded with thinly laminated leptynites and quartzites. This formation was formed in a vast neritic carbonate-platform sedimentary environment, emplaced by Paleozoic to Mesozoic granites.

3.1.2. Heiwaizi Formation

The Heiwaizi Formation, exposed merely in the southern Hongqiling deposit, is controlled by the Huifahe depression fault zone. It spreads in nearly EW, with a dip direction of south and a dip angle of about 20° in general. Its outcrops are dominated by yellowish-green sandstones and sandy conglomerates from bottom to top, with thinly laminated sandy shales and feldspar sandstones found locally (Xu ZH, 2020). This formation, in angular unconformity with the underlying marbles of the Huangyingtun Formation's upper member, is overlain by Quaternary Upper Pleistocene strata.

3.2. Structures

Structures within the Hongqiling deposit encompass folds and faults. The folds primarily include the Balidong, Dulihe-Gaoliguo, and Zhaojiagou-Xiaolingzi anticlines, while the faults are mostly NE- and NW-trending. These crisscrossing structures constitute the general structural profile of the Hongqiling deposit (Fig. 4).

3.2.1. Folds

The Balidong anticline, with an axial plane strike of 310°, is a nearly vertical tight fold intruded by Variscan mafic-

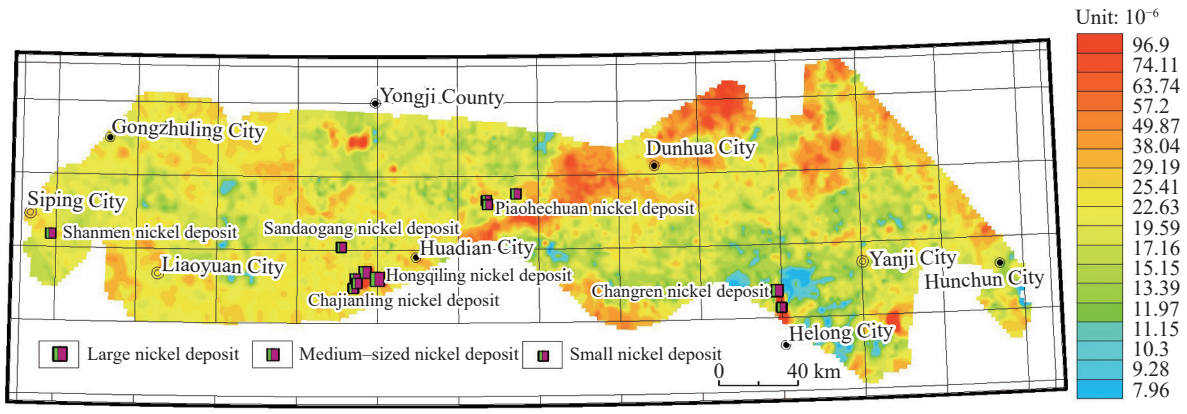

Fig. 3. Map showing the geochemical characteristics of Ni and the distributions of nickel deposits in the Jizhong-Yanbian metallogenic belt.

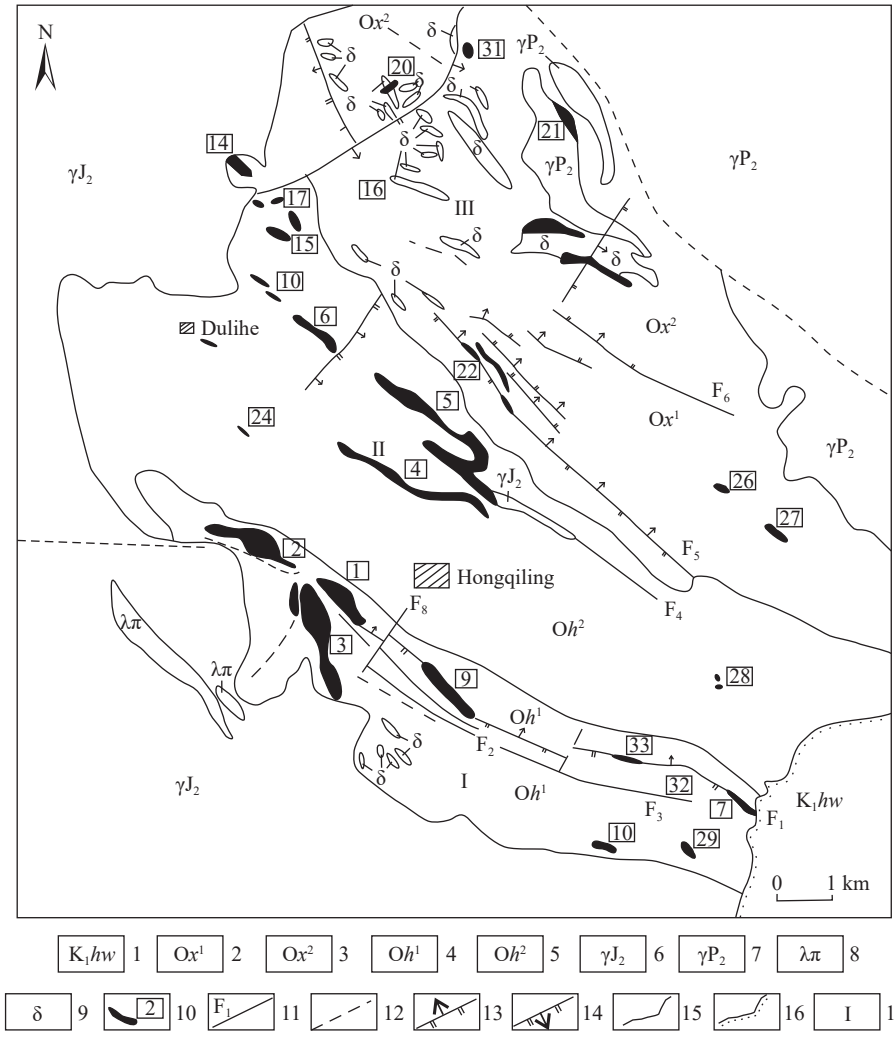

Fig. 4. Geological map of the Hongqiling deposit in Panshi City, Jilin Province (after Sun YH et al., 2016). 1–Cretaceous Heiwaizi Formation; 2–lower member of the Xiaosangedingzi Formation; 3–upper member of the Xiaosangedingzi Formation; 4–lower member of the Huangyingtun Formation; 5–upper member of the Huangyingtun Formation; 6–Middle Jurassic granite; 7–Middle Permian granite; 8–quartz porphyry; 9–diorite; 10–mafic or ultramafic rock and its number; 11–fault of practical survey; 12–infer fault; 13–reverse fault; 14–normal fault; 15–geological boundary; 16–angular unconformity boundary; 17–rock belt number.

ultramafic rocks along its core. The Dulihe-Gaoliguo anticline is a tight anticline structure with axial plane strikes ranging from 315° to 330°. The Zhaojiagou-Xiaolingzi anticline, exposed on the southeast side of Hongqiling Town, is also a tight anticline structure, with the axial plane strike gradually shifting from NWW in the south to N-NNW in the north, a length of about 9 km, and a width of 2.5 km. In the Beixinglong area, this anticline is intruded by the Nos.1 and 2 Indosinian mafic-ultramafic plutons of the Hongqiling deposit. Its southwest flank, with a dip direction of SW and dip angles ranging from 40° to 90°, is incomplete due to the intrusion by Yanshanian granites in the Zhaojiagou area and the deconstruction by later faults. Its northeast flank, with a dip direction of NE northeast and dip angles varying between 40° and 70°, has been partly destroyed by NW-trending faults.

3.2.2. Faults

Faults within the Hongqiling deposit are mostly NE- and NW-trending (Fig. 4). The NW-trending faults are proved to be primary ore-hosting faults in the study area, with attitudes generally consistent with those of strata. Some of these faults are connected to the deep-seated Huifahe fault, being considered secondary faults of the latter formed by its prolonged activity. The NW-trending faults primarily include Fujia-Pianlianzi(F1), Xiaolingtun-Zhaojiagou (F2, F3), and Xiaozhuqi-Mingdetun (F4, F5) faults (Fig.3), jointly governing the distributions of 33 mafic-ultramafic plutons in the Hongqiling deposit.

The attitudes of the Nos. 1 and 7 plutons in the Hongqiling deposit, as well as their variations, indicate that the NW-trending rock- and ore-controlling faults feature multistage activity. Specifically, these faults exhibited left-lateral compression in the early stage, right-lateral tension in the primary diagenetic and mineralization stages, and left-lateral compression during the emplacement of residual fertile magmas, with the Indosinian transtensional tectonic activity period identified as a critical ore-controlling period (Zhi XJ, 2005).

The NE-trending faults, dominated by transpressive faults, align parallel with the regional deep-seated Huifahe fault, featuring multistage activity. Their intersections with NW-

trending faults tend to host clusters of mafic-ultramafic plutons.

3.3. Intrusive rocks

Prolonged, frequent tectonic movements and significant magmatic activities in the Hongqiling area have led to the formation of Caledonian, Variscan, Indosinian, and Yanshanian intrusive rocks, which include Variscan and Yanshanian granites, Caledonian, Variscan, and Indosinian mafic-ultramafic rocks, as well as some quartz porphyry, granite pegmatite, and diorite dikes .

3.3.1. Granites

Variscan granites, primarily distributed in the eastern Hongqiling deposit, intrude into the metamorphic rock series of the Ordovician Hulan Group as stocks. They consist primarily of medium- and medium- to coarse-grained granodiorites and biotite monzogranites. The Yanshanian granites, principally distributed in the west of the Hongqiling deposit, intrude into the metamorphic rock series of the Ordovician Hulan Group as batholiths or stocks. They predominantly comprise medium- to fine-grained biotite granites and granites.

3.3.2. Mafic-ultramafic rocks

A total of 33 mafic-ultramafic plutons have been identified in the Hongqiling deposit. They exhibit zonal distributions along NW-trending faults, exposed on a small scale. These plutons are categorized into three rock belts based on their occurrence positions, types, and characteristics (Fig. 4; Table 3).

Rock belt I is distributed in the NW-trending Fujia-Hejiagou-Beixinglong-Changsheng fault zone. It extends over a length of 15 km in the NW direction (325°), with Nos.1, 2, 3, 9, 10, 29, 24, 30, and 7 plutons exposed within this belt. The surrounding rocks of these plutons are composed of biotite gneisses interbedded with thinly laminated hornblende plagiogneisses and marbles in the lower member of the Hulan Group's Huangyingtun Formation. The major ore-bearing plutons of the Hongqiling deposit are almost located in this rock belt. They exhibit various types, including the gabbro-pyroxenite-peridotite (Nos. 1 and 2), gabbro-pyroxenite (No. 3), hornblende peridotite (No. 9), peridotite (plutons in the footwall of fault F1), and orthopyroxenite (No. 7) types (Fig. 5).

Rock belt II is situated in the Huangguaying-Songbaitun-Mingdetun-Xinlitun fault zone. This fault zone is an interlaminar fault formed along the contact zone between hornblende plagiogneisses and chert band-bearing marbles. It extends over a length of 14 km in the NW direction. With rock belt II, Nos. 4, 5, 6, 18, 19, and 14 plutons, as well as No. 15 pluton in the north, are exposed. The plutons in this belt are primarily of the hornblende peridotite and peridotite types. They show simple lithofacies, consisting of a few mineralized plutons and ore-free plutons.

Rock belt III is located within the Xiaosangedingzi-Nangudingzi fault zone in the eastern Hongqiling deposit. This belt shows a NW strike (330°) and a total length of over 5 km, holding Nos. 8 and 31 meta-alkaline mafic-ultramafic plutons. The plutons are primarily of hornblende peridotite and peridotite types. They exhibit simple lithofacies, roughly lacking Ni mineralization (Xue HR, 2020). The mafic-ultramafic plutons in this rock belt were subjected to regional metamorphism and deformations, with minerals such as pyroxenes displaying a gneissic directional arrangement.

3.3.3. Characteristics of primary ore-bearing plutons

(i) No. 7 ore-bearing pluton

The No. 7 ore-bearing pluton, situated at the NW-trending fault zone's southwest end that is the closest to the Huifahe fault (Fig. 3), exhibits a zonal distribution on a horizontal plane and appears as a dyke form on the cross section (Fig. 6). Its roof is composed of granitic gneisses and hornblende schists interbedded with marbles, while its floor comprises biotite gneisses (Dong YS, 2003). This pluton has an exposed area of 0.013 km^2, strikes ranging from 300° to 330°, a dip direction of NE, and dip angles ranging from 75° to 80°. Moreover, it manifests a length of 700 m and an average width of 35 m, extending for a maximum of 520 m in its dip direction.

Regarding rock types, the No. 7 pluton primarily includes enstatites (intensively sub-amphibolized into altered pyroxenites locally) and a small quantity of norites. The enstatites, the dominant rocks in the pluton, account for 96% of its total volume. The norites are mostly distributed at the

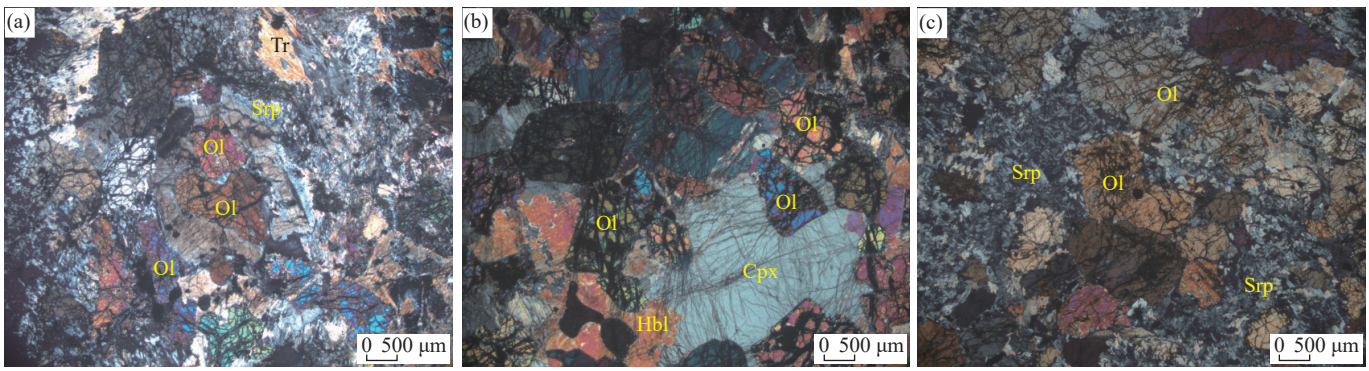

Fig. 5. Altered hornblende peridotites (a) and hornblende olivine pyroxenites (b) of the No.1 pluton and serpentinized peridotites (c) of the No. 33 pluton in rock belt I of the Hongqiling area. Cpx–Clinopyroxene; Hbl–Hornblende; Ol–Olivine; Srp–Serpentine; Tr–Tremolite.

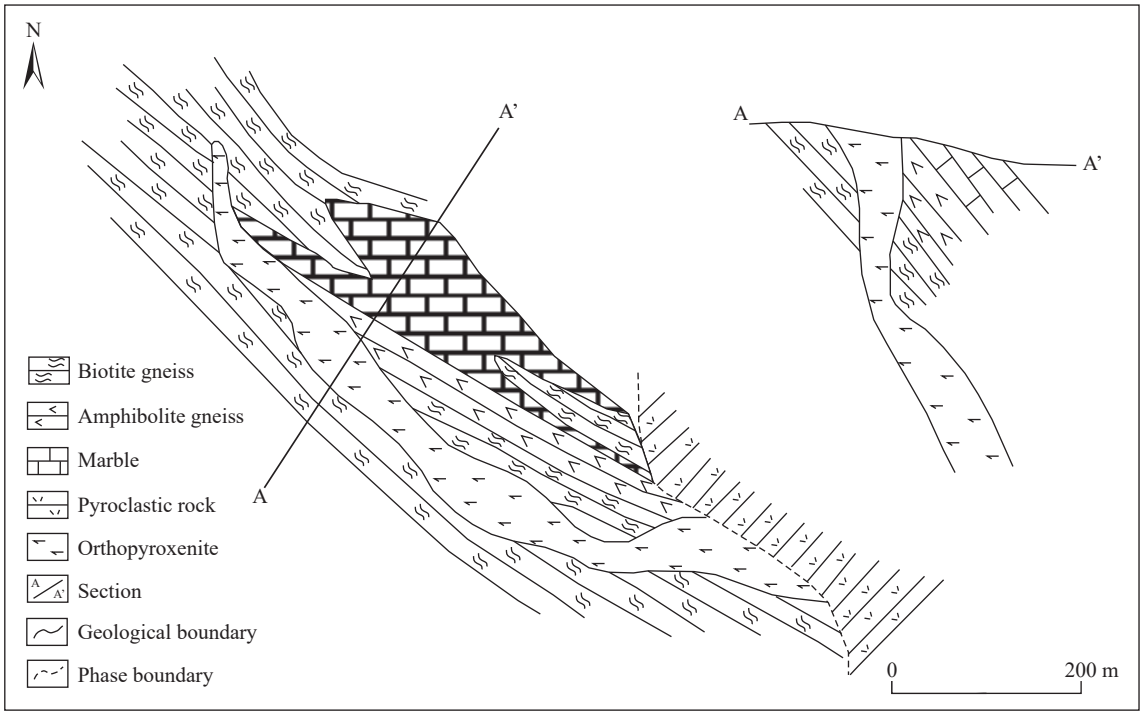

Fig. 6. Geological map and section of the No. 7 pluton in the Hongqiling deposit in Panshi City (modified from Qin K, 1995).

edges of the pluton, in structurally fractured contact with surrounding rocks. Pyroxene peridotite dykes are frequently found on the pluton's side close to strata in the middle portion of the pluton. These dykes partially shift to peridotites or olivine pyroxenites due to their changes in the relative contents of olivines and orthopyroxenes.

Based on the analyses of the geological characteristics of the Nos. 7, 32, and 33 plutons, Yin GZ et al. (2019a) conducted modeling for the lithofacies and orebodies of these plutons. The results indicate that the three plutons were formed by comagmas' differential denudation and modification from the No. 7 pluton's deep part in the southeast toward the northwest.

(ii) No. 1 ore-bearing pluton

The No. 1 ore-bearing pluton in the southern Hongqiling deposit intrudes along the NW-trending fault, in unconformity with the surrounding biotite gneisses. This pluton presents a fusiform pattern on a horizontal plane, with a NW strike (40°), a length of 980 m, widths ranging from 150 m to 280 m, and a depth of 560 m. On the cross section, with both ends tilting toward its center, this pluton has a dip angle of 75° at the northwest end and 36° at the southeast end, appearing as an asymmetric lopolith pitching northwestward (Fig. 7a). The longitudinal projection reveals that this pluton deepens gradually from south to north, with mineralization extremely significant at the southern tip that warps up (Fig. 7b; Fu DB et al., 1988).

The No. 1 pluton is obliquely cut by reverse-oblique fault F1. Its roof is composed of the upper No. 1 pluton, two small blind plutons, and two orebodies within gneisses, while its floor consists of the lower No. 1 pluton and the No. 1 pluton' part within gneisses, with only the upper No. 1 pluton exposed (Yin GZ et al., 2019b). The upper No. 1 pluton largely intrudes into the biotite gneisses, generally pitching northwestward at an angle of 39°. It exhibits a NW strike, a length of approximately 980 m, and widths roughly ranging from 150 m to 280 m (average: about 200 m; narrow ends and wide central part). Its dip angle is relatively stable, ranging from 70° to 75°. From the center to both sides, surface to deep part, and northwest to southeast, the upper No. 1 pluton features gabbros, pyroxenites, peridotites, and olivine pyroxenites in sequence, forming a lopolith structure (Yin GZ et al., 2019b). Peridotites, the dominant lithofacies of the No. 1 pluton, account for about 81% of its total volume. Olivine pyroxenites, ore-bearing rocks at the pluton bottom, represent about 12% of its total volume (Yin GZ et al., 2019b).

(iii) No. 2 ore-bearing pluton

The No. 2 ore-bearing pluton is located at the northwesternmost end of rock belt I in the Hongqiling area. Its surrounding rocks consist of biotite gneisses on its northeast side and hornblende schists on its southwest side (Fig. 4). This pluton has a strike of NW (310°) in the south and EW in the west. The outcrops of the pluton have a length of approximately 1700 m and widths ranging from 60 m to 350 m, covering an area of 0.28 km^2. The pluton is lentoid in shape on a horizontal plane (Fig. 8a). On the cross section, it inclines inward on both sides, appearing as a wedge that is wide in the upper part and narrow in the lower part. This pluton has a lithofacies assemblage of gabbro-pyroxenite-peridotite. This assemblage is highly differentiated, consisting of gabbros, pyroxenites (partly altered pyroxenites and feldspar-bearing pyroxenites), and pyroxene peridotites from top to bottom (Li A, 2019).

(iv) No. 3 ore-bearing pluton

The No. 3 ore-bearing pluton hosts the most widely exposed mafic-ultramafic rocks in rock belt I. This pluton,

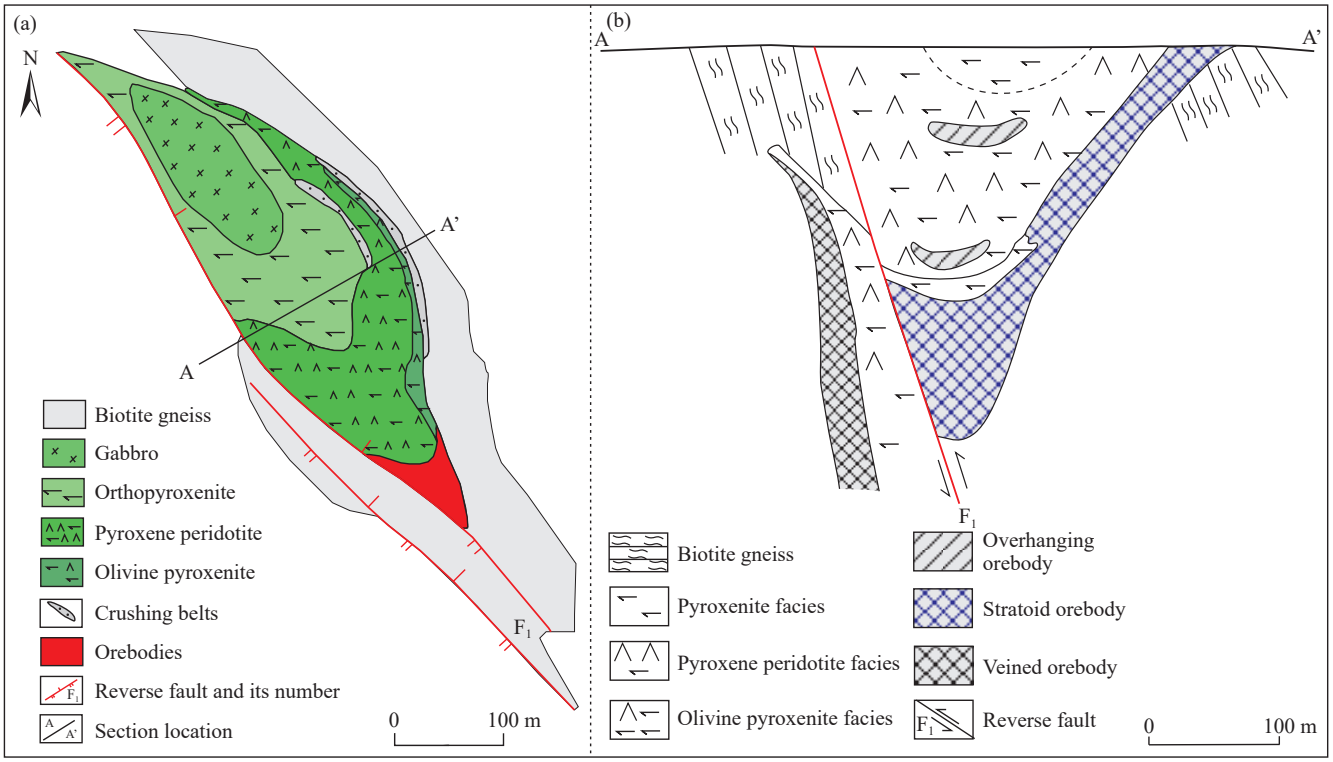

Fig. 7. Geological map and cross section of the No. 1 pluton of the Hongqiling deposit in Panshi City (a after Team 607 of Jilin Nonferrous Metal Geological Exploration Bureau, 2008; b after Hao LB et al., 2014).

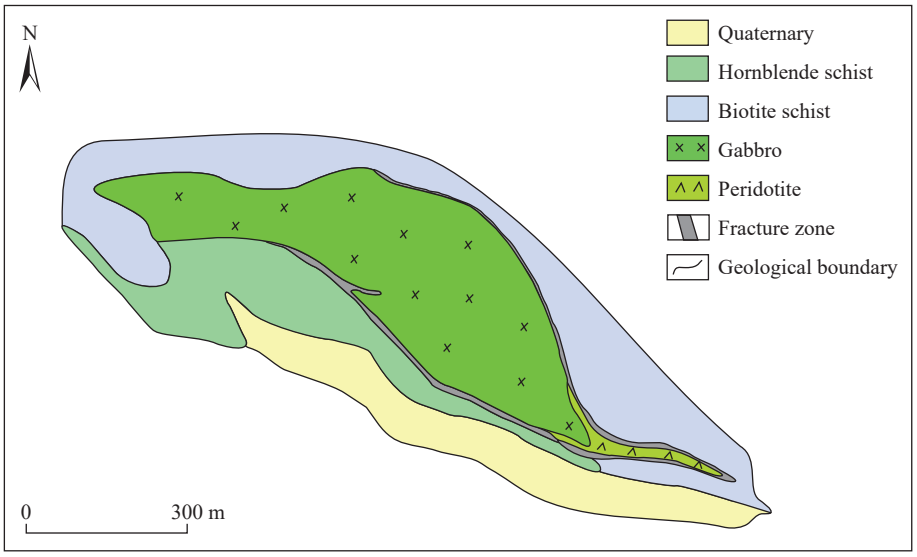

Fig. 8. Geological map of the No. 2 pluton in the Hongqiling deposit (after Team 607 of Jilin Nonferrous Metal Geological Exploration Bureau, 2008).

located in the central part of rock belt I, is adjacent to the No. 2 pluton to the north and the No. 1 pluton to the east (Fig. 3). This pluton intrudes into the granitic gneisses, hornblende schists, marbles, and other rocks of the Hulan Group. It is composed primarily of gabbros, with a length of approximately 2500 m and widths ranging from 40 m to 500 m, resembling a long tadpole characterized by a wide northern part and a narrow southern part (Fig. 9a). On the cross section, this pluton appears as a steep dyke (Fig. 9b), with a length-width-depth ratio of 9∶4∶1 and an exposed area of about 0.4 km^2. It has a strike of nearly SN (350°) and dips towards the east (70°–80°). Based on its outcrop location, the No. 3 pluton can be segmented into the old and the young No. 3 plutons, which are combined at an elevation of 150 m. Regarding lithofacies, this pluton is primarily composed of gabbros and pyroxenite facies, which are distributed on the north side of the old No. 3 pluton and the south side of the No. 3 pluton, respectively (Liu JY et al., 2010).

4. Mineralized alterations

The Hongqiling deposit is primarily composed of the H-7

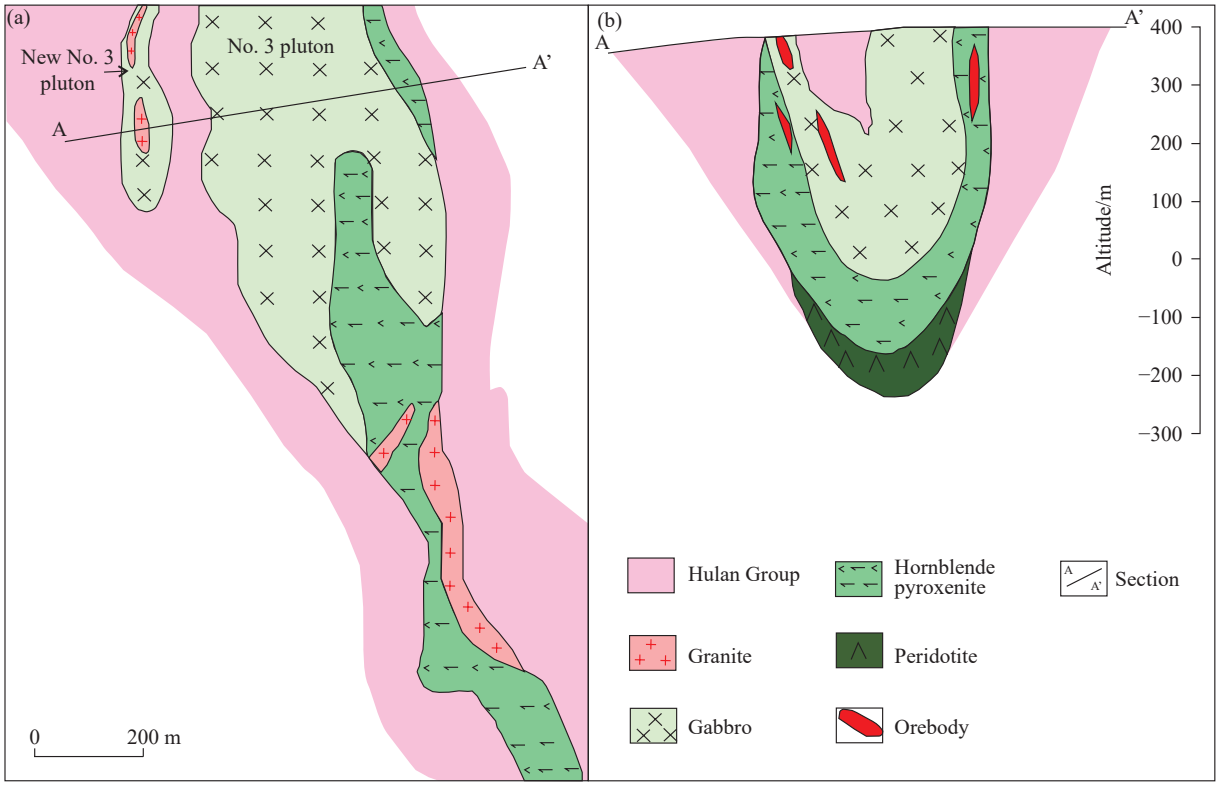

Fig. 9. Geological map (a) and cross section (b) of the No. 3 pluton in the Hongqiling deposit (modified from Li A, 2019).

large deposit, the H-1 and H-3 medium-sized deposits, and small deposits such as H-2 and H-9.

4.1. Characteristics of orebodies

4.1.1. H-7 large deposit

The H-7 large deposit (within the No. 7 pluton), i.e., the Fujia deposit, consists primarily of tabular, veined, and pure-sulfide veined orebodies (Fig. 6; Dong YS, 2003).

Tabular orebodies. These orebodies are mostly industrial orebodies with extensive metal sulfides. Their morphologies and attitudes are roughly consistent with those of plutons. The ore-bearing rocks predominantly comprise enstatites or altered pyroxenites, along with a small quantity of norites. The ores exhibit sideronitic structures largely, followed by trace quantities of disseminated structures, with lumpy structures locally found. The metallic mineral assemblage principally encompasses pyrrhotite, pentlandite (including minor amounts of violarite), and chalcopyrite, with relative contents of 54%, 33%, and 13%, respectively. Additionally, the ores exhibit a Ni/Cu ratio of around 3.3.

Veined orebodies. These orebodies predominantly occur in pyroxene peridotite veins. They are veined in shape, with morphologies and attitudes roughly consistent with those of the veins they occur. Their ores primarily include sideronitic and spotted ores. Their dominant metallic mineral assemblage consists of pyrrhotite, pentlandite, and chalcopyrite, with relative contents of 56%, 39%, and 5%, respectively. Compared to the tabular orebodies, these orebodies manifest higher Ni grades, with a Ni/Cu ratio of 5.2.

Pure-sulfide veined orebodies. These orebodies occur in the contact fracture zone between enstatites and pyroxene peridotites, with the three manifesting distinct boundaries and abrupt shifts. They are all composed of dense massive ores. Their metallic minerals principally comprise pyrrhotite (58×10^{-2}), pentlandite (35×10^{-2}), and chalcopyrite (7×10^{-2}), as well as minor amounts of olivine, enstatite, and brown hornblende. Among them, pentlandite usually displays an elliptical directional arrangement, suggesting its migration characteristics during the orebodies' formation (Qin K, 1995). The pure-sulfide orebodies, exhibiting minimal changes in strike and dip direction, remain a stable vein shape, with lengths exceeding depths.

4.1.2. H-1 medium-sized deposit

The H-1 medium-sized deposit (within the No. 1 pluton), i.e., the Daling deposit, primarily hosts stratoid, overhanging lentoid, veined, and pure-sulfide veined orebodies/mineralized bodies. Among them, stratoid orebodies are identified as the most important industrial orebodies within the No. 1 pluton (Fig. 7).

Stratoid orebodies. These orebodies occur within the olivine pyroxenite facies at the bottom of the upper No. 1 pluton, with distinct boundaries between them and the overlying peridotite facies. Their morphologies and attitudes are roughly consistent with those of their ore-hosting lithofacies, presenting a stratoid pattern (Wang ZG, 2012). Their flanks incline toward their centers on the cross section and gently incline toward the NW on the longitudinal section (Qin K, 1995). These orebodies are composed principally of sideronitic and spotted ores, along with some disseminated ores. Generally, the sideronitic ores are found at the bottom

Table 3. Characteristics of major mafic-ultramafic plutons within the Hongqiling deposit.

Rock belt	Rock-controlling structure	Pluton No.	Exposed area/ km^2	Pluton scale	Pluton morphology	Pluton attitude	Lithofacies	Degree of differentiation	Mineralization evaluation	Diagenetic epoch/Ma	Geochemical characteristics of rocks (average M/F ratio)
Rock belt I	NW-trending Fujia-Hejiagou-Beixinglong-Changsheng fault zone	Upper No. 1 pluton	0.2	Length: 980 m; average width: 200 m	A fusiform shape on a horizontal plane, and a lopolith shape on the cross section	Strike: 320°; dip direction: 60–65°, with both sides dipping toward the center	Gabbro-pyroxenite-peridotite-ore-bearing olivine pyroxenite	Highly differentiated	Large to medium-sized deposit	216–239	0.99–6.05 (4.60)
		Lower No. 1 pluton		Length: 1000 m; width: 30–170 m; depth: 30–900m	Narrow band	Strike: 320°; dip direction: northwest; dip angle: 60°–65° (80°–85° in the deep part)	Peridotite	Insignificantly differentiated	Medium-sized orebodies at the edge of the pluton		
		No. 2 pluton	0.28	Length: 1712 m; maximum width in the central part: 350 m	Resembling a mouse on a horizontal plane and a basin and wedge on the cross section	Strike: 310°; dip angle: 65°–85°; with both sides dipping inward	Gabbro-norite-pyroxene-peridotite	Highly differentiated, with the transition differentiation facies between the upper and lower parts	Small orebodies in the deep area	212–237	3.47–5.93 (4.77)
		No. 3 pluton (including the new No. 3 pluton)	0.4	Length: 2500 m; width: up to 500 m in the north, gradually decreasing to 40–50 m southward	Appearing as a steep dyke	Strike: 350°; steep in the north and extending and dipping eastward in the south; dip angle: 70°–80°	Gabbro-norite, felsite-bearing hornblende pyroxene - orthopyroxenite	Differentiated, including two major lithofacies	Small orebodies in the Su Changyan anomaly body	234.6±5.6	3.56–6.02 (4.38)
		No. 9 pluton	0.0996	Length: 1400 m; maximum width: 200 m	Narrow at both ends and wide in the central part, resembling a rock hammer on the vertical section	Strike: 320°; with both sides dipping toward the center	Hornblende peridotite primarily, followed by peridotite and olivine pyroxene veins	Poorly differentiated	Industrial value of pure Ni ore is not significant		4.7
		No. 7 pluton	0.0078	Length: 700 m; average width: about 35 m	Appearing as dykes on both a horizontal plane and the cross section	Strike: 300°–330°; dip direction: northeast; dip angle: 70°–85°	Orthopyroxene primarily, followed by norite	Insignificantly differentiated	Large deposit		0.87–5.48 (3.87)

Table 3. (*Continued*)

Rock belt	Rock-controlling structure	Pluton No.	Exposed area/ km^2	Pluton scale	Pluton morphology	Pluton attitude	Lithofacies	Degree of differentiation	Mineralization evaluation	Diagenetic epoch/Ma	Geochemical characteristics of rocks (average M/F ratio)
		No. 10 pluton		Length:120 m in the north and 300 m in the south; width: 58 m in the north and 18 m in the south	Veined	Strike: 290°; dip direction: 70° in the north and NW in the south (50 °)	Hornblende peridotite - felsite-bearing hornblende peridotite	Poorly differentiated			
		No. 32 pluton		Length: 120 m; width: 10–16 m	Veined	Strike: 320°; dip direction: NE, dip angles: 75°-80°	Orthopyroxene and pyroxene peridotite	Insignificantly differentiated	Small deposit		
		No. 33 pluton		Length: 80 m; width: 10 m	Veined	Strike: 320°; dip direction: NE	Orthopyroxene		Mineralization		
Rock belt II	Huangguaying-Songbaitun-Mingdetun-Xinlitun fault zone	No. 4 pluton			Narrow strip	Strike: NW	Metamorphic pyroxene and hornblendite, and peridotite	Insignificantly differentiated	No economically valuable copper Ni mineralization has been discovered		
		No. 5 pluton			S-shaped strip extending northwestward	Strike: NW	Gabbro - hornblende pyroxenite - hornblende peridotite	Insignificantly differentiated		272±4	
		No. 6 pluton			Spindle shaped on a horizontal plane	Strike: NW	Gabbro, peridotite	Insignificantly differentiated		258±3	
		No. 15 pluton			Veined	Strike: NW	Metamorphic hornblendite	Insignificantly differentiated			
		No. 24 pluton			Veined	Strike: NW	metamorphic pyroxenites	Insignificantly differentiated			
Rock belt III	Xiaosangedingzi-Nangudingzi fault	No. 8 pluton			Lentoid	Strike: NW	Diorite and pyroxenite	Insignificantly differentiated	No mineralization	238±3	
		No. 31 pluton		Length: about 280 m; width: nearly 140 m	Elliptically shaped on a plane	Strike: NW; dip direction: NE	Diorite - hornblende gabbro - felsite-bearing hornblende peridotite felsite-bearing hornblende peridotite	Differentiated, including three major lithofacies		218.1±3.5	

Note: The M/F ratios and chronological data of plutons originate from Li A, 2019; Wu FY et al., 2004; Liu JY et al., 2010; Hao LB et al., 2013; and Wei B et al., 2013.

and center of the orebodies, while spotted ores occur on their top and edges (Wang ZG, 2012). The metallic minerals in the ores encompass pyrrhotite (60×10^{-2} ±), pentlandite (30×10^{-2} ±), chalcopyrite (5×10^{-2} ±), and minor amounts of magnetite, pyrite, vallerite, and ilmenite. Besides, the ores exhibit a Ni/Cu ratio of about 5.

Overhanging lentoid orebodies. These orebodies occur primarily within the central and upper portions of the upper No. 1 pluton's peridotite facies. They present irregular morphologies like lentoid or thinly laminated shapes. They are composed principally of fine-grained disseminated ores, in which the metallic mineral assemblage encompassing pyrrhotite (60×10^{-2} ±), pentlandite (35×10^{-2} ±), chalcopyrite (5×10^{-2} ±), and a minor amount of magnetite. Additionally, the ores exhibit a Ni/Cu ratio of around 4.6.

Veined orebodies. These veined orebodies occur within the altered pyroxenite veins of the lower No. 1 pluton. Their vein rocks comprise uralites (above 90×10^{-2}) and minor quantities of brown hornblendes, talcs, chlorites, and phlogopites. The metal sulfides, with content roughly ranging from 2×10^{-2} to 6×10^{-2}, exhibit spotted and disseminated sparse, uneven distributions in rocks, occasionally constituting orebodies (Wang ZG, 2012). Consequently, these veined orebodies are unstable in space. The metallic minerals in the ores principally include pyrrhotite, pentlandite, and chalcopyrite, with relative contents of 76×10^{-2}, 20×10^{-2}, and 4×10^{-2}, respectively. The Ni/Cu ratio of the ores is close to 5.

Pure-sulfide veined orebodies. These orebodies are frequently found within the primary joints of stratoid orebodies or, influenced by variable primary joints, are veined or lentiform in shape. Their widths range from several to over 10 cm, with a maximum of above 20 cm. They are exposed discontinuously and composed of dense massive ores (Wang ZG, 2012). Their dominant metal minerals include pyrrhotite (69×10^{-2} ±) and pentlandite (29×10^{-2} ±), along with a minor amount of chalcopyrite, with pyrite and magnetite visible occasionally. The ores exhibit a Ni/Cu ratio of up to 20, with intense alterations observed in some surrounding rocks on both sides of the pure-sulfide veins.

Additionally, in the orthopyroxenite schlieren of the peridotite facies, mineralization is occasionally observed in some gabbro pegmatites, with metal sulfides being scattered or lumpy in shape. The metal minerals are dominated by pyrrhotite (80×10^{-2}), succeeded by pentlandite (18×10^{-2}), as well as minor amounts of chalcopyrite, magnetite, and ilmenite.

In the altered pyroxenites near the contact fracture zone between stratoid orebodies and gneisses, the mineralization of metal sulfides, irregularly lumpy, veinlet-like, and disseminated, are occasionally observed. The metallic mineral assemblage consists of pyrrhotite (50×10^{-2} to 92×10^{-2}), chalcopyrite (1×10^{-2} to 45×10^{-2}), and pentlandite (5×10^{-2} to 20×10^{-2}), which exhibit significantly varying contents and are dominated by the former two. Additionally, minerals like niccolite, temiskamite, and molybdenite, as well as tourmaline, biotite, chlorite, and quartz, are identified locally. Such mineralization features a low Ni grade and a low Ni/Cu ratio.

4.1.3. H-3 medium-sized deposit

The H-3 deposit (within the No. 3 pluton) primarily holds veined and chambered orebodies, occurring within gabbros and hornblende pyroxenites. Their orebodies have lengths ranging from 100 m to 300 m, depths from 54 m to 265 m, thicknesses from 1.5 m to 164.27 m, and dip angles from 4° to 25° (Xu ZH et al., 2022).

Recently, five veined orebodies have been discovered in the No. 3 pluton (Fig. 10), with Ni ores estimated at 32259 t and an ore grade up to 0.36%. Among them, the No. 2 orebody is the thickest, with burial depths ranging from 700 m to 1100 m and average Ni, Cu, and Co grades of 0.39%, 0.11%, and 0.03%, respectively (Xu ZH et al., 2022).

4.2. Ore and mineral characteristics

The ores in the Hongqiling deposit consist of Cu-Ni sulfides. The metal minerals in the ores primarily encompass pyrrhotite, pentlandite, chalcopyrite (Fig. 11), violarite, and pyrite, succeeded by chloanthite, niccolite, sphalerite, magnetite, galena, vallerite, molybdenite, and ilmenite.

The ore textures predominantly comprise hypidiomorphic to xenomorphic granular, flame-shaped, and rimmed textures, as well as interstitial, myrmekitic, poikilitic, nodular, and metasomatic textures. In the ores of the Hongqiling deposits, sulfides like pyrrhotite, pentlandite, and chalcopyrite are frequently paragenetic and metasomatized by sphalerite. Most especially, pentlandite is often metasomatized by sphalerite along its cleavage (Figs. 11a, c).

The ore structures principally include disseminated, spotted, sideronitic, and dense massive structures, succeeded by lumpy, veinlet-disseminated, and brecciated structures. Various ore-bearing plutons in the deposit differ somewhat in ore structure. Specifically, the No. 1 pluton primarily exhibits disseminated, spotted, and lumpy ore structures, the No. 2 pluton predominately hosts spotted ore structures, the No. 3 pluton principally contains disseminated ore structures, while the No. 7 pluton mainly holds densely disseminated ore structures, followed by scant, sparsely distributed disseminated and lumpy ore structures (Li A, 2019). Moreover, orebodies with different morphologies feature distinctive ore structures. Disseminated structures are the most common in the overhanging orebodies and the bottom stratoid orebodies in peridotites. In contrast, sideronitic structures are primarily present in segments hosting olivine pyroxenites and orthopyroxenites (Dong YS et al., 2004).

Pyrrhotite, pentlandite, chalcopyrite, and pyrite constitute the dominant metal mineral assemblage of the Hongqiling deposit. Their characteristics are described as below.

Pyrrhotite is the most common metal sulfide in ores, also serving as a primary carrier mineral of Cu, Ni, and Co (Lv LS et al., 2017). Pyrrhotite, together with other metal sulfides like pentlandite and chalcopyrite, occurs among silicate mineral grains (Fig. 12a) or spread among idiomorphic pentlandite

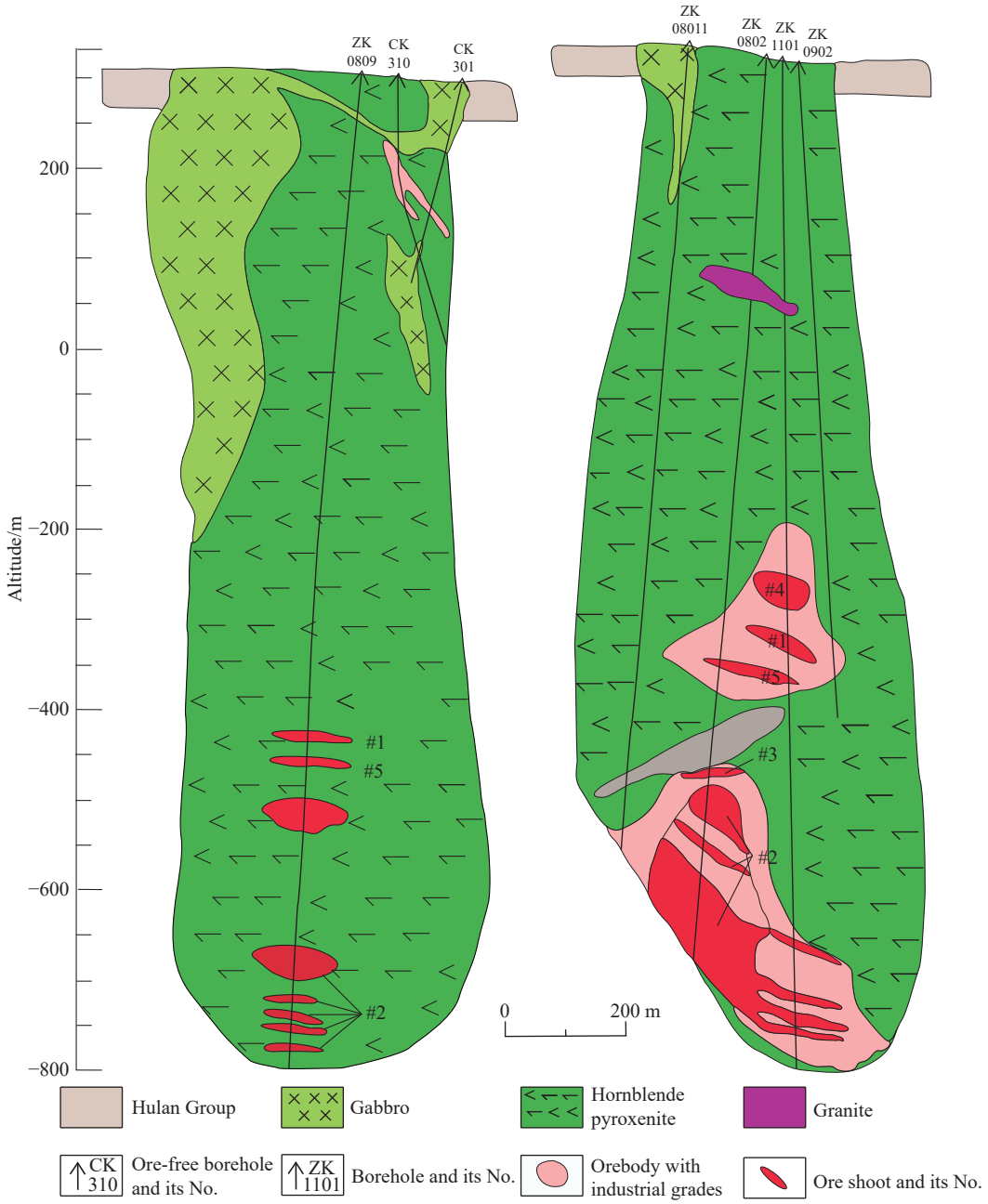

Fig. 10. Drilling verification results of Cu and Ni ores at the bottom of the No. 3 pluton in the Hongqiling deposit (after Xu ZH et al., 2022).

grains as xenomorphic grains (Wei B, 2013). The Ni and Co in ores of the No. 7 pluton are primarily distributed randomly within pyrrhotite as free sulfides (or sulfarsenides), micro-fine inclusions, or exsolutions, with minor amounts of Ni and Co distributed within pyrrhotite lattices by replacing Fe through isomorphism (Ding KS et al., 2007).

Pentlandite is proved to be the dominant nickel-bearing mineral in the Hongqiling deposit. In ores of the No. 7 pluton, pentlandite exhibits elongated pisolitic textures, a directional arrangement, and rhyolitic structures (Lv LS et al., 2017). In this pluton, pentlandite occurs in massive ores as idiomorphic mineral aggregates, while xenomorphic pyrrhotite and pyrite are distributed among pentlandite grains (Wei B, 2013). In ores of the No. 1 pluton, pentlandite is frequently paragenetic with pyrrhotite and chalcopyrite as hypidiomorphic to xenomorphic mineral aggregates, metasomatized by sphalerite along its cleavage (Fig. 11c). Based on its morphological characteristics and intergrowth relationships with surrounding minerals, pentlandite can be categorized into three generations: Pn (1), Pn (2), and Pn (3). Pn (1) is monocrystal granular pentlandite derived from high-temperature crystallization. Pn (2) is fine-grained pentlandite with synneusis textures, derived from low-temperature exsolution. Pn (3) is microscopic flaky exsolved pentlandite derived from low-temperature crystallization (Xi AH et al., 2004). Pentlandite of varying generations shows increasing Ni/Fe ratios with the Ni content, with compositions showing somewhat inheritance (Lv LS et al., 2017). Iron and Ni in the ores are commonly metasomatized by Co and Cu through isomorphism (Lv LS et al., 2017).

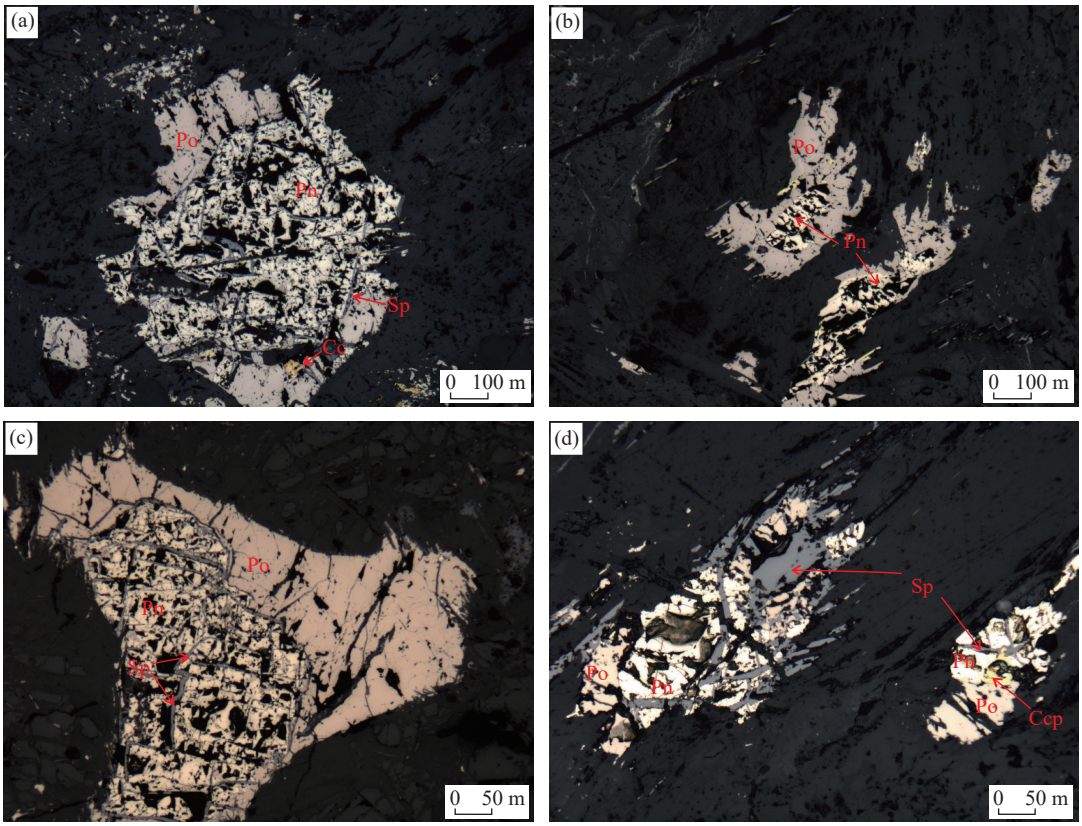

Fig. 11. Microscopic images of primary ore minerals in the No. 1 pluton of the Hongqiling deposit. Ccp–Chalcopyrite; Sp–Cphalerite; Po-pyrrhotite; Pn–Pentlandite.

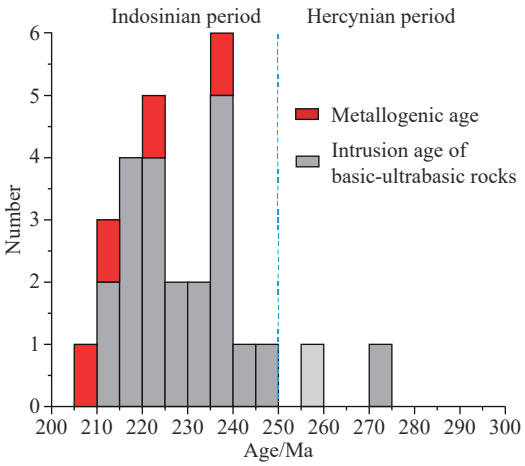

Fig. 12. Histogram showing the diagenetic and metallogenic ages of major copper-nickel deposits on the northern margin of the North China Plate (data shown in Table 6).

Chalcopyrite is identified as the predominant Cu-bearing mineral in the Hongqiling deposit. Based on its morphological characteristics, attitudes, and intergrowth relationships with surrounding minerals, chalcopyrite in ores can be categorized into two generations: Ccp (1) and Ccp (2). Ccp (1) is xenomorphic, granular chalcopyrite, paragenetic with pyrrhotite and pentlandite (Figs. 11a, b). Ccp (2) is drop-like chalcopyrite, forming exsolution textures with sphalerite. In the deposit of the No. 7 pluton (i.e., the Fujia deposit), minor amounts of Cu and iron in chalcopyrite are replaced by nickel and Co through isomorphism (Lv LS et al., 2017).

Pyrite is commonly found in dense massive and disseminated ores. Based on its morphologies, attitudes, and intergrowth relationships with surrounding minerals, pyrite in ores can be categorized into four generations: Py (1), Py (2), Py (3), and Py (4). Py (1) is hypidiomorphic to xenomorphic granular pyrite. It frequently appears as residual pyrite due to metasomatism, identified as metal sulfides crystallized in the early stage. Py (2) is fascicular or myrmekitic pyrite, exhibiting a somewhat directional arrangement. Py (3) is idiomorphic granular pyrite, with high Ni and Co contents but almost bearing no Cu. Py (4) is veinlet or stockwork pyrite. Pyrite of various generations differs in the contents and characteristics of trace elements, further reflecting the changes in ore-forming fluids in varying mineralization stages (Xi AH et al., 2004).

Useful components in ores primarily include Ni, Co, Cu, sulfur (S), selenium (Se), and tellurium (Te), with average contents of 1.13%, 0.034%, 0.20%, 3.22%, 0.00057%, and 0.0004%, respectively.

4.3. Alterations of surrounding rocks

The ore-bearing plutons within the Hongqiling deposit generally show relatively weak alterations, primarily including uralite, talc, chlorite, hornblende, biotite, phlogopite, sericite, and serpentine alterations, as well as carbonation. Some uralite, serpentine, and chlorite alterations are closely associated with mineralization. However, the tremolite, chlorite, and talc alterations and carbonation,

caused by late-stage hydrothermal alteration, are proved unrelated to mineralization (Xue HR, 2020).

Uralite alteration is the most extensive, especially in the enstatites of the No. 7 pluton and the gabbros of the No. 3 pluton. Such alteration is frequently accompanied by chlorite alteration.

The serpentine and talc alterations, comparatively intense, primarily occur in the olivine and pyroxene minerals within olivine websterites, lherzolites, and hornblende pyroxenites. These alterations are accompanied by uralite, chlorite, and biotite alterations, as well as iron precipitation.

4.4. Mineralization phases and stages

Tang ZL et al. (1998) posited that the Hongqiling deposit and the Jinchuan copper-nickel deposit experienced similar metallogenic processes involving deep liquation and magma ascent and emplacement. They segmented the magmatic mineralization of both deposits into four successive mineralization stages: silicate magma, sulfide-bearing magma, sulfide-rich magma, and sulfide liquation.

Based on the characteristics of orebodies and ores, Sun LJ (2013) divided the Ni mineralization of the Hongqiling deposit into three major stages: magmatic liquation, ore magma penetration, and hydrothermal superimposed enrichment. The magmatic liquation mineralization stage witnessed the formation of major stratoid orebodies. In the late ore magma penetration mineralization stage, unconsolidated sulfide-bearing magmas penetrated into the stratoid orebodies along their primary joints, forming small-scale sulfide-rich veins. In the hydrothermal superimposed enrichment stage, silicate minerals like olivine and pyroxene in early-stage rocks and orebodies experienced alterations, further releasing Ni, which was superimposed and enriched within the existing orebodies or surrounding rocks. Consequently, some veinlet quartz-carbonate-sulfide mineralization occurred, or disseminated ores were transformed into lumpy ones.

Han CM et al. (2014) categorized the Cu-Ni mineralization in the Hongqiling deposit into three stages: magma crystallization, autometamorphism, and the hydrothermal stage sequentially. In the magma crystallization stage, disseminated and massive ores occurred, forming the ore mineral assemblage composed of pentlandite, violarite, millerite, and magnetite. The autometamorphism stage witnessed the formation of massive and veined high-grade Cu-Ni ores, with the Cur- and Ni-bearing minerals typified by chalcopyrite and pyrrhotite. The hydrothermal stage, the third mineralization stage, exhibited chlorite alteration and carbonation, as well as a mineral assemblage composed of carbonate, pyrite, and pyrrhotite, occurring as veins.

Xu ZH (2020) divided the magmatic mineralization phase of the Hongqiling deposit into the deep liquation - crystal fractionation stage, the late-stage magmatic mineralization stage, and the ore magma-related mineralization stage. Moreover, he considered that the weak hydrothermal mineralization phase and the supergene oxidation phase were superimposed onto the magmatic mineralization phase (Table 4). The mineralization characteristics of various mineralization phases and stages are as described as follows:

(i) The magmatic mineralization phase. This phase can be divided into three stages: The deep liquation – crystal fractionation stage, the late-stage magmatic mineralization stage, and the ore magma-related mineralization stage.

Deep liquation – crystal fractionation stage. In this stage, primary magmas underwent fractional crystallization of olivines and clinopyroxenes in deep magma chambers. Concurrently, metal sulfides underwent liquation due to the contamination by crustal materials, leading to the separation of sulfide melt facies from silicate lavas. As a result, magmas and ore magmas, bearing sulfide melts to different degrees, were formed.

Late-stage magmatic mineralization stage. This predominant mineralization stage witnessed the formation of various ores and the placement of orebodies. Ore-bearing magmas or ore magmas underwent pulsed ascent and emplacement, followed by in situ liquation in shallow magma chambers. In the early stage, the in situ liquation primarily featured the crystallization of olivines and pyroxenes. In the late stage, it was characterized by significant exsolution of metal sulfides like pyrrhotite, pentlandite, and minor chalcopyrite. These sulfides initially occurred as droplets. In fertile magmas, numerous sulfide droplets continuously accumulated, fused, and grew while sinking to the bottom, forming sideronitic and densely disseminated ores, and even local massive ores. In contrast, in ore-deficient magmas, sulfide droplets were insufficient for further fusion and growth, finally forming dotted, spotted, and sparsely disseminated ores. For ore magmas, they (possibly entraining minor silicate minerals like olivine) were directly emplaced along faults, forming massive orebodies like the No. 7 pluton. Besides, minor quantities of hornblendes and phlogopites were formed in this stage. With the crystallization of various minerals, the volatile content in magmas increased. In this case, the previously formed lithogenetic minerals experienced autometamorphism such as serpentine and talc alterations.

Ore magma-related mineralization stage. In this stage, the ore magmas formed by deep liquation penetrated into the previously formed plutons and orebodies, leading to the formation of dense massive ores. Consequently, chalcopyrite-rich massive ores possibly occurred at this stage.

(ii) Late hydrothermal mineralization phase. This phase primarily witnessed the formation of tremolites, talcs, and serpentines, along with minor metal sulfides like chalcopyrite and pyrrhotite.

(iii) Supergene oxidation phase. In this phase, primary orebodies were oxidized and leached, forming minerals like annabergite and malachite.

4.5. Resources of the Hongqiling deposit

As of the end of 2018, the Hongqiling deposit had proven

Ni reserves of 22.01×10^4 t, proven associated Cu reserves of 2.47×10^4 t, and proven associated Co reserves of 0.53×10^4 t, with average Ni, Cu, and Co grades of 1.13%, 0.20%, and 0.034%, respectively. Additionally, associated Se, Te, and S are also found in the deposit (Jilin Institute of Geological Survey, 2023). Statistics show that the proven Ni reserves in the Hongqiling deposit ranks 10th among China's magmatic nickel deposits on the premise that average Ni grade is ignored (Table 5; Sun T et al., 2019). The No. 7 pluton (the Fujia nickel deposit; Ni content: 16.03 ×10^4 t; Sun T et al., 2019) is identified as the predominant contributor to the Ni reserves of the Hongqiling deposit. This pluton has an average Ni grade of 1.974%, ranking top among large and above magmatic nickel deposits of China (Sun T et al., 2019).

5. Discussion

5.1. Diagenetic and metallogenic epochs

The diagenetic and metallogenic epochs of the Hongqiling deposit were initially considered the Hercynian. The Geology and Mineral Exploration and Development Bureau of Jilin Province (1988) conducted K-Ar dating on the pyroxenes in pegmatites and gabbros of the No. 1 pluton in the Hongqiling deposit, determining diagenetic ages ranging from 331 to 350 Ma. Qin K (1995) reported that the pyroxenes in the Nos. 1 and 7 plutons of the Hongqiling deposit have K-Ar isotope ages between 330 Ma and 355 Ma. These results limit the formation epoch of ore-bearing mafic-ultramafic plutons in the Hongqiling deposit to the Hercynian.

Table 4. Mineralization phases and stages of the Hongqiling deposit (after Xu ZH, 2020).

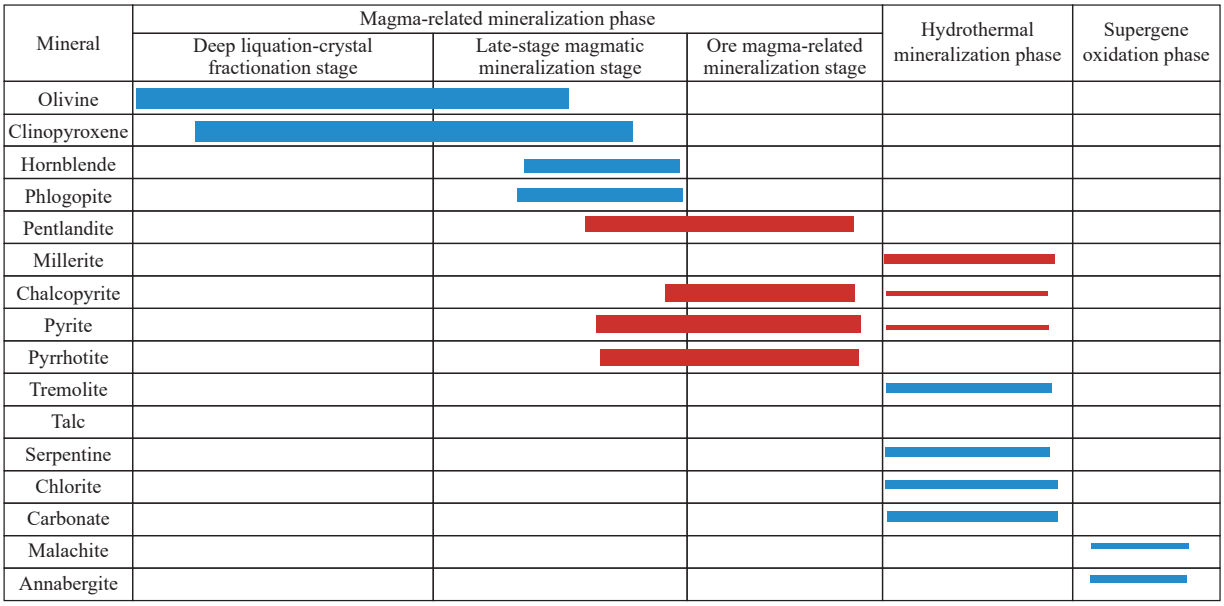

Table 5. Profile of major magmatic nickel deposits in China.

Rank	Deposit	Province	Metal content /10^4 t	Average Ni grade/%	Scale	Data source	Comments
1	Jinchuan	Gansu	552.60	0.72	Supergiant	Sun T et al., 2019	
2	Xiarihamu	Qinghai	110.40	0.66	Supergiant	The Fifth Geological Exploration Institute of Qinghai Province, 2014; Sun T et al., 2019	
3	Poyi	Xinjiang	92.79	0.5	Supergiant	The Sixth Geological Team of the Bureau of Geology and Mineral Resources of Xinjiang Uygur Autonomous Region, 2012; Sun T et al., 2019	
4	Huangshandong	Xinjiang	38.36	0.52	Large	Sun T et al., 2019	
5	Yangliuping	Sichuan	36.80	0.44	Large	Sun T et al., 2019; Liang et al., 2023	
6	Jianchaling	Shaanxi	34.29	0.626	Large	Sun T et al., 2019	
7	Huangshan (west)	Xinjiang	32.7	0.48	Large	Sun T et al., 2019	
8	Zhouan	Henan	32.43	0.34	Large	Zhou Q and Gao S, 2008; Sun T et al., 2019	
9	Karatungk	Xinjiang	26.68	0.65	Large	Sun T et al., 2019; Wang et al., 2022	Metal quantity as of the end of 2012
10	Hongqiling	Jilin	22.01	1.974 (No. 7) 0.53 (No. 1)	Large	Sun T et al., 2019	

Since the start of the 21st century, with the advancement in isotopic dating technology, researchers have investigated the isotope chronology of the mafic-ultramafic plutons in the Hongqiling deposit using Ar-Ar dating, as well as LA-ICP-MS and SHRIMP zircon U-Pb dating, for monominerals like hornblende and biotite (Fig. 12; Table 5). Zhang GL and Wu FY (2005) reported that the leucogabbros in the No. 1 pluton have a SHRIMP zircon U-Pb age of 216±5 Ma. Using the Ar-Ar dating of biotite and hornblende, Xi AH et al. (2006) determined that the Nos. 1 and 8 plutons have crystallization ages of 225 Ma and 250 Ma, respectively. Liu JY et al. (2010) conducted Ar-Ar dating on hornblendes in hornblende pyroxenites of the No. 3 pluton, yielding a crystallization age of 228±3 Ma. It was successively reported that the Nos. 1, 2, 3, 8, and 31 plutons in the Hongqiling deposit have diagenetic ages ranging from 207 Ma to 238 Ma (Feng GY et al., 2011; Hao LB et al., 2012; Wei QQ, 2015). Additionally, some researchers conducted detrital zircon U-Pb dating for the Hulan Group metamorphic sedimentary rocks —the surrounding rocks of the mafic-ultramafic plutons, determining the youngest detrital zircon ages of 272.2±4.3 Ma and 287±6 Ma (Wu FY et al., 2007; Lv LS et al., 2011). These findings suggest that these mafic-ultramafic plutons were emplaced later than the Middle-Late Permian. The above isotopic dating data indicate that the ore-bearing mafic-ultramafic plutons in the Hongqiling deposit were largely formed during the Indosinian (208–239 Ma). To determine the accurate diagenetic epoch of the Hongqiling deposit, researchers conducted Re-Os isotopic dating on the Nos. 1 and 7 plutons, successively reporting isochron ages of 208±21 Ma (Lv LS et al., 2011), 222.9±9.1 Ma (Han CM et al., 2014), and 237±16 Ma (Hao LB et al., 2014). These ages align with the abovementioned diagenetic ages of the ore-bearing mafic-ultramafic plutons, implying that the Indosinian is the predominant diagenetic and metallogenic epoch of the Hongqiling deposit. Besides, the available isotopic dating data show that the emplacement of mafic-ultramafic plutons in the Hongqiling deposit also occurred during the Late Hercynian (258–272 Ma) (Wei QQ, 2015), devoid of significant mineralization.

On the northern margin of the North China Plate, besides the Hongqiling deposit, its adjacent areas host medium-sized Changren copper-nickel deposit and some small-scale copper-nickel deposits or ore occurrences like Chajianling, Piaohechuan, Shanmen, Sandaogang, and Erdaogou (Fig. 1). These deposits are primarily distributed along the giant fault zone on the northern margin of the North China Plate. Available isotopic dating data indicate that the mafic-ultramafic plutons related to these copper-nickel sulfide deposits were emplaced at 213–243 Ma (Fig. 13; Wu FY et al., 2004; Xie HQ et al., 2007; Wang ZG et al., 2011; Wang ZG, 2012; Hao LB et al., 2013; Wu Q et al., 2019; Xue HR, 2020; Zhang LS, 2022), aligning with the diagenetic and metallogenic epoch of the Hongqiling deposit. Hence, the northern margin of the North China Plate underwent significant Indosinian magmatic Cu-Ni mineralization, with its east and west sides governed by the Huifahe and Gudonghe deep-seated faults, respectively.

5.2. Diagenesis

5.2.1. Magma sources

The primary ore-bearing plutons within the Hongqiling deposit include the Nos. 1, 2, 3, 7, and 9 plutons in rock belt I. The geochemical testing data of trace elements, rare earth elements (REE), and similar platinum-group elements (PGEs) reveals that rocks of various lithologies in the ore-bearing plutons within the deposit exhibit almost the same REE and trace element patterns (Fig. 13) and similar PGE characteristics (Dong GZ et al., 2012; Li A et al., 2019). These findings suggest the consanguinity of the magma sources of primary ore-bearing mafic-ultramafic plutons within the Hongqiling deposit (Dong GZ et al., 2012; Li A et al., 2018) and that rocks of various lithologies are the products of comagmatic evolution (Xi AH et al., 2002; Li A et al., 2018).

It has been roughly recognized that the primitive magmas of major ore-bearing mafic-ultramafic plutons within the Hongqiling deposit originated principally from the upper

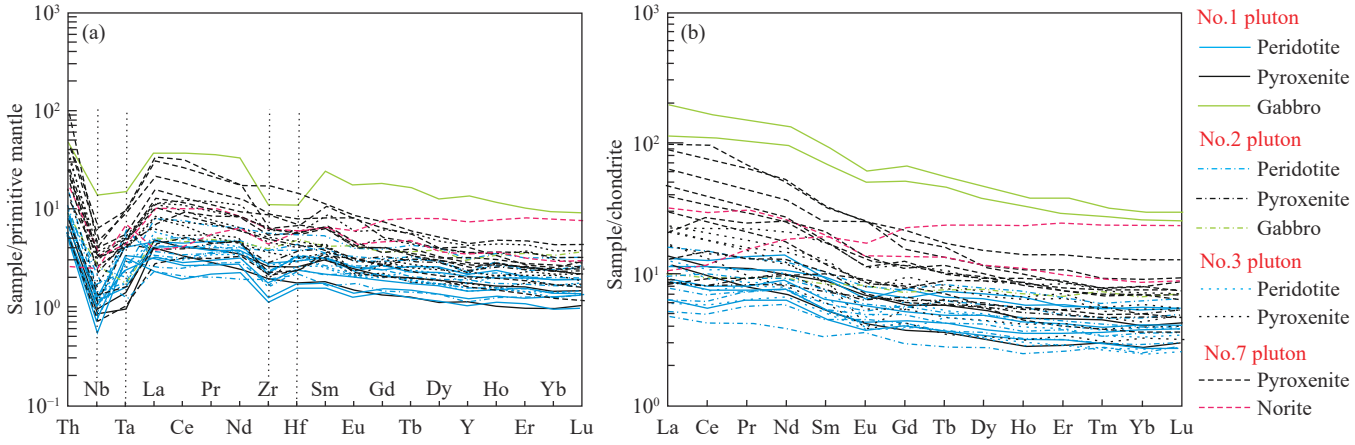

Fig. 13. Primitive mantle-normalized diagram of trace elements (a) and chondrite-normalized diagram of rare earth elements (b) for mafic-ultramafic rocks from the Nos. 1, 2, 3, and 7 plutons of the Hongqiling deposit (sample data from Li A, 2019).

Table 6. Chronological data of mafic-ultramafic rocks and ores within the Hongqiling deposit and its adjacent areas.

Deposit	Rocks/minerals for dating	Dating method	Age/Ma	Data sources
Hongqiling	Biotite in the No. 1 pluton	^{40}Ar-^{39}Ar	225±0.9	Xi AH et al., 2006
	Gabbro in the No. 1 pluton	SHRIMP U-Pb	216±5	Wu FY et al., 2004
	Disseminated ores in the No. 1 pluton	Re-Os	237±16	Hao LB et al., 2014
	Sulfides in the No. 1 pluton	Re-Os	222.9±9.1	Han CM et al., 2014
	No. 2 pluton	^{40}Ar-^{39}Ar	237.7±2.2	Wei QQ, 2015
	Gabbro and diorite pegmatite in the No. 2 pluton	SHRIMP U-Pb	212.5–212.2	Hao LB et al., 2012
	Disseminated ores in the No. 2 pluton	Re-Os	215±24	Hao LB et al., 2014
	No. 3 pluton	^{40}Ar-^{39}Ar	236.4±4.6	Wei QQ, 2015
	No. 3 pluton	LA-ICP-MS U-Pb	220.6±2	Feng GY et al., 2011
	Hornblende in the No. 3 pluton	^{40}Ar-^{39}Ar	228–230	Liu JY et al., 2010
	Gabbro in the No. 5 pluton	SHRIMP U-Pb	272.2±3.6	Wei QQ, 2015
	Gabbro in the No. 6 pluton	SHRIMP U-Pb	258.8±3.4	Wei QQ, 2015
	Diorite in the No. 8 pluton	LA-ICP-MS U-Pb	238.1±2.7	Wei QQ, 2015
	Hornblende in the No. 8 pluton	^{40}Ar-^{39}Ar	250.8±0.25	Xi AH et al., 2006
	Sulfides in the No. 7 pluton	Re-Os	208±21	Lv LS et al., 2011
	No. 31 pluton	LA-ICP-MS U-Pb	218.1±3.5	Wei QQ, 2015
Chajianling	Hornblende in the No. 1 pluton	^{40}Ar-^{39}Ar	231.2±2.6	Wei QQ, 2015
	Gabbro in the No. 1 pluton	SHRIMP U-Pb	239.6±2.6	Hao LB et al., 2013
Sandaogang	Gabbro	LA-ICP-MS U-Pb	232.75±0.95	Wang ZG et al., 2011
Piaohechuan	Gabbro in the No. 4 pluton	SHRIMP U-Pb	217±3	Wu FY et al., 2004
	Gabbro in the No. 5 pluton	SHRIMP U-Pb	222±8	Xie HQ et al., 2007
Shanmen	Gabbro	LA-ICP-MS U-Pb	225.1	Xi AH et al., 2008
Erdaogou	Hornblende gabbro in the No. 115 pluton	LA-ICP-MS U-Pb	213.0±1.1	Zhang LS, 2022
Shirengou	Gabbro	LA-ICP-MS U-Pb	225.6±7	Xue HR, 2020
Changren	Peridotite	LA-ICP-MS U-Pb	243.0±1.1	Xue HR, 2020
	Olivine pyroxenolite	LA-ICP-MS U-Pb	226±1	Wu Q et al., 2019
Zhangxiang	Peridotite	LA-ICP-MS U-Pb	237.0±1.1	Xue HR, 2020

mantle (Wu FY et al., 2004; Feng GY et al., 2011; Lv LS et al., 2012; Wei B et al., 2013; Wei QQ, 2015; Li A, 2019; Zhang LS, 2022). However, due to varying interpretations of the geochemical characteristics of these plutons, the magma sources remains controversial, such as the asthenospheric or lithospheric mantle and the enriched or depleted mantle.

The pyroxenite and leucogabbro samples from the No. 1 pluton and the orthopyroxenite samples from the No. 7 pluton yielded low initial $^{87}Sr/^{86}Sr$ ratios (0.703 to 0.705) and positive $\varepsilon Nd(t)$ values (+0.2 to +4.3), suggesting the enrichment in large-ion lithophile elements (LILEs) and depletion in high field strength elements (HFSEs) like Nb and Ta of the trace elements. Given that the La/Yb and Th/Ta ratios of these samples were significantly higher than those of mid-ocean ridge basalts (MORBs), Wu FY et al. (2004) proposed that the magma sources of the mafic-ultramafic plutons in the Hongqiling deposit were the juvenile lithospheric mantle, undergoing somewhat enrichment of incompatible elements and the contamination by trace quantities of crustal materials. This view is highly consistent with previous geochemical findings on the major and trace elements, Sr-Nd isotopes, and zircon Lu-Hf isotopes of olivine pyroxenites in the No. 1 pluton (Feng GY et al., 2011). Based on the analysis of mixing between two end-members, as well as the relatively high and uniform $\varepsilon Hf(t)$ values of zircons (+9.6 – +14.4), Feng GY et al. (2011) further inferred that the parental magmas of mafic-ultramafic rocks in the Hongqiling deposit experienced no significant contamination by crustal materials, suggesting a relatively simple source of primitive parental magmas. Besides, they held that the enrichment in LILEs like Rb and Sr and depletion in HFSEs like Nb, Ta, Zr, and Ti of ultramafic rocks in the Hongqiling deposit are associated with the metasomatism of fluids in the source area.

Based on the aforementioned results and given that the Nb/Zr and Nb/La ratios of the regional Indosinian mafic-ultramafic rock samples were very close to those of enriched MORBs (E-MORBs), Wei QQ (2015) proposed that the samples were characteristic of the depleted asthenospheric mantle. Moreover, she posited that the primitive magmas of the regional Indosinian mafic-ultramafic rocks were largely derived from the lithospheric mantle metasomatized by subduction fluids, mixed with asthenospheric mantle materials.

However, Li A (2019) determined a high temperature of parental magmas in the Hongqiling area, reaching up to 1400°C, ruling out the possibility of magma origin from the lithospheric mantle. Instead, she posited that the magmas were derived from the depleted asthenospheric mantle based on the positive $\varepsilon Nd(t)$ values (1.63 to 10.34) of mafic-ultramafic rocks in the Hongqiling area. From the perspective of mineralization, Zhang LS (2022) also considered that the magmas of mafic-ultramafic rocks in the Hongqiling area were more likely derived from the asthenospheric mantle,

probably mixed with trace quantities of lithospheric mantle materials. The reason is that the primitive magmas originating predominantly from the asthenospheric mantle feature high melting ratios. Consequently, these magmas are more prone to form primitive magmas rich in metal elements but unsaturated with S, creating favorable conditions for the formation of large copper-nickel deposits.

5.2.2. Magmatic evolutionary process

The structure and composition of lithogenetic minerals in igneous rocks keep a record of the entire magmatic evolutionary process in magma chambers (involving crystal fractionation, crustal contamination, and magma mixing; Lv LS et al., 2012). Based on the petrological, mineralogical, and mineral chemical characteristics of dominant ore-bearing mafic-ultramafic rocks in the Hongqiling deposit, previous researchers explored the magmatic evolutionary process of dominant ore-bearing plutons in the deposit.

(i) Fractional crystallization

Field observations reveal that the Nos. 1 and 7 plutons in the Hongqiling deposit exhibit significant lithofacies zoning and high differentiation degrees, with rocks' maficity degree gradually decreasing from bottom to top or from the center to edges. The No. 1 pluton features peridotite or pyroxene peridotite facies, pyroxenite facies, and gabbro facies. In contrast, the No. 7 pluton exhibits peridotite, pyroxenite, and norite facies. In both plutons, various lithofacies display gradual transition, indicating that the rocks underwent varying crystal accumulation processes during their formation and are thus supposed to be the product of in situ fractional crystallization (Lv LS et al., 2012).

For the mineralogy of ore-bearing mafic-ultramafic plutons in the Hongqiling deposit, the contents and grain sizes of their lithogenetic minerals gradually transition. Poikilitic and interstitial textures are extensive in these plutons. Specifically, spinels are enclosed by olivines, pyroxenes, or hornblendes, while olivines are enclosed by orthopyroxenes or clinopyroxenes. Furthermore, olivines, early cumulate minerals, exhibit a roughly directional arrangement, with clinopyroxenes filled in the interstices among olivine minerals. These characteristics indicate that significant fractional crystallization occurred during the magmatic evolution of these plutons. Moreover, in these plutons, spinels and olivines crystallized earlier, followed by minerals like orthopyroxenes, clinopyroxene, and feldspar (Lv LS et al., 2012; Li A, 2019).

Additionally, whole-rock geochemical characteristics also reflect the significant fractional crystallization of ore-bearing rocks in the Hongqiling area. For the ore-bearing rocks in the Hongqiling deposit, there is a positive correlation between whole-rock FeOT and MgO contents, suggesting the fractional crystallization of olivines and orthopyroxenes (Feng GY et al., 2011). The weakly or moderately negative europium (Eu) anomalies (average δEu value: 0.88) suggest the fractional crystallization of plagioclases (Li A, 2019). The Si/Ti *vs.* (Mg+Fe)/Ti diagram (Fig. 14a) indicates that the dominant ore-bearing rocks in the Hongqiling deposit experienced the fractional crystallization of olivines and pyroxenes (Stanley CR et al., 1989).

Overall, the ore-bearing mafic-ultramafic plutons in the Hongqiling deposit experienced significant fractional crystallization during their magmatic evolution. The primary lithogenetic minerals crystallized in the sequential order of olivines, orthopyroxenes, clinopyroxenes, plagioclases, hornblendes, and biotites (Lv LS et al., 2012).

(ii) Crustal contamination

Crustal contamination played a significant role in S supersaturation during the formation of a typical magmatic copper-nickel sulfide deposit (Naldrett AJ, 2010; Xue SC et al., 2022; Ripley EM and Li C, 2013). For the ore-bearing ultramafic rocks in the Nos. 1 and 7 plutons, primary lithogenetic minerals include olivines, orthopyroxenes, clinopyroxenes, hornblendes, plagioclases, and biotites. The presence of orthopyroxenes, alongside olivines with reaction rims of orthopyroxenes, indicates that supersaturated SiO_2 might arise from crustal contamination. Additionally, the chemical analysis results of the primary lithogenetic minerals indicate that the same lithogenetic minerals like clinopyroxenes, hornblendes, and plagioclases in various lithofacies of both plutons exhibit significant or minimal

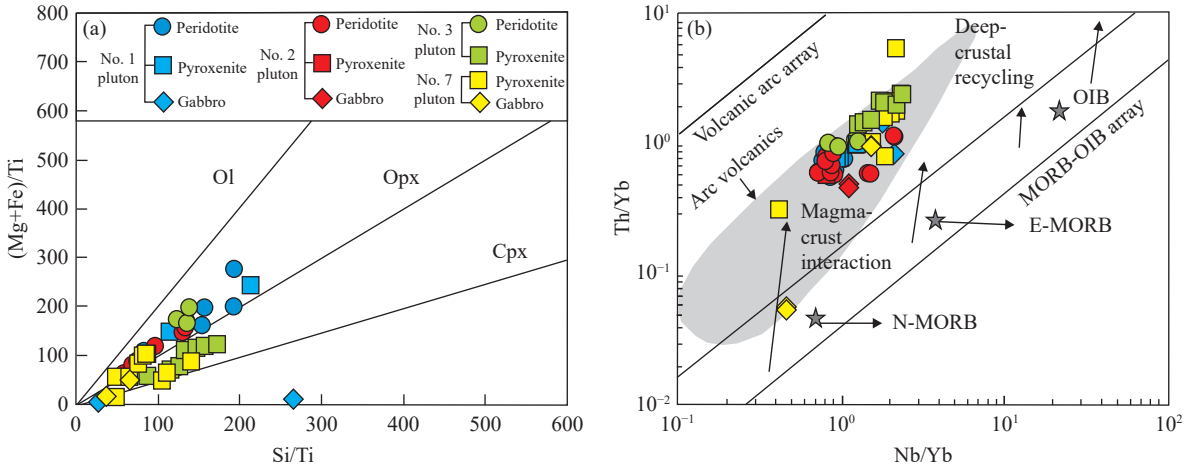

Fig. 14. Si/Ti *vs.* (Mg+Fe)/Ti and Nb/Yb *vs.* Th/Yb diagrams of predominant ore-bearing rocks in the Hongqiling deposit (after Li A, 2019).

differences in chemical compositions. This phenomenon is potentially associated with the mixing of crustal-derived materials to varying degrees (Lv LS, 2012).

The geochemical characteristics of trace elements in the mafic-ultramafic rocks of the Hongqiling deposit also reveal the occurrence of crustal contamination during the magmatic evolution. Typically, the mantle exhibits an average Ce/Pb ratio of 25±5, while the crust has an average Ce/Pb ratio below 15 (Hofmann AW, 1986). The Ce and Pb elements show similar partition coefficients, and the Ce/Pb ratio will not change with partial melting and magmatic differentiation (Li A, 2019). For the ore-bearing mafic-ultramafic plutons in the Hongqiling deposit, various rocks exhibit Ce/Pb ratios ranging from 0.59 to 5.82, with an average of 3.30, which is lower than that of the mantle but closer to that of the crust (Hofmann AW, 1986). This result is consistent with the illustration of the Nb/Yb *vs.* Th/Yb diagram (Fig. 14b), where the mafic-ultramafic rock samples from the Hongqiling deposit fell into the crust-mantle interaction zone. Besides, the $(^{187}Os/^{188}Os)_i$ ratios of these samples fell between those of the mantle and crust (detailed below), demonstrating that the ore-bearing plutons in the Hongqiling deposit underwent somewhat crustal contamination. This aligns with the enrichment in light rare earth elements (LREEs) and depletion in HFSEs (like Nb and Ta) of the mafic-ultramafic rocks in the Nos. 1 and 7 plutons, suggesting mafic-ultramafic magmas might have been mixed with crustal materials during their ascent and emplacement (Wei QQ, 2015).

The ultramafic rocks in the Hongqiling deposit exhibit relatively low $(^{87}Sr/^{86}Sr)_i$ ratios (0.70394 to 0.70408), positive $\varepsilon_{Nd}(t)$ values (3.5 to 4.0), and positive $\varepsilon_{Hf}(t)$ values (9.6 to 14.4), suggesting insignificant crustal contamination during the magmatic evolution (Feng GY, 2011). Based on the Sr-Nd isotopes, Wu FY et al. (2004) conducted crustal contamination simulations using the upper continental crust- and upper mantle-derived basalts as end members, revealing that Nos. 1 and 7 plutons featured 5%–7% crustal contamination. However, Feng GY et al. (2011) examined the degree of contamination by continental crust materials through the analysis of mixing between two end-members, concluding that the diagenetic process involved no upper crustal materials and minimal lower crustal contamination (1%–2%). Wei B (2013) posited that mantle-derived magmas of the No. 7 pluton in the Hongqiling deposited experienced 10–30 wt.% contamination of A-type granitic magmas in the deep part and approximately 5% upper crustal contamination in the shallow crust.

Overall, the predominant ore-bearing mafic-ultramafic rocks in the Hongqiling deposit experienced different degrees of crustal contamination during the diagenetic process. However, the origin of crustal materials and the contamination degree remain controversial.

5.2.3. Metasomatism by subduction fluids from the Paleo-Asian Ocean

Extensive studies indicate that metasomatism by subduction fluids plays a significant role in the formation of ore-bearing mafic-ultramafic rocks in the Hongqiling deposit (Xi AH et al., 2006; Feng GY et al., 2011; Wei QQ, 2015; Li A et al., 2018; Li A, 2019). Through microscopic observations, Li A (2019) revealed the presence of primary hornblendes in the ore-bearing plutons of the Hongqiling deposit. This finding suggests that the primitive magmas in the deposit contained water, implying that the magma sources experienced fluid metasomatism. The olivine samples from ore-bearing mafic-ultramafic rocks in the Hongqiling deposit yielded Ca content of less than 1000×10^{-6} (Li A, 2019), coinciding with the presence of low-Ca olivines within island-arc basalts and relevant mafic-ultramafic rocks (Li CS and Ripley EM, 2012). Additionally, the relative enrichment in LILEs (like Rb and Sr) and depletion in HFSEs (like Nb, Ta, Zr, and Ti) of the ore-bearing rocks in the deposit indicate that the magma sources experienced significant metasomatism by subduction fluids (Xi AH, et al., 2006; Feng GY, et al., 2011; Wei QQ, 2015). The influence of fluids or sediments on a magma source can be determined using changes in the Ba/La, Th/HREE, and LREE/HREE ratios (Woodhead et al., 2001). The Ba/La *vs.* Th/Yb diagram (Fig. 15a) shows significant changes in the Ba/La ratio, suggesting that the magma sources were influenced by subduction fluids. As illustrated in the Th/Zr *vs.* Nb/Zr diagram (Fig. 15b), the samples exhibited a trend of metasomatism by fluid subduction. All these pieces of evidence suggest that the magma sources of the ore-bearing mafic-ultramafic rocks in the Hongqiling deposit were subjected to metasomatism by subduction fluids.

During the Paleozoic, the east-central portion of Jilin Province, where the Hongqiling deposit is situated, experienced the evolution of the Paleo-Asian Ocean tectonic domain. During the Late Paleozoic, characterized by the subduction of the Paleo-Asian Ocean, this region underwent "accordion tectonics" characterized by extension alternating with compression (Wei QQ, 2015; Zhao Y et al., 2017). During the subduction of the oceanic crust, materials in the subducting slab dehydrated and released fluids as the temperature and pressure in the subduction zone increased. Then, the fluids ascended, transforming the magma sources of the ore-bearing mafic-ultramafic rocks in the Hongqiling deposit (Feng GY et al., 2011; Wei QQ, 2015). Studies have indicated that fluids rich in volatiles such as water promoted the intense differentiation of ore-forming plutons, while mantle-derived components that preserve the metasomatism by subduction fluids might have expedited the migration of ore-forming minerals (Wei QQ, 2015). Therefore, the metasomatism by the subduction fluids from the Paleo-Asian Ocean possibly played a significant role in the formation of the Hongqiling deposit.

5.3. Mineralization

5.3.1. Source of ore-forming materials

Extensive sulfur isotope analyses have been conducted for sulfides in the primary Nos. 1, 3, and 7 ore-bearing plutons of the Hongqiling deposit (Table 7). The results indicate that the sulfides in plutons Nos. 1, 3, and 7 exhibit $\delta^{34}S$ values ranging from −1.83‰ to +0.9‰, from −1.4‰ to −0.7‰, and from

−4.7‰ to +2.13‰ (primarily between −2.8‰ and +2.13‰), respectively. Overall, the $\delta^{34}S$ values of various ore-bearing plutons vary in similar ranges, mostly around zero, approaching those of mantle-derived S (0±2‰; Ripley EM and Li C, 2013). This result suggests that the sulfur in the Hongqiling deposit might originate from the upper mantle and undergo weak fractionation (Zhao ZH et al., 2023; Liang SS etal., 2024; Chen J et al., 2024; Zhang S et al., 2023). For the No. 1 pluton, the surrounding rocks and contaminated rocks within the external contact zone exhibit $\delta^{34}S$ values ranging from −8.4‰ to −3.9‰ (Chen MY, 1979), significantly lower than those of the mafic-ultramafic rocks (ores) within the Nos. 1 and 3 plutons. This result suggests relatively low crustal S effects on the Nos. 1 and 3 plutons, and thus the magmas might have been saturated with S probably attributed to their own evolution (Li Ai, 2019). For the No. 7 pluton, some pyrite exhibits lower $\delta^{34}S$ values, varying between −4.7‰ and −1.9‰, closer to those of its surrounding rocks and contaminated rocks within its external contact zone. This finding implies that the No. 7 pluton experienced slight contamination by crustal materials during its magmatic evolution. Additionally, the S isotopic composition of sulfides in the No. 1 pluton exhibits $\delta^{34}S_{Po}$ (average: −0.63‰) > $\delta^{34}S_{Pn}$ (average: −0.65‰), and that of sulfides in the No. 7 pluton also shows $\delta^{34}S_{Po}$ (average: 0.278) > $\delta^{34}S_{Pn}$ (average: 0.013) > $\delta^{34}S_{Py}$ (average: −0.988). This result demonstrates

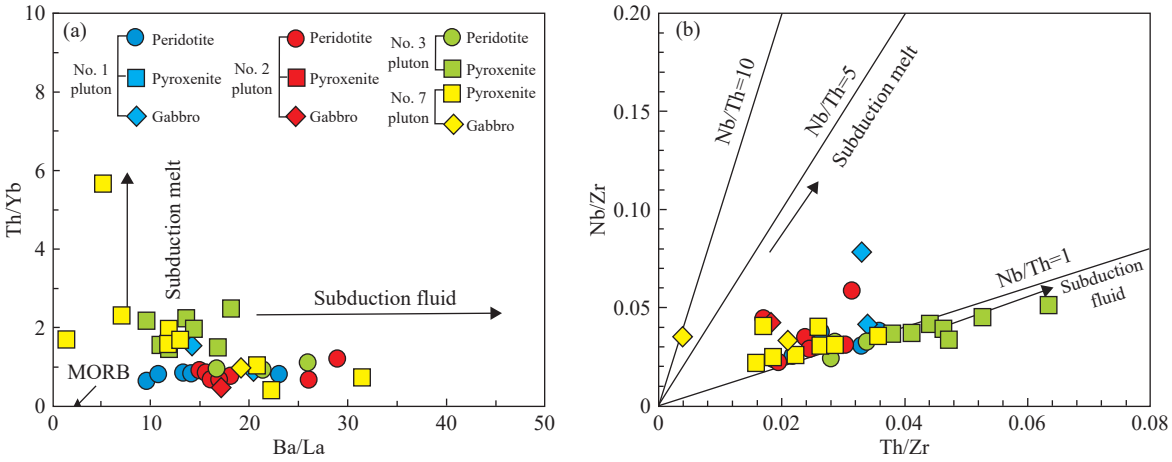

Fig. 15. Ba/La *vs.* Th/Yb (a) and Th/Zr *vs.* Nb/Zr (b) diagrams of mafic-ultramafic plutons in the Hongqiling deposit (base maps after Hanyu T et al., 2013 and Woodhead JD et al., 2001, respectively; sample data from Li A, 2019).

Table 7. Sulfur isotopic compositions of sulfides in the Hongqiling deposit.

Pluton	No.	Mineral	$\delta^{34}S$/‰	Data source	Pluton	No.	Mineral	$\delta^{34}S$/‰	Data source
No. 1 pluton	1	Pyrrhotite	−0.7	Li A, 2019	No. 7 pluton	13	Pyrrhotite	−1.9	Lv LS et al., 2017
	2	Pyrrhotite	0.21	Li A, 2019		14	Pyrrhotite	1.79	Xi AH, 2002
	3	Pyrrhotite	−1.83	Li A, 2019		15	Pyrrhotite	2.13	Xi AH, 2002
	4	Pyrrhotite	−0.2	Li A, 2019		16	Chalcopyrite	−0.11	Li A, 2019
	5	Pentlandite	−0.66	Li A, 2019		17	Pyrite	0.54	Han et al., 2014
	6	Pentlandite	−0.47	Li A, 2019		18	Pyrite	0.39	Han et al., 2014
	7	Chalcopyrite	0.9	Sun LJ, 2013		19	Pyrite	−0.31	Han et al., 2014
	8	Pentlandite	−1.2	Sun LJ, 2013		20	Pyrite	−0.01	Han et al., 2014
	9	Pentlandite	−0.6	Sun LJ, 2013		21	Pyrite	0.29	Han et al., 2014
	10	Pentlandite	−0.3	Sun LJ, 2013		22	Pyrite	0.43	Han et al., 2014
No. 3 pluton	1	Pentlandite	−0.7	Sun LJ, 2013		23	Pyrite	0.41	Han et al., 2014
	2	Pentlandite	−1.4	Sun LJ, 2013		24	Pyrite	−4.3	Lv LS et al., 2017
No. 7 pluton	1	Pentlandite	0.3	Li A, 2019		25	Pyrite	−4.4	Lv LS et al., 2017
	2	Pentlandite	0.18	Li A, 2019		26	Pyrite	−4.7	Lv LS et al., 2017
	3	Pentlandite	0.52	Li A, 2019		27	Pyrite	−1.9	Lv LS et al., 2017
	4	Pentlandite	−0.21	Li A, 2019		28	Pyrite	−2.8	Liu M, 2005
	5	Pentlandite	−0.7	Li A, 2019		29	Pyrite	2.13	Liu M, 2005
	6	Pyrrhotite	0.11	Li A, 2019		30	Pyrite	1.94	Liu M, 2005
	7	Pyrrhotite	0.06	Li A, 2019		31	Pyrite	−2.53	Xi AH, 2002
	8	Pyrrhotite	0.07	Li A, 2019		32	Pentlandite	−0.2	Sun LJ, 2013
	9	Pyrrhotite	−0.2	Li A, 2019		33	Pentlandite	0.2	Sun LJ, 2013
	10	Pyrrhotite	0.06	Li A, 2019		34	Chalcopyrite	−2.2	Sun LJ, 2013
	11	Pyrrhotite	0.13	Li A, 2019		35	Chalcopyrite	−0.5	Sun LJ, 2013
	12	Pyrrhotite	0.53	Li A, 2019		36	Chalcopyrite	−1.3	Sun LJ, 2013

that the S in the ore-forming melts of the Hongqiling deposit has reached equilibrium.

The Re-Os isotopic system serves as both a powerful tracer for the formation of sulfide deposits and a highly sensitive indicator for the mixing degree of crustal materials during mineralization (Lambert et al., 1999). In recent years, researchers have conducted Re-Os isotope analyses on ores and metal sulfides in the Nos. 1, 2, and 7 plutons of the Hongqiling deposit (Table 8). Available data indicate that the disseminated ores of the No. 1 pluton exhibit Re and Os contents ranging from 0.634×10^{-9} to 22.632×10^{-9} and from 0.029×10^{-9} to 2.581×10^{-9}, respectively. In contrast, the disseminated ores of the No. 2 pluton manifest Re and Os contents ranging from 0.31×10^{-9} to 5.102×10^{-9} and from 0.004×10^{-9} to 0.556×10^{-9}, respectively. For the No. 7 pluton, the Re content varies significantly across various ores or

Table 8. Re-Os isotopic composition of molybdenite in the Hongqiling deposit.

Pluton	Sample No.	Sample type	Re/10^{-9}	Os/10^{-9}	$^{187}Re/^{188}Os$	2σ	$^{187}Os/^{188}Os$	2σ	$(^{187}Os/^{188}Os)i$	γOs(t)	Age/Ma	Data source
No. 7	HQ-55	Sulfide-deficient orthopyroxenite	2.55	0.23	55.6474	0.1251	0.4556	0.0012	0.255	103	216	Wei B et al., 2013
	HQ-58		1.03	0.18	28.7668	0.0672	0.3384	0.0017	0.2347	87		
	HQ-59	Disseminated ore	6.22	0.67	46.5505	0.0747	0.4418	0.0012	0.274	118		
	HQ-69		6.64	0.24	145.4041	0.1742	0.8075	0.0023	0.2833	126		
	HQ-63	Stockwork ore	77.79	1.05	435.7394	0.7863	1.8441	0.0045	0.2733	118		
	HQ-64		84.67	4.61	93.5673	1.0404	0.5693	0.0064	0.232	85		
	HQ-65		12.72	0.53	123.5128	0.8086	0.6338	0.0065	0.1885	50		
	HQ-67		15.47	0.61	131.9452	0.6052	0.7352	0.0024	0.2595	107		
	HQ-71		40.85	5.56	36.7902	0.05	0.4356	0.0186	0.3029	141		
	HQ-74	Massive ore	122.8	5.65	112.9183	0.733	0.7359	0.0044	0.3289	162		
	HQ-75		138.68	7.25	99.2135	0.2536	0.7184	0.0016	0.3607	187		
	HQ-78		76.69	2.82	143.4702	0.4063	0.8675	0.0064	0.3502	179		
	HK7-01	Massive ore Pyrrhotite	80.66	2.643	146	2.1	0.8048	0.0195	0.2982	137	208±21	Lv LS et al., 2011
	HK7-04		118.7	3.839	147.9	1.8	0.8416	0.0103	0.3282	161		
	HK7-17		166.5	6.268	127	1.5	0.7592	0.0072	0.3181	153		
	HK7-29		81.84	1.855	210.9	2.4	1.0463	0.0119	0.314	150		
	HK7-47		178.6	7.82	109.2	1.4	0.6895	0.0067	0.3104	147		
	HK7-53		167.3	6.721	119	1.4	0.7331	0.0111	0.3198	155		
No. 1	HQ01-1	Disseminated ore	1.804	0.029	350.26	4.5978	1.5723	0.0091	0.215±0.043	146.6	237±16	Hao LB et al., 2014
	HQ01-2		3.741	0.069	306.94	3.9248	1.4277	0.0048		155.8		
	HQ01-3		0.634	0.015	227.63	1.6934	1.1255	0.0063		142.8		
	HQ01-4		0.697	0.018	214.16	2.1096	1.0393	0.0085		112.8		
	HQ01-5		1.123	0.039	151.46	1.6721	0.806	0.0055		107		
	HQ01-6		7.062	0.367	98.8	2.236	0.6358	0.0008		122.7		
	HQ01-7		22.632	2.581	43.55	3.5917	0.3673	0.0015		67.5		
	HQ01-8		6.835	0.245	146.39	1.4959	0.8089	0.0018		123.9		
No. 2	HQ02-1	Disseminated ore	5.102	0.556	46.15	0.7955	0.4644	0.0013	0.302±0.089	139.8	215±24	
	HQ02-2		4.313	0.196	114.38	1.1415	0.7316	0.0029		160.3		
	HQ02-3		0.56	0.012	261.95	1.5636	1.2956	0.0065		193.6		
	HQ02-4		0.407	0.004	744.82	5.3844	3.0208	0.0226		206.9		
	HQ02-5		0.31	0.004	410.43	3.3066	1.7208	0.0148		113.9		
	HQ02-6		0.561	0.017	180.32	1.5175	0.9067	0.0045		113.9		
	HQL-1	Disseminated ore	106.8	3.65	141.3	1.6	0.8179	0.011	0.2921	132.74	222.9±9.1	Han CM et al., 2014
	HQL-2	Massive ore	138.8	6.31	106.2	1.2	0.6942	0.0082	0.299	138.24		
	HQL-3	Massive ore	236.6	13.17	86.75	1.34	0.6223	0.0093	0.2995	138.62		
	HQL-4	Disseminated ore	116.2	4.906	114.4	1.7	0.7151	0.0102	0.2894	130.59		
	HQL-5	Disseminated ore	93.17	2.793	161.2	2.8	0.8751	0.0186	0.2753	119.32		
	HQL-6	Massive ore	131.5	5.569	114.1	3	0.7186	0.0191	0.294	134.26		
	HQL-7	Disseminated ore	113.9	5.319	103.4	2	0.6739	0.0134	0.2892	130.37		
	HQL-8	Massive ore	83.78	2.392	169.2	2	0.9316	0.0088	0.302	140.62		
	HQL-9	Disseminated ore	134.7	5.65	115.1	4.8	0.7073	0.0375	0.279	122.3		
	HQL-10	Massive ore	91.84	2.68	165.5	3.2	0.9200	0.0213	0.3042	142.35		

metal sulfides. Specifically, sulfide-deficient orthopyroxenites exhibit the lowest Re content (1.03×10^{-9} to 2.55×10^{-9}), followed by disseminated ores (6.22×10^{-9} to 6.64×10^{-9}), while stockwork/massive ores and pyrrhotite they contain exhibit the highest Re content (12.72×10^{-9} to 166.5×10^{-9}). The samples from the No. 7 pluton had Os content varying between 0.18×10^{-9} and 7.82×10^{-9}. Additionally, the ores or metal sulfides from the Nos. 1, 2, and 7 plutons present similar $(^{187}Os/^{188}Os)_i$ ratios, which are 0.215±0.043, 0.302±0.089, and 0.1885–0.3607, respectively, suggesting similar sources of Cu-Ni ore-forming materials in various ore-bearing plutons. Overall, the $(^{187}Os/^{188}Os)_i$ ratios of the Hongqiling deposit are slightly higher than those of the Kambalda copper-nickel sulfide deposit with a pure mantle source (0.108±0.00035; Foster JG et al., 1996), and significantly lower than those of the Canadian Sudbury copper-nickel sulfide deposit with a crust source (8.73±0.37; Walker RJ et al., 1991). Therefore, the ore-forming materials of the Hongqiling deposit primarily originated from the mantle, possibly mixed with some crustal materials.

Additionally, γOs(t) is a critical parameter used to discriminate the source of ore-forming materials (Walker RJ et al., 1994). The disseminated ores in the Nos. 1 and 2 plutons of the Hongqiling deposit display γOs(t) values varying from 67.5 to 155.8 (average: 122.4) and from 113.9 to 206.9 (average: 153.7), respectively. Samples from the No. 7 pluton showed significantly varying γOs(t) values, ranging between 50 and 187 (average: 131.4). The γOs(t) values of samples from the three plutons are close to those of the Kevitsa deposit with a mantle source in Finland (130–170), significantly higher than those of the Sakatti deposit with a mixed crust-mantle source in northern Finland (21–56), and lower than those of the Canadian Sudbury deposit dominated by a crust source (430–814; Walker RJ et al., 1991; Sproule RA et al., 1999; Moilanen M et al., 2021). Therefore, the Os in the Hongqiling deposit originated primarily from the mantle, mixed with some crust-derived Os.

In the Hongqiling deposit, pure sulfide veins are frequently paragenetic with quartz and calcite veins. Xi AH (2002) conducted carbon isotope analyses on these calcite veins, obtaining $\delta^{13}C$ values ranging from −8.94‰ to −2.89‰. These values approach those of calcite-bearing mafic-ultramafic rocks of the Jinchuan nickel deposit (−9.0‰ to −2.9‰). It is considered that in the Jinchuan nickel deposit, the surrounding rocks (marbles) and mafic-ultramafic rocks experienced weak chemical mixing near their contact zone (Xue SC et al., 2022). The mafic-ultramafic rocks of the Hongqiling deposit primarily occur in the Hulan Group's Huangyingtun Formation, which is composed predominantly of biotite schists and siliceous banded marbles. Therefore, it can be inferred that the Hongqiling deposit was subjected to carbonate contamination.

As indicated by both S and Re-Os isotopic compositions, the ore-forming materials of the Hongqiling deposit originated predominantly from the mantle, mixed with some crustal materials. Moreover, the Nos. 1, 2, and 7 plutons feature different mixing degrees of crustal materials. Specifically, the No. 7 pluton exhibits a relatively broad S isotopic composition, which is possibly attributed to the mixing of more crustal materials.

5.3.2. Magmatic liquation mineralization

The Hongqiling deposit hosts the pyrrhotite-pentlandite-chalcopyrite paragenetic assemblage, typical of copper-nickel sulfide deposits. The nickel-rich ores in the Fujia deposit, occurring within the No. 7 pluton, exhibit typical liquation textures like ocellar and peritectic textures (Lv LS et al., 2012). This reflects the liquid immiscibility between sulfides and silicates, representing the liquation mineralization of sulfide-rich silicate magmas during their early high-temperature stage. The liquation origin of the Hongqiling deposit is also evidenced by the presence of sideronitic, droplet-shaped, disseminated, and pisolitic ore structures in the deposit. Additionally, the minimum Cu/Pd ratio (238×10^3) of the ores from the Hongqiling deposit is significantly higher than that of the primitive mantle (7.69×10^3; McDonough WF and Sun SS, 1995), substantiating that the primitive magmas of plutons in the Hongqiling deposit underwent sulfide liquation in their early evolutionary stage (Li A, 2019). The Hongqiling deposit exhibit deep liquation and in situ magmatic liquation, which primarily occurred in the Nos. 7 and 1 plutons, respectively (Wu DY, 1987; Sun LJ, 2013).

In the No. 7 pluton, deep magmatic liquation occurred either in the magma source area or within relatively stable magma chambers as magmas ascended toward the crust. In the case where magmas were saturated with S, they differentiated into the upper and lower molten lava due to gravitational effects, with the lower molten lava enriched in ions like Mg^{2+}, Fe^{2+}, and Ni^{2+} and the upper portion enriched in Al_2O_3, SiO_2, and CaO. The upper molten lava absorbed hydroxyl ions $(OH)^-$ from surrounding rocks. In contrast, the lower molten lava became relatively enriched in sulfide ions (S^{2-}), which combined with Ni, Co, and Cu ions to form compounds. These led to the immiscibility between sulfides and silicates, with the sulfide droplets sinking to the bottom of magma chambers. As ore-bearing magmas continued to ascend, the two types of melts were emplaced sequentially due to their difference in specific gravity, with sulfide-rich melts penetrating to form ores (Zhang LS, 2022).

In the No. 1 pluton, sulfide-bearing molten lava was intruded into a relatively shallow position of the crust. As the temperature decreased, some mafic silicate crystals precipitated, leading to a decrease in Mg^{2+} and Fe^{2+} ions and relative enrichment in Si^{4+}, Ca^{2+}, and Al^{3+} ions in the melts. Consequently, conditions for S saturation were changed, leading to in situ magmatic liquation (Wu DY, 1987). The lithofacies in the No. 1 pluton exhibits gradual transition, along with normal zoning and rhythmic layering, suggesting pronounced characteristics of in situ magmatic liquation (Sun LJ, 2013).

5.3.3. Late hydrothermal modification

Late hydrothermal modification is relatively common in magmatic nickel-copper deposits, exemplified by the

Kambalda Dome deposit in Western Australia (Heath C et al., 2001), the Enterprise deposit in Zambia (Capistrant PL et al., 2015), and the Sancha copper-nickel-gold deposit in Northwest China (Li L et al., 2022). In these deposits, late hydrothermal processes further activated and modified the early Ni-Cu ores. This characteristic is also evident in the Cu-Ni mineralization within the northern Bushveld Complex (Holwell DA et al., 2017).

Within the No. 7 pluton in the Hongqiling deposit, continuous gradational transition can be observed between disseminated ores and pure-sulfide veined orebodies, indicating that extensive volatile-rich hydrothermal fluids activated and enriched the metal sulfides within pre-existing orebodies following the consolidation of the pluton (Lv LS et al., 2012). Large quantities of massive chalcopyrite aggregates or mottled chalcopyrite commonly occur near the contact zone between the mottled ores/pluton and surrounding rocks. Electron probe microanalysis (EPMA) reveals the hydrothermal metasomatic origin of the chalcopyrite. The slightly higher Cu content and lower S and PGE contents of the chalcopyrite suggest that hydrothermal metasomatism occurred in the presence of S-rich volatile components (Xi AH et al., 2004). The carbon and oxygen isotopic compositions ($\delta^{13}C$: −8.94‰ to −2.89‰; $\delta^{18}O$: +3.75‰ to +14.42‰) in the quartz and calcite veins paragenetic with pure-sulfide veins indicate that some of the materials in these veins originated from the upper mantle and were affected by hydrothermal fluids in their mineralization process (Xi AH, 2002). The aforementioned geological, elemental, and isotopic evidence all suggests the presence of late hydrothermal modification in the Ni mineralization of the Hongqiling deposit.

In the late stage of magmatic activity, hydrothermal fluids affected the consolidated rocks and orebodies, causing silicate minerals like olivines and pyroxenes to undergo tremolite, talc, and chlorite alterations, as well as carbonation. Then, the released Ni was further superimposed and enriched on the original orebodies or surrounding rocks. Consequently, some veinlet quartz-carbonate-sulfide mineralization occurred, or disseminated ores were transformed into lumpy ones. Therefore, the late hydrothermal modification played a crucial role in the Ni mineralization of the Hongqiling deposit. Concurrently, this stage contributed significantly to the PGE mineralization and partial Cu mineralization of the Hongqiling deposit (Sun LJ, 2013).

5.4. Origin and metallogenic model of the Hongqiling deposit

5.4.1. Comparison with domestic typical mafic-ultramafic magmatic copper-nickel sulfide deposits

The Hongqiling, Xiarihamu, and Huangshandong deposits are China's significant magmatic copper-nickel sulfide deposits occurring in orogenic belts (Li A, 2019). They share some similarities in geological characteristics, petrogeochemistry, and mineral chemistry while exhibiting differences (Table 9). Comparative research on typical copper-nickel deposits within orogenic belts can provide a crucial basis for both the theoretical research into magmatic copper-nickel deposits and the exploration of similar deposits.

In terms of geological characteristics, the three typical magmatic deposits all occur near deep-seated faults and are governed by secondary fault structures. The dominant ore-bearing mafic-ultramafic plutons of the Hongqiling deposit (e.g., the Nos. 1 and 7 plutons) occur on the north side of the deep-seated Huifahe fault, governed by secondary NW-trending fault structures. Similarly, the Xiarihamu and Huangshandong deposits are dictated by the Kunbei fault and the Kangguer deep-seated fault, respectively. In the three deposits, the primary ore-bearing mafic-ultramafic plutons all exhibit relatively small exposed areas (0.013–2.8 km²), demonstrating the characteristic of small plutons constituting large deposits (Tang ZL, 1996). However, the three deposits differ in lithofacies assemblages, pluton morphologies, and orebody morphologies. The plutons of the Hongqiling deposit are exposed as veins, while those of the latter two deposits exhibit elliptical and rhombic outcrops, respectively. The ore-bearing mafic-ultramafic plutons of the Hongqiling (the Nos. 1 and 7 plutons), Xiarihamu (the No. 1 pluton), and Huangshandong deposits all manifest transition from mafic gabbros to ultramafic peridotites. However, these plutons differ significantly in the proportions of different rocks. Specifically, the No. 7 pluton of the Hongqiling deposit exhibits the lowest proportion of mafic rocks, followed by the pluton of the Xiarihamu deposit, with the plutons of the Huangshandong deposit featuring the highest proportion (Qin KZ et al., 2009; Wang G, 2014; Song XY et al., 2016; Liu YG et al., 2018). In the No. 7 pluton of the Hongqiling deposit and the pluton of the Xiarihamu deposit, ultramafic rocks are composed predominantly of pyroxene peridotites, olivine pyroxenites, and pyroxenites. In contrast, in the plutons of the Huangshandong deposit, mafic rocks are dominated by gabbros and norites, with diorites locally visible (Gu LX et al., 1994; Zhou MF et al., 2004; Qin KZ et al., 2009). Nevertheless, the ore-hosting lithofacies of the three deposits are all identified as the peridotite and pyroxenite facies. Except for the Nos. 1 and 7 plutons of the Hongqiling deposit, where pure-sulfide veins occur, the plutons of the three deposits share similar orebody morphologies, dominated by stratoid and lentoid shapes, and primarily exhibit disseminated, densely disseminated, and lumpy mineralization. In the three deposits, the average Ni grade decreases in the order of the No. 7 pluton of the Hongqiling deposit, the No. 1 pluton of the Xiarihamu deposit, and the plutons of the Huangshandong deposit. Additionally, all these three deposits contain minor amounts of associated Co (0.018–0.048 wt.%).

Regarding mineral chemistry, the ore-bearing lithofacies of the Hongqiling, Xiarihamu (No. 1 pluton), and Huangshandong deposits are dominated by the peridotite and pyroxenite facies, with olivines serving as the primary mineral of these ore-hosting rocks. The Ni content and Fo value of olivines are commonly employed to discriminate the

Table 9. Comparison of characteristics of the Hongqiling, Xiarihamu, and Huangshandong deposits.

Deposit	Hongqiling (No. 1 pluton)	Hongqiling (No. 7 pluton)	Xiarihamu (No. 1 pluton)	Huangshandong
Surrounding rock type	Metamorphic rocks of the Paleozoic Hulan Group's Huangyingtun Formation		Metamorphic rocks of the Proterozoic Jinshuikou Group and Neoproterozoic garnet-bearing granite gneisses	Iron-bearing siltstones, carbonaceous ferruginous slates, and bioclastic limestones of the Lower Carboniferous Gandun Formation
Geotectonical location	Eastern Xing'an-Mongolian orogenic belt		Central part of the East Kunlun orogenic belt	Northeastern part of the Neopaleozoic trench-arc zone in Jueluotage
Pluton-controlling structure	deep-seated Huifahe fault and secondary NW-trending faults		Kunbei fault, nearly EW- and NEE-trending fault structures	Kanggur deep-seated fault and secondary Huangshan fault
Pluton type	Single		Complex	Complex
Pluton strike	NW 30°–60°		Nearly EW	NEE
Pluton morphology	Vein zone		Elliptical	Rhombic
Exposed area	0.2 km^2	<0.013 km^2	0.7 km^2	2.8 km^2
Primary lithofacies	Gabbro, pyroxenite, peridotite, and ore-bearing olivine pyroxenite	Peridotite facies (harzburgite), pyroxenite facies (orthopyroxenite), and norite facies (norite)	Peridotite facies (dunite, harzburgite, and lherzolite), pyroxenite facies (olivine pyroxenite, pyroxenite, and feldspar-bearing websterite), and norite-gabbro facies (olivine gabbro, dark gabbronorite, gabbro, and leucogabbro)	Peridotite facies (lherzolite) and norite-gabbro facies (diorite, hornblende gabbro, olivine gabbro, and gabbronorite)
Ore-hosting lithofacies	Olivine pyroxenite and altered pyroxenite facies	Peridotite facies (harzburgite) and pyroxenite facies (orthopyroxenite)	Peridotite and pyroxenite facies predominantly, with dotted sulfide mineralization visible in gabbronorite	Gabbro, norite, olivine pyroxenite, and olivine norite
Mineralization type	Disseminated, spotted, and lumpy	Disseminated and lumpy	Disseminated, densely disseminated, and lumpy primarily, and densely massive locally	Primarily densely and moderately disseminated, followed by massive and sparsely disseminated
Orebody morphology	Stratoid, overhanging lentoid, and veined orebodies, and pure-sulfide veins	Tabular, veined, and pure-sulfide veined	Thickly stratoid and lentoid orebodies primarily, along with small quantities of funnel-shaped and irregular overhanging orebodies	Stratoid and lentoid orebodies primarily, with small quantities of veined and branching-recombining orebodies
Ore mineral assemblage	Pyrrhotite, pentlandite, chalcopyrite, and minor amounts of magnetite, pyrite, vallerite, and ilmenite	Pyrrhotite, pentlandite (including a small amount of violarite), and chalcopyrite	Pyrrhotite, pentlandite, chalcopyrite, pyrite, chrome spinel, and violarite	Pyrrhotite, pentlandite, and chalcopyrite
Average grades of Ni, Cu, and Co	Ni: 0.53 wt.%; Cu: 0.11 wt.%	Ni: 1.974 wt.%; Cu: 0.63 wt.%	Ni: 0.65 wt.%; Cu: 0.14 wt.%; Co: 0.013 wt.%	Ni: 0.52 wt.%; Cu: 0.27 wt.%; Co: 0.024 wt.%
Fo value of olivine	83.69–89.00	85.04 (83.02–87.27)	87.26 (83.02–90.77)	79.86 (67.20–85.1)
Ni content of olivine	(601.75–1726.61) $\times10^{-6}$	1988×10^{-6} (721×10^{-6} to 2782×10^{-6})	2121×10^{-6} (558×10^{-6} to 4370×10^{-6})	1114×10^{-6} (558×10^{-6} to 4370×10^{-6})
m/f ratio	0.99–6.05(4.60)	3.87(0.87–5.48)	4.90(2.06–7.45)	2.98(0.78–4.96)
Deposit scale	Medium-sized	Large	Supergiant	Large
Diagenetic and metallogenic epochs	Indosinian		Late Silurian to Early Devonian	Middle Permian
References	Wu FY et al., 2004; Wei B al., 2013; Li A, 2019; Yin GZ et al., 2019b; Xue HR, 2020; Xu ZH, 2020		Wang G, 2014; Zhang ZW et al., 2015, 2017; Pan T, 2015; Song XY et al., 2016; Liu YG et al., 2018	Qin KZ et al., 2009; Fu YG et al., 2019; Wang SM et al., 2021; Zhao Q and Zhang MJ, 2022

metallogenic potential of mafic-ultramafic rocks (Li A, 2019). The No. 1 pluton of the Xiarihamu deposit shows the highest Fo values, which vary from 83.02 to 90.77 (average: 87.26; Li CS et al., 2015; Zhang ZW et al., 2017; Liu YG et al., 2018), followed by the No. 7 pluton of the Hongqiling deposit, whose Fo values range between 83.02 and 87.27 (average: 85.04; Li A, 2019). The Huangshandong deposit displays the lowest Fo values of olivines, which range from 67.20 to 85.1 (average: 79.86; Liu YR et al., 2012; Deng Y et al., 2014; Mao YJ et al., 2015). The Fo values of the three deposits all fall within the Fo value range (80–86 mostly and 65–80 occasionally) of olivines proposed by Jiang CY et al. (2012) for mafic-ultramafic rocks of copper-nickel sulfide deposits, suggesting favorable conditions for mineralization. The Ni content in the three deposits decreases in the order of the Xiarihamu, Hongqiling (No. 7 pluton), and Huangshandong

deposits, with average of 2121×10^{-6} (Li CS et al., 2015; Zhang ZW et al., 2017; Liu YG et al., 2018), 1988×10^{-6} (Li A, 2019), and 1114×10^{-6} (Liu YR et al., 2012; Deng et al., 2014; Mao et al., 2015), respectively. Hence, in the three deposits, olivines are all depleted in Ni, as evidenced by Ni content below 2200×10^{-6}, indicating favorable conditions for mineralization (Naldrett AJ, 1999).

In terms of petrogeochemistry, the m/f ratio and its range are critical indicators used to discriminate the metallogenic potential and mineralization types of mafic-ultramafic rocks (Wu LR, 1963; Liu YG et al., 2019). In the Hongqiling, Xiarihamu, and Huangshandong deposits, the ore-bearing plutons show significantly varying m/f ratios, primarily between 2 and 6. This result suggests high differentiation degrees of the plutons, conducive to the formation of copper-nickel sulfide deposits (Wu LR, 1963; Liu YG et al., 2019). Additionally, the ore-bearing plutons of the three deposits exhibit similar REE distribution patterns, characterized by enrichment in LREEs and depletion in heavy REEs (HREEs), implying similar magma sources (Li A, 2019).

5.4.2. Origin and metallogenic model of the Hongqiling deposit

There are several views on the tectonic setting of copper-nickel sulfide deposits and related mafic-ultramafic plutons in the east-central region of Jilin Province. Initially, it was believed that the formation of these copper-nickel sulfide deposits is associated with the subduction of the Pacific Plate or the activity of the mantle plume (Xi AH, 2002). Some researchers posited that these deposits were formed during the synorogenic period of the Xing'an-Mongolian orogenic belt, corresponding to the orogeny-related tectonic setting of compression alternating with extension (Xi AH et al., 2005; 2006). Others proposed that their formation predated the collisional orogeny between the North China and the Siberian plates, possibly corresponding to a continental-margin rift setting (Xie HQ et al., 2007). In recent years, an increasing number of researchers underpin that the Indosinian copper-nickel deposits and related mafic-ultramafic plutons in the east-central region of Jilin Province were formed in an extensional environment related to post-collisional orogeny between the North China Plate and the Songnen-Zhangguangcai Range block (Wu FY et al., 2004; Wei QQ, 2015; Zhao Y et al., 2017; Li A et al., 2018; Li A, 2019; Zhang LS, 2022; Ma YF et al., 2022).

During the Late Triassic, significant lithospheric extension led to decompressional partial melting of the upper mantle that was enriched in ore-forming materials and retained subduction-related metasomatic fluids, leading to the formation of primitive ore-bearing parental magmas. Then, the ore-bearing magmas ascended along the deep-seated Huifahe fault to magma chambers in the deep crust. Crustal extension and stress release tend to occur intermittently, causing pulsed magma ascent and emplacement, which is characterized by the regularity consisting of ascent and emplacement, residence, and ascent and emplacement again (Tang ZL et al., 1998). This process continued until magmas intruded into the shallow crust and reached stress equilibrium. Then, as the temperature gradually decreased, the primitive parental magmas consolidated, forming rocks and minerals (Tang ZL et al., 1998; Fig. 16).

During the magma ascent and emplacement, each residence led to the formation of a middle magma chamber, followed by further magma ascent and emplacement. Due to lag effects, light, medium, and heavy magmas would be distributed from top to bottom. As magmas entered a middle magma chamber, they would be distributed based on their sequential order and density, progressively constituting a magma chamber with a four-layered structure composed of magmas, ore-bearing magmas, fertile magmas, and ore magmas from top to bottom (Tang ZL et al., 1998).

Accompanied by the pulsed, intermittent activity of magma-conducting and -hosting structures, magmas with low density and sulfide content at the top of a magma chamber first intruded, forming the gabbro facies of the No. 1 pluton. Then, the magmas crystallized and differentiated, forming gabbros and plagioclase websterites. Subsequently, magmas with slightly higher sulfide content and a higher maficity degree immediately arrived and were emplaced, in intrusive contact with the gabbro facies. They formed the pyroxene peridotite and olivine pyroxenite facies of the No. 1 pluton. With a decrease in temperature, mafic silicates crystallized, the residual magmas experienced in situ liquation, forming overhanging orebodies and stratoid orebodies at the bottom (Fig. 16). Fertile magmas at the bottom of the magma chamber ascended last. Accordingly, the upper melts were emplaced at the basal axial position of the No. 1 pluton and experienced in situ liquation and gravity effect, leading to the vertical zoning of ores with the ore-hosting lithofacies and the formation of pure-sulfide veins.

The high-viscosity melts more enriched in sulfides in the lower part penetrated into transtensional faults as dykes under tectonic driving forces, forming the peridotite and pyroxenite facies of the No. 7 pluton. These lithofacies are enriched in metal sulfides, constituting high-grade tabular orebodies (Fig. 16). Significant dynamic forces led to insufficient in situ liquation. The melts, composed almost of sulfides, that were residual in the magma chamber finally penetrated into the contact fracture zone between enstatites and pyroxene peridotite veins, forming the pure-sulfide veins in the No. 7 pluton (Wu DY, 1987).

5.5. Prospecting indicators and model

5.5.1. Prospecting indicators

This study summarized favorable mineralization conditions and prospecting indicators of the Hongqiling deposit by combining the aforementioned in-depth analysis and insights into the ore-controlling geological factors and diagenetic and mineralization processes, as well as the exploration results achieved and orebodies revealed.

(i) Favorable geological setting

The Hongqiling deposit, along with its adjacent magmatic copper-nickel deposits like Chajianling, Piaohechuan, and

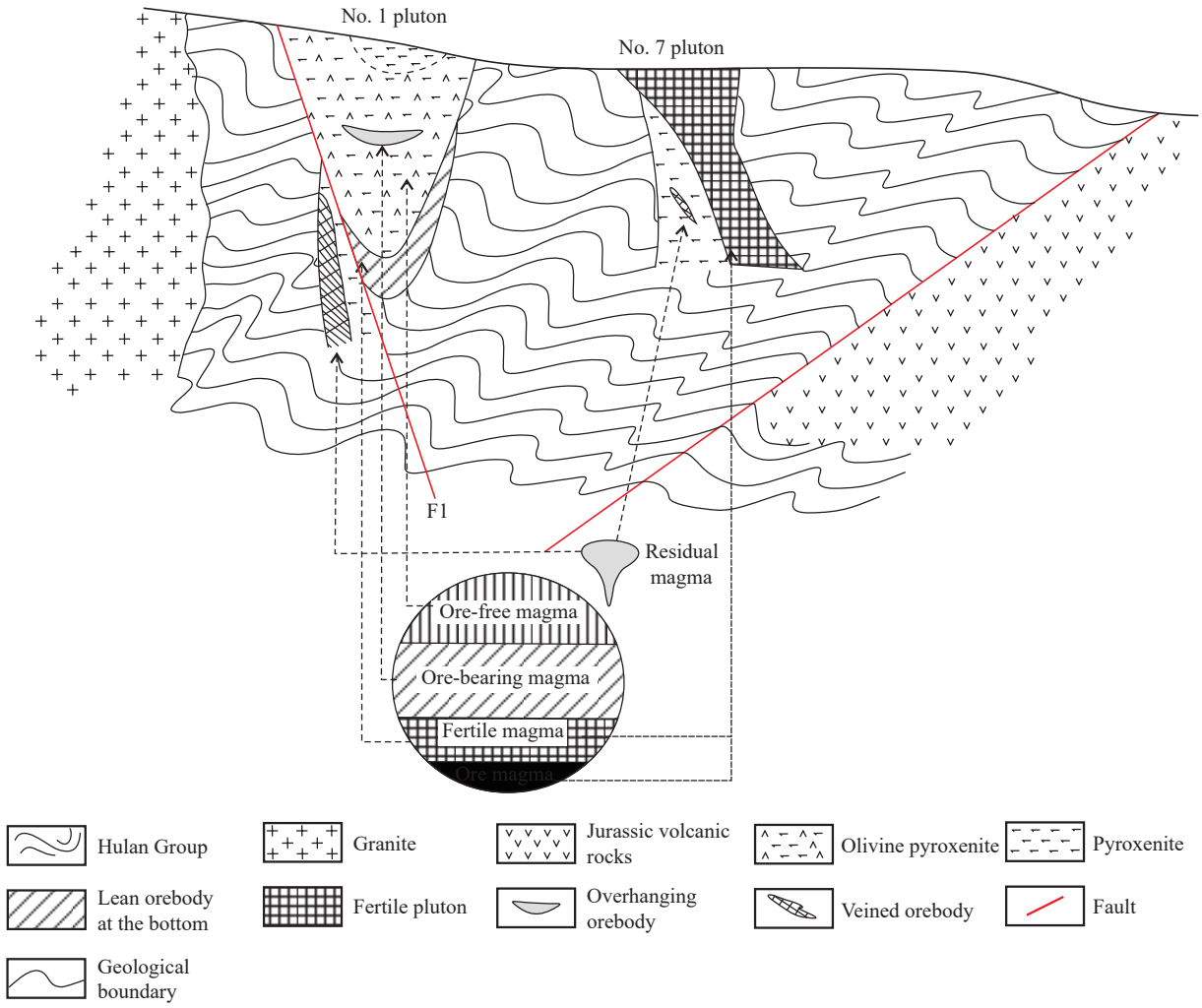

Fig. 16. Diagram showing the metallogenic model of the Hongqiling copper-nickel deposit in Panshi City, Jilin Province (modified from Tang ZL et al., 1998; Xing SW et al. 2014).

Changren deposits, is located in the eastern segment of the Xing'an-Mongolian orogenic belt, falling within the superimposed zone between the Paleo-Asian Ocean and Paleo-Pacific tectonic domains. This zone exhibits well-developed fault structures featuring frequent prolonged and inherited activity, as well as intense magmatic activity. Furthermore, this zone was in an intense post-orogenic extensional tectonic environment during the Indosinian. These conditions created a favorable geological setting for the formation of various minerals like Au, Au, Pb, Zn, Cu, and Ni in the region.

(ii) Indicators of surrounding rocks

The Huangyingtun Formation of the Hulan Group is composed primarily of tourmaline- and garnet-bearing two-mica plagiogneisses, biotite-plagioclase leptynites, hornblende-plagioclase leptynites, and kyanite schists, interbedded with multi-layered siliceous banded marbles. As stated above, both the magmatic evolutionary process and material source of the Hongqiling deposit's mafic-ultramafic plutons are somewhat associated with the metamorphic rocks of the Hulan Group's Huangyingtun Formation. The crustal material contamination plays a significant role in promoting magmas to reach S saturation and undergo sulfide liquation (Arndt NT et al., 2005). Therefore, the metamorphic rocks of the Hulan Group's Huangyingtun Formation serve as the indicators of surrounding rocks for exploring similar types of deposits.

(iii) Rock assemblage indicators

For copper-nickel sulfide deposits, mafic-ultramafic rocks, as ore-forming parental rocks, control the entire diagenetic and mineralization processes (Zhang LS, 2022). In the Hongqiling area, rocks favorable for the nickel mineralization encompass Middle-Late Triassic gabbros, pyroxenites, olivine pyroxenites, peridotites, orthopyroxenites, and norites, with the dominant ore-hosting lithofacies including peridotite facies (harzburgite) and pyroxenite facies (orthopyroxenite). These ore-bearing ores have average m/f ratios ranging from 3.87 to 4.77, which fall within the m/f ratio range (2–6.5) of ferrous ultramafic rocks favorable for Cu and Ni mineralization.

(iv) Structural indicators

In terms of the tectonic setting, the Hongqiling deposit was formed in an intense extension environment related to post-collisional orogeny between the North China Plate and the Songnen-Zhangguangcai Range block. Furthermore, this deposit is governed by the NE-trending deep-seated Huifahe fault, which, characterized by considerable cutting depths and

frequent inherited activity, serves as a significant rock- and ore-controlling structural zone (Dong YS et al., 2004). The primary ore-bearing plutons in the Hongqiling deposit all occur within the NW-trending Fujia-Pianlianzi fault derived from the deep-seated Huifahe fault. The NW-trending transtensional fault activity governs the emplacement of fertile magmas and the localization of orebodies (Zhi XJ, 2005). Besides, areas with multiple superimposed structures are favorable for mineralization (Sun YH et al., 2016).

(v) Mineralized alteration indicators

Pyrrhotite, pentlandite, and chalcopyrite constitute the predominant metallic mineral assemblage in the Hongqiling deposit, also acting as the primary carriers of useful elements like Cu, Co, and Ni. Therefore, this assemblage is identified as a direct prospecting indicator for the mineralization of mafic-ultramafic plutons in the deposit. The uralite, serpentine, and chlorite alterations, closely associated with mineralization, serve as indirect prospecting indicators for the mineralization of the mafic-ultramafic plutons.

(vi) Lithogenetic mineral indicators of ore-forming plutons

In the Hongqiling deposit, olivines in the primary ore-bearing mafic-ultramafic rocks exhibit high Fo values, ranging from 83.02 to 87.27 (average: 85.04; Li A, 2019), and high Ni content, averaging 1988×10^{-6}. All these values fall within the ranges of Fo values and Ni content of olivines in mafic-ultramafic rocks hosting copper-nickel sulfide deposits (Naldrett AJ, 1999; Jiang CY et al., 2012).

(vii) Geophysical indicators

The 1∶10000 high-precision surface magnetic survey proves highly effective in locating mafic-ultramafic plutons in the Hongqiling deposit, showing strong correlations between mafic-ultramafic plutons and geomagnetic anomalies. The morphologies of plutons agree well with the anomaly patterns (Qiu W et al., 2012). The geomagnetic anomaly amplitudes range from 10 nT to 2100 nT, with larger mafic-ultramafic plutons corresponding to higher anomaly amplitude (Sun LJ, 2013), which reaches up to 4000 nT (Sun YH et al., 2016). The 1∶10000 high-precision surface gravity survey results reveal that the Nos. 1 and 3 plutons in the Hongqiling deposit correspond to high-amplitude gravity anomaly areas, with high anomaly values of approximately 12×10^{-5} m/s^2, effectively delineating mafic-ultramafic plutons (Xu ZH et al., 2022). The 1∶10000 Bouguer gravity anomaly map shows that the positions of the Nos. 1, 2, 3, and 9 plutons in rock belt I of the Hongqiling area correspond significantly to independent, high-value anomaly traps. Hence, the Bouguer gravity method can effectively locate high-density mafic-ultramafic plutons (Sun LJ, 2013).

In terms of measured physical properties, the orebodies of the No. 1 pluton exhibits high density (2.85–3.04 g/cm^3, average: 2.95 g/cm^3), magnetic susceptibility (1453×10^{-6} to 4620×10^{-6} SI, average: 2600×10^{-6} SI), and polarizability (5.65%–40%, average: 22%) and significantly lower resistivity (847–5994 Ω·m, average: 3130 Ω·m) than surrounding rocks and other plutons (6000–15000 Ω·m). These physical properties make it significantly distinguished from local strata and intermediate-acidic intrusive rocks.

Transient electromagnetic (TEM) surveys show that the resistivity of the ore-bearing plutons generally ranges from 10 Ω·m to 300 Ω·m, differing insignificantly from that of the surrounding rocks. However, the ores and the surrounding rocks differ greatly in resistivity, with differences exceeding two orders of magnitude (Sun YH et al., 2016).

The induced polarization (IP) sounding reveals apparent polarizability anomalies (ηs) of plutons greater than 4% (Sun YH et al., 2016).

(viii) Geochemical indicators

The 1∶200000 stream sediment survey results indicate that single-element anomalies of Cu, Co, Ni, and chromium (Cr) agree well with the location of the Hongqiling deposit. Moreover, zones with high Ni/Co ratios (12–20) of stream sediments correlate highly with the Hongqiling deposit, suggesting that the Ni/Co ratio of stream sediments can effectively reveal large-scale ore-bearing mafic-ultramafic plutons, with minimal influence from the lithological background. Additionally, the 1∶10000 soil anomaly survey demonstrates that the composite anomaly of Cu, Co, and Ni proves highly effective in locating mafic-ultramafic plutons in the Hongqiling deposit (Sun LJ, 2013).

5.5.2. Prospecting model

This study established a prospecting model for the Hongqiling deposit based on the aforementioned metallogenic geological setting and geological characteristics of the deposit, as well as deposit prediction factors extracted from the geophysical, geochemical, and remote sensing data (Table 10).

6. Conclusions

(i) The Hongqiling deposit, a large magmatic nickel-copper-cobalt deposit in Jilin Province, boasts proven Ni reserves of 22.01×10^4 t, proven associated Cu reserves of 2.47×10^4 t, and proven associated Co reserves of 0.53×10^4 t, with Ni reserves ranking 10th among China's magmatic nickel deposits. The nickel deposit hosted by the No. 7 pluton is identified as the predominant contributor to the Ni reserves of the Hongqiling deposit, with an average Ni grade of 1.974%, ranking top among large and above magmatic nickel deposits in China.

(ii) The primary ore-hosting plutons of the Hongqiling deposit comprise the Nos. 1 (medium-sized nickel deposit) and 7 (large nickel deposit) plutons in rock belt I, with ore-hosting lithofacies encompassing peridotite and (olivine) pyroxenite facies. These plutons host stratoid, overhanging lentoid, veined, and pure-sulfide veined orebodies, along with disseminated, lumpy/massive, and mottled ore structures. They are generally governed by the secondary NW-trending Fujia-Hejiagou-Beixinglong-Changsheng fault zone of the deep-seated Huifahe fault.

(iii) The Hongqiling deposit underwent three mineralization phases, i.e., magmatic mineralization, late hydrothermal modification, and supergene oxidation, with magmatic mineralization characterized by deep (represented

Table 10. Prospecting model for the Hongqiling deposit in Panshi City, Jilin Province.

Metallogenic factor		Description	Category
Characteristic description		Magmatic differentiation deposit	
Geological environment	Geotectonic location	Eastern segment of the Xing'an-Mongolian orogenic belt, falling within the superimposed zone between the Paleo-Asian Ocean and Paleo-Pacific tectonic domains	Important
	Strata	Metamorphic rocks of the Hulan Group's Huangyingtun Formation	Important
	Magmatic rocks	Gabbro-pyroxenite-peridotite (No. 1 pluton) and orthopyroxenite-norite (No. 7 pluton)	Necessary
	Structures	Huifahe translithospheric fault and its secondary NW-trending fault structures	Necessary
	Mineralization epoch	Indosinian	Necessary
Deposit characteristics	Mineral assemblage	Metallic minerals primarily include pyrrhotite, pentlandite, chalcopyrite, violarite, and pyrite, followed by temiskamite, niccolite, magnetite, galena, vallerite, molybdenite, and ilmenite.	Important
	Textures and structures	Common ore textures comprise hypidiomorphic to xenomorphic granular, flame-shaped, rimmed textures, as well as interstitial and myrmekitic textures. Ore structures principally include disseminated, spotted, sideronitic, and massive structures, followed by lumpy, veinlet-disseminated, and brecciated structures.	Secondary
	Alterations	Alterations primarily include talc, uralite, biotite, saponite, serpentine, and sericite alterations, with uralite, serpentine, and chlorite alterations being closely associated with mineralization.	Important
	Ore-controlling conditions	The metamorphic rocks of the Hulan Group's Huangyingtun Formation create favorable stratigraphic conditions for mineralization. The Huifahe translithospheric fault and its derived NW-trending faults govern the emplacement of mafic-ultramafic plutons and the locations of orebodies. The primary ore-bearing rock assemblages include the gabbro-pyroxenite-peridotite and orthopyroxenite-norite assemblages.	Necessary
Geophysical, geochemical, and remote sensing anomalies	Gravity survey	Regionally, the Hongqiling deposit resides in the southern portion of the equiaxial high-amplitude gravity anomaly zone of the Hongqiling area, with the highest anomaly value of -23.6×10^{-5} m/s^2. The primary ore-bearing plutons within the deposit show high-amplitude gravity anomalies, with high anomaly values of approximately 12×10^{-5} m/s^2.	Important
	Magnetic survey	Regionally, the Hongqiling deposit is located in the NWW-striking zone with local positive magnetic anomaly values, with a maximum anomaly value of 266 Nt. Primary ore-bearing plutons within the deposit display high-amplitude magnetic anomalies, with anomaly values ranging between 10 nT and 2100 nT.	Important
	Geochemical survey	Elements like Cr, Ni, Cu, and Co exhibit high anomaly intensity, distinct zoning, pronounced concentration centers, and large scales. Moreover, the composite anomalies dominated by Ni and Cu are tightly overlayed in spatial distribution.	Important
	Remote sensing	Several linear and circular structures are determined in the Hongqiling area using the interpretation of remote sensing data. Ferric contamination anomalies are relatively concentrated in the intersections of faults of multiple directions and areas occupied by circular structures.	Important

by the No. 7 pluton) and in situ liquation (typified by the No. 1 pluton).

(iv) The primary ore-bearing mafic-ultramafic plutons of the Hongqiling deposit exhibit δ^{34}S values ranging from −4.7‰ to +2.13‰, mostly around zero. These values are similar to those of mantle-derived S, suggesting that the S in the Hongqiling deposit originated primarily from the upper mantle. Some sulfide samples from a pluton in the deposit showed lower δ^{34}S values ranging between −4.7‰ and −1.9‰, which approached those of surrounding rocks and contaminated rocks in the external contact zone. This result suggests slight contamination by crustal materials during the magmatic mineralization, aligning with the Re-Os isotopic analysis results.

(v) The ore-bearing mafic-ultramafic plutons of the Hongqiling deposit manifest crystallization ages varying between 208 Ma and 239 Ma, roughly matching the Re-Os isochron ages (208 Ma to 237 Ma) of the ores or metal sulfides. This result limited the diagenetic and metallogenic epoch of the deposit to the Indosinian, corresponding to the extensional setting post-collisional orogeny between the North China Plate and the Songnen-Zhangguangcai Range block.

(vi) From the perspective of the metallogenic geological setting, surrounding rocks, ore-controlling structures, and rock assemblages, this study identifies one favorable metallogenic condition and seven significant prospecting indicators for the Hongqiling deposit and develops a prospecting model for the deposit.

CRediT authorship contribution statement

Cong Chen, Yu-chao Gu, and Di Zhang conceived of the presented idea and performed the computations. Tao-tao Wu and Ai Li assisted in plotting the maps. All authors discussed the results and contributed to the final manuscript.

Declaration of competing interest

The authors declare no conflicts of interest.

Acknowledgement

This study was funded by projects of the China Geological Survey (Nos. DD20242070, DD20230763, DD20221695, DD20190379, and DD20160346).

References

Arndt NT. 2005. The conduits of magmatic ore deposits. In: Mungall JE(ed) Exploration for platinum-group element deposits. Mineralogical Association of Canada. Short Course Series 35, 181–201.

Cai QS, Fan YX, Yan XY, Wang Y, Gao MM, Yang GL, Zhang MJ, Bi K, Zhang HF, Li XH. 2023. Paleozoic rapid denudation of the Proterozoic Jinchuan Ni-Cu-PGE sulfide deposit, NW China: Insights from single-grain zircon (U-Th)/He thermochronology. Journal of Asian Earth Sciences, 255, 105762. doi: 10.1016/j.jseaes.2023.105762.

Capistrant PL, Hitzman MW, Wood D, Kelly NM, Williams G, Zimba M, Kuiper Y, Jack D, Stein H. 2015. Geology of the enterprise hydrothermal Ni deposit, North-Western Province, Zambia. Economic Geology, 110, 9–38. doi: 10.2113/econgeo.110.1.9.

Chen C. 2017. Late Paleozoic-Mesozoic tectonic evolution and regional metallogenic regularity of the eastern Yanbian area, NE China. Changchun, Jilin University, Ph. D thesis, 1–201 (in Chinese with English abstract).

Chen J, Zhao ZH, Yang YJ, Li CL, Yin YC, Zhao X, Zhao N, Tian JW, Li HN. 2024. Metallogenic prediction based on fractal theory and machine learning in Duobaoshan Area, Heilongjiang Province. Ore Geology Reviews, 168, 106030. doi: 10.1016/j.oregeorev.2024.106030.

Chen MY. 1979. Sulfur istopes of various types of copper deposits in China. Geology and Exploration, 06, 6–17 (in Chinese).

Dai M, Yan GS, Li YS, Jia WB, Qi FY, Ju X. 2023. Melt extraction and mineralization: A case study from the Shuangjianzishan supergiant Ag-Pb-Zn deposit (208 Mt), Inner Mongolia, NE China. China Geology, 6(4), 623–645. doi: 10.31035/cg2022044.

Deng Y. 2014. Geochemistry of the Huangshandong Ni-Cu deposit in northwestern China: Implications for the formation ofmagmatic sulfide mineralization in orogenic belts. Ore Geology Reviews, 56(1), 181–198. doi: 10.1016/j.oregeorev.2013.08.012.

Dong GZ, Ye MH, Dai XG, Sun C. 2012. Petrology and geochemistry characteristics of the Cu-Ni sulfide deposits of the 3rd rocks in Hongqiling area, Jilin. Mineral Exploration, 3(3), 297–305 (in Chinese with English abstract).

Ding KS, Qin KZ, Xu YX, Sun H, Xu XW, Tang DM, Mao Q, Ma YG. 2007. Typomorphic characteristics and ore—forming significance of pyrrhotite in the majorCu —Ni deposits, EastTianshan, Xinjiang. Mineral Deposits, 26 (11: 109 —119(in Chinese with English abstract).

Dong YS, Fan JZ, Yang YC, Sun DY. 2004. Study on the metallogenic feature and ore genesis of Hongqiling copper-nickel deposit, Jilin Province. Geoscience, 18(2), 197–202 (in Chinese with English abstract).

Dong YS. 2003. Synthesis prospecting model of copper-nickel deposit of Hongqiling, Jilin Province. Journal of Jilin University (Earth Science Edition), 2, 32–35, 57 (in Chinese with English abstract).

Editorial Board of Jilin Volume of The Discovery History of Mineral Deposits of China. 1991. The discovery history of mineral deposit of China, volume of Jilin Province. Beijing, Geological Publishing House, 1–137 (in Chinese).

Feng GY, Liu S, Feng CX, Jia DC, Zhong H, Yu XF, Qi YQ, Wang T. 2011. Zircon U-Pb age, Sr-Nd-Hf isotope geochemistry and the petrogenesis of the ultramafic pluton in Hongqiling, Jiling Province. Acta Petrologica Sinica, 27(6), 1594–1606 (in Chinese with English abstract).

Foster JG, Lambert DD, Frick LR, Maas R. 1996. Re-Os isotopic evidence for genesis of Archaean nickel ores from uncontaminated komatiites. Nature, 382(6593), 703–706. doi: 10.1038/382703a0.

Fu DB, Chen EZ. 1988. Metallogenetic regularities of Cu-Ni sulfide deposits in Jilin Province. Jilin Geology, 2, 138–158 (in Chinese with English abstract).

Fu YG, Gao JW, Ma MS. 2019. The discovery of Early Permian pyroxenite in Heiyingshan region in the western Inner Mongolia. Geology in China, 46(3), 668–669 (in Chinese with English abstract).

Geology and Mineral Exploration and Development Bureau of Jilin Province. 1985. Regional geological survey report of Hulan Town and Hongqiling Town map sheets (1∶50000) (in Chinese).

Geology and Mineral Exploration and Development Bureau of Jilin Province 1988. Regional Geology of China, volume of Jilin Province. Beijing, Geological publishing house (in Chinese).

Gu LX, Zhu JL, Guo JX, Liao JJ, Yan ZF, Yang H, Wang JZ. 1994. The east Xinjiang-type mafic-ultramafic copplexes in orogenic environments. Acta Petrologica Sinica, 10(4), 339–356 (in Chinese with English abstract).

Han CM, Xiao WJ, Zhao GC. 2014. Re–Os Isotopic Age of the Hongqiling Cu-Ni Sulfide Deposit in Jilin Province, NE China and its Geological Significance. Resource Geology, 64(3), 247–261. doi: 10.1111/rge.12039.

Hanyu T, Tatsumi Y, Nakai SI, Chang Q, Miyazaki T, Sato K, Tani K, Shibata T, Yoshida T. 2013. Contribution of slab melting and slab dehydration to magmatism in the NE Japan arc for the last 25 Myr: Constraints from geochemistry. Geochemistry Geophysics Geosystems, 7(8), 1–29. doi: 10.1029/2005GC001220.

Hao LB, Sun LJ, Zhao YY, Lu JL, Lü CD, Ma C. 2012. The No. 2 Mafic-ultramafic intrusion SHRIMP U-Pb zircon dating and its geological significance in Hongqiling area of Jilin Province, China. Journal of Jilin University (Earth Science Edition), 42(3), 166–178 (in Chinese with English abstract).

Hao LB, Sun LJ, Zhao YY, Lu JL. 2013. SHRIMP Zircon U-Pb Dating of Chajian Mafic-Ultramafic Rocks in Hongqiling Mine Field, Jilin Province, and Its Implications. Earth Science, 38(2), 233–240 (in Chinese with English abstract).

Hao LB, Wu C, Sun LJ, Jiang YM, Zhao YY, Lu JL, Li J. 2014. Re-Os Isotope characteristics of Hongqiling Cu-Ni Sulfide deposit in Province and its significance. Journal of Jilin University (Earth Science Edition), 44(2), 507–517 (in Chinese with English abstract).

Heath C, Lahaye Y, Stone WE, Lambert DD. 2001. Origin of variations in Ni tenor along the strike of the Edwards Lode Ni sulfide ore body, Kambalda, Western Australia. Canadian Mineral, 39(2), 655–671. doi: 10.2113/gscanmin.39.2.655.

Hofmann AW. 1986. Chemical differentiation of the earth-The relationship between mantle, continental crust, and oceanic crust. Earth and Planetary Science Letters, 90(3), 297–314. doi: 10.1016/0012-821X(88)90132-X.

Holwell DA, Adeyemi Z, Ward LA, Smith DJ, Graham SD, McDonald I, Smith JW. 2017. Low temperature alteration of magmatic Ni-Cu-PGE sulfides as a source for hydrothermal Ni and PGE ores: A quantitative approach using automated mineralogy. Ore Geology Reviews, 91, 718–740. doi: 10.1016/j.oregeorev.2017.08.025.

Jiang CY, Ling JL, Zhao YF, Kang Z, Song YF, Wang Y. 2012. Ore-Bearing Potential Evaluation Index System of Mafic and Ultramafic Intrusions —Used to Search for Magmatic Sulfide Deposits. Northwestern Geology, 45(4), 51–60 (in Chinese with English abstract).

Jilin Institute of Geological Survey. 2023. Geology of Mineral Resources in China, Volume of Jilin. Beijing, Geological publishing house (in Chinese).

Kang Z, Qin KZ, Mao JW, Tang DM, Yao ZS. 2020. The formation of a magmatic Cu-Ni sulfide deposit in mafic intrusions at the Kalatongke, NW China: Insights from amphibole mineralogy and composition. Lithos, 352–353, 105317. doi: 10.1016/j.lithos.2019.105317.

Lambert DD, Foster JG, Frick LR, Li C, Naldrett AJ. 1999. Re-Os Isotopic Systematics of the Voisey's Bay Ni-Cu-Co Magmatic Ore System, Labrador, Canada. Lithos, 47, 69–88. doi: 10.1016/S0024-4937(99)00008-0.

Li A, Wang J, Song Y, Liu JG, Xue SC. 2018. Geochemistry Characteristics of the ore-bearing mafic-ultramafic intrusions in the

Hongqiling Ni-Cu sulfide deposit, NE China and its petrogenesis significance. Acta Geologica Sinica, 92(2), 263–277 (in Chinese with English abstract).

Li A. 2019. Mineralogy, petrogeochemistry and Ni-Cu mineralization for the mafic-ultramafic intrusions from the Hongqiling area, Jilin Province. Changchun, Jilin University, Ph. D thesis, 1–133 (in Chinese with English abstract).

Li CS, Ripley EM. 2012. Low-Ca contents and kink-banded textures are not unique to mantle olivine: Evidence from the Duke Island Complex, Alaska. Mineralogy and Petrology, 104(3–4), 147–153. doi: 10.1007/s00710-011-0188-0.

Li CS, Zhang ZW, Li WY. 2015. Geochronology, petrology and Hf-S isotope geochemistry of the newly-discovered Xiarihamu magmatic Ni-Cu sulfide deposit in the Qinghai-Tibet plateau, western China. Lithos, (216-217), 224–240. doi: 10.1016/j.lithos.2015.01.003.

Li L, Sun FY, Li BL, Bai Y, Wang C, Qian Y, Sun YG, Tan SC. 2022. Identification of hydrothermal alteration and mineralization in the Sancha magmatic Cu-Ni-Au sulfide deposit, NW China: Implications for timing and genesis of mineralization. Ore Geology Reviews, 143, 104770. doi: 10.1016/j.oregeorev.2022.104770.

Li ZT, Li CG (editor in chief). 1994. Geological characteristics, metallogenic traditions and prospecting directions of Au-Ag polymetallic deposits in Panshi-Shuangyang areas, Jilin Province. Changchun, Jilin Science and Technology Publishing House, 1–23 (in Chinese).

Liang QL, Song XY, Long TM, Wirth R, Dai ZH. 2023. The effect of platinum-group minerals on differentiation of platinum-group elements in magmatic sulfide deposits: Evidence from the Cu-Ni-PGE deposits in the Yangliuping area of the Emeishan large igneous province, SW China. Chemical Geology, 636, 121645. doi: 10.1016/j.chemgeo.2023.121645.

Liang SS, Zhao ZH, Li CL, Yin YC, Li HN, Zhou JZ. 2024. Age and petrogenesis of ore–forming volcanic-subvolcanic rocks in the Yidonglinchang Au deposit, Lesser Xing'an Range: Implications for late Mesozoic Au mineralization in NE China. Ore Geology Reviews, 165, 105875. doi: 10.1016/j.oregeorev.2024.105875.

Lightfoot PC, Evans-Lamswood D. 2015. Structural controls on the primary distribution of mafic-ultramafic intrusions containing Ni-Cu-Co-(PGE) sulfide mineralization in the roots of large igneous provinces. Ore Geology Reviews 64, 354–386. doi: 10.1016/j.oregeorev.2014.07.010.

Liu JY, Xi AH, Ge YH, Sun HT, Gong PH. 2010. Mineralization age of the No. 3 ore-bearing intrusion and its petrological significance in Hongqiling Cu-Ni sulfide deposits, Jilin Province. Journal of Jilin University (Earth Science Edition), 40(2), 321–328 (in Chinese with English abstract).

Liu M. 2005. Study on geological characteristics and genesis of Cu-Ni sulfide deposit in Hong Qi ling Ji Lin. Changchun, Jilin University, Master thesis, 1–54 (in Chinese with English abstract).

Liu YG, Chen ZG, Li WY, Xu XH, Kou X, Jia QZ, Zhang ZW, Liu F, Wang YL, You MX. 2019. The Cu-Ni mineralization potential of the Kaimuqi mafic-ultramafic complex and the indicators for the magmatic Cu-Ni sulfide deposit exploration in the East Kunlun Orogenic Belt, Northern Qinghai-Tibet Plateau, China. Journal of Geochemical Exploration, 198, 41–53. doi: 10.1016/j.gexplo.2018.12.002.

Liu YG, Li WY, Jia QZ, Zhang ZW, Wang ZA, Zhang ZB, Zhang JW, Qian B. 2018. The dynamic sulfide saturation process and a possible slab break-off model for the giant Xiarihamu magmatic nickel ore deposit in the east Kunlun Orogenic Belt, Northern Qinghai-Tibet Plateau, China. Economic Geology, 113(6), 1383–1417. doi: 10.5382/econgeo.2018.4596.

Liu YR, Lv XB, Mei W, Hui WD. 2012. Compositions of olivine from the mafic-ultramafic complexs in eastern Tianshan, Xinjiang and implications to petrogenesus: Examples from Huangshandong and Tulargen complexes. Geochemica, 41(1), 78–88 (in Chinese with English abstract).

Lv LS, Li HB, Zhou ZH, Xu LG, Yang XN, Mao B. 2017. Mineral chemistry and sulfur isotopic characteristics of ores from the Fujia Deposit in Hongqiling Area, Jilin Province: Constraints on the genesis and ore-forming processes of Ni-Cu sulfide deposit. Acta Geoscientica Sinica, 38(2), 193–207 (in Chinese with English abstract).

Lv LS, Mao JW, Li HB. 2011. Pyrrhotite Re-Os and SHRIMP zircon U-Pb dating of the Hongqiling Ni-Cu sulfide deposits in Northeast China. Ore Geology Reviews, 43, 106–119. doi: 10.1016/j.oregeorev.2011.02.003.

Lv LS, Mao JW, Zhou ZH, Li HB, Zhang ZH, Wang YF. 2012. Mineral chemistry of ore-bearing ultramafic rocks from the Hongqiling No. 1 and 7 instrusions in Jilin Province: Constraints on the magmatic processes and the metallogenesis of Ni-Cu sulfide deposits. Acta Petrologica Sinica, 28(1), 319–344 (in Chinese with English abstract).

Ma JX, Li ZT, Zhang YP, Fang WC, Yang S. 1998. Paleozoic tectonic-magmatic activity and gold-silver mineralization of central Jilin Province, China. Beijing, Geological Publishing House, 1–163 (in Chinese with English abstract).

Ma YF, Liu YJ, Peskov AY, Wang Y, Song WM, Zhang YJ, Cheng Q, Liu TJ. 2022. Paleozoic tectonic evolution of the eastern Central Asian Orogenic Belt in NE China. China Geology, 5, 555–578. doi: 10.31035/cg2021079.

Manor MJ, Scoates JS, Nixon GT, Ames DE. 2016. The giant mascot Ni-Cu-PGE deposit, British Columbia: Mineralized conduits in a convergent margin tectonic setting. Economic Geology, 111(1), 57–87. doi: 10.2113/econgeo.111.1.57.

Mao YJ, Qin KZ, Li CS, Tang DM. 2015. A modified genetic model for the Huangshandong magmatic sulfide deposit in the Central Asian Orogenic Belt, Xinjiang, western China. Mineralium Deposita, 50(1), 65–82. doi: 10.1007/s00126-014-0524-5.

McDonough WF, Sun SS. 1995. The composition of the Earth. Chemical Geology, 120(3–4), 223–253.

Moilanen M, Hanski E, Yang SH. 2021. Re-Os isotope geochemistry of the Palaeoproterozoic Sakatti Cu-Ni-PGE sulphide deposit in northern Finland. Ore Geology Reviews, 132, 104044. doi: 10.1016/j.oregeorev.2021.104044.

Mudd GM, Jowitt SM. 2014. A detailed assessment of global nickel resource trends and endowments. Economic Geology, 109(7), 1813–1841. doi: 10.2113/econgeo.109.7.1813.

Naldrett AJ. 2004. Magma Sulfide Deposits: Geology, Geochemistry and Exploration. Berlin, Springer, 1–17.

Naldrett AJ. 2010. Secular variation of magmatic sulfide deposits and their source magmas. Economic Geology, 105(3), 669–688. doi: 10.2113/gsecongeo.105.3.669.

Naldrett AJ. 1999. World-class Ni-Cu-PGE deposits: Key factors in their genesis. Mineralium Deposita, 34(3), 227–240. doi: 10.1007/s001260050200.

Pan T. 2015. The prospecting for magmatic liquation type nickel deposits on the southern and northern margin of Qaidam Basin, Qinghai Province: A case study of the Xiarihamu Ni-Cu sulfide deposit. Geology in China, 42(3), 713–723 (in Chinese with English abstract).

Piña R, Romeo I, Ortega L, Lunar R, Capote R, Gervilla F, Tejero R, Quesada C. 2010. Origin and emplacement of the Aguablanca magmatic Ni-Cu-(PGE) sulfide deposit, SW Iberia: A multidisciplinary approach. Canadian Mineralogist, 122(5-6), 915–925.

Qian ZZ, Duan J, Li CS, Xu G, Feng YQ, Ren M. 2018. Paleozoic mafic-intermediate intrusions (320-287 Ma) in the Kalatongke area,

south Altai, NW China: Products of protracted magmatism in a convergent tectonic setting. Jounal of Asian Earth Sciences, 159, 1367–9120. doi: 10.1016/j.jseaes.2016.12.038.

Qin K. 1995. Geological features of magmatic sulfide Cu-Ni deposit at the Hongqiling, Jilin Province. Jilin Geology, 14(3), 17–30 (in Chinese with English abstract).

Qin KZ, Sun H, Tang DM, Xiao QH, Su BX, San JZ, Cao MJ, Liu PP, Li GM. 2009. Evaluation of metallogenic potentiality of mafic-ultramafic rocks and Cu-Ni (PGE) metallogenic regularity and location prediction of concealed deposit in East Tianshan. Acta Mineralogica Sinica, 29(s1), 80–81 (in Chinese).

Qiu W, Zhao J, Ding L, He Z. 2012. Application of the ground high precision magnetic survey in Hongqiling nickel resource succeeding exploration. Jilin Geology, 31(3), 69–73 (in Chinese with English abstract).

Regional Geology and Mineral Survey Institute of Jilin Province. 2016. Regional Geology of China, volume of Jilin Province. Beijing, Geological publishing house (in Chinese).

Ripley EM, Li C. 2013. Sulfide saturation in mafic magmas: is external sulfur required for magmatic Ni-Cu-(PGE) ore genesis. Economic Geology, 108, 45–58. doi: 10.2113/econgeo.108.1.45.

Song J, Liu ZH, Wang C, Liu XW, Bao SB, Li XH. 2017. Zircon U-Pb dating and geochemistry of Beigou granites from Hongqiling area in central Jilin and its geological implication. Global Geology, 36(2), 391–402 (in Chinese with English abstract).

Song XY, Yi JN, Chen LM, She YW, Liu CZ, Dang XY, Yang QA, Wu SK. 2016. The Giant Xiarihamu Ni-Co Sulfide Deposit in the East Kunlun Orogenic Belt, Northern Tibet Plateau, China. Economic Geology, 111, 29–55. doi: 10.2113/econgeo.111.1.29.

Sproule RA, Lambert DD, Hoatson DM. 1999. Re-Os Isotopic Constraints on the Genesis of the Sally Malay Ni-Cu-Co Deposit, East Kimberley, Western Australia. Lithos, 47, 89–106. doi: 10.1016/S0024-4937(99)00009-2.

Stanley CR, Russell JK. 1989. Petrologic hypothesis testing with Pearce element ratio diagrams: Derivation of diagram axes. Contributions to Mineralogy and Petrology, 103(1), 78–89. doi: 10.1007/BF00371366.

Sun LJ. 2013. Geological and geochemical characteristics of Hongqiling Cu-Ni Sulfide deposit and prospecting techniques for the same type deposit. Changchun, Jilin University, Ph. D thesis, 1–171 (in Chinese with English abstract).

Sun T, Wang DH (editor in chief). 2019. Geology of Mineral Resources in China, Volume of Nickel. Beijing, Geological Publishing House, 1–878 (in Chinese).

Sun YH, Zhou SL, Yi X, 2016. Geochemistry and genesis of No. 3 rock body in the Hongqiling orefield, Jilin Province. Geology and Resources, 1, 15–21 (in Chinese with English abstract).

Tang ZL, Barnes SJ. 1998. Mineralization Mechanism of Magmatic Sulfide Deposits. Beijing, Geological Publishing House, 1–60 (in Chinese).

Tang ZL. 1996. Main types of magma sulfide deposits in China. Acta Geologica Gansu, 3, 237–243 (in Chinese with English abstract).

Team 607 of Jilin Nonferrous Metal Geological Exploration Bureau. 2008. Exploration report of nickel mine replacement resources of Hongqiling deposit, Panshi City, Jilin Province (in Chinese).

The Fifth Geological Exploration Institute of Qinghai Province. 2014. Detailed investigation report for NO. Hs26 anomaly area of the Xiarihamu Cu-Ni deposit in Geermu City, Qinghai Province (in Chinese).

The Sixth Geological Team of the Bureau of Geology and Mineral Resources of Xinjiang Uygur Autonomous Region. 2012. Survey report of nickel deposit in Pobei-Xuanwoling areas in Ruoqiang County, Xinjiang, 1–230 (in Chinese).

Walker RJ, Morgan JW, Naldertt AJ, Li C, Fassett JD. 1991. Rhenium-osmium isotope systematics of nickel-copper sulfide ores, Sudbury Igneous Complex, Ontario: Evidence for a major crustal component. Earth and Planetary Science Letters, 105, 416–429. doi: 10.1016/0012-821X(91)90182-H.

Walker RJ. 1994. Re-Os isotopic evidence for an enriched-mantle source for the Noril'sk-type, ore-bearing intrusions, Siberia. Geochimica Et Cosmochimica Acta, 58(19), 4179–4197. doi: 10.1016/0016-7037(94)90272-0.

Wang G. 2014. Metallogenesis of Nickel deposits in Eastern Kunlun Orogenic Belt, Qinghai Province. Changchun, Jilin University, Ph. D thesis, 1–200 (in Chinese with English abstract).

Wang SM, Wu CZ, Muhtar, MN, Lei RX, Brzozowski MJ. 2021. Mobilization of ore-forming metals during post-magmatic hydrothermal overprinting of the Huangshandong Ni-Cu sulfide deposit, Eastern Tianshan, NW China. Ore Geology Reviews, 137, 104315. doi: 10.1016/j.oregeorev.2021.104315.

Wang XH, Xu XW, Zhang BL, Niu L, Ke Q. 2022. Protracted mafic magmatism and two-stage mineralization of the Kalatongke Cu-Ni sulfide deposit in the Central Asian Orogenic Belt. Ore Geology Reviews, 141, 104669. doi: 10.1016/j.oregeorev.2021.104669.

Wang ZG, Xi AH, Ge YH, Gong PH, Wang B. 2011. Chronology Significance of the Intrusion Group in Sandaogang Cu-Ni Sulfide Deposit, Panshi, Jilin Province. Journal of Jilin Unviersity (Earth Science Edition), 42(S1), 126–133 (in Chinese with English abstract).

Wang ZG. 2012. Study on Metallogenesis of Mesozoic Endogenetic Metal Deposits in the Eastern Part of Jilin Province. Changchun, Jilin University, Ph. D thesis, 1–193 (in Chinese with English abstract).

Wei B, Wang YC, Li CS, Sun YL. 2013. Origin of PGE-Depleted Ni-Cu Sulfide Mineralization in the Triassic Hongqiling No. 7 Orthopyroxenite Intrusion, Central Asian Orogenic Belt, Northeastern China. Economic Geology, 108, 1813–1831. doi: 10.2113/econgeo.108.8.1813.

Wei B. 2013. Platinum-group element and Re-Os isotopic compositions of the magmatic Ni-Cu sulfide deposits in the Hongqiling-Chajianling-Piaohechuan region, eastern part of the Central Asian Orogenic Belt. Guangzhou, Guangzhou institute of Geochemistry, Chinese Academy of Sciences, Ph. D thesis, 1–157 (in Chinese with English abstract).

Wei QQ. 2015. Late Hercynian-Indosinian Mafic-ultramafic rocks of the Central-Eastern Part of Jilin Province and Cu-Ni Metallization. Changchun, Jilin University, Ph. D thesis, 1–124 (in Chinese with English abstract).

Woodhead JD, Hergt JM, Davidson JP, Eggins SM. 2001. Hafnium isotope evidence for 'conservative' element mobility during subduction zone processes. Earth and Planetary Science Letters, 192(3), 331–346. doi: 10.1016/S0012-821X(01)00453-8.

Wu DY. 1987. Rerecognition of diagenesis and metallogeny of the Hongqiling Cu-Ni sulfide deposit in Jilin. Jilin Geology, 4, 45–56 (in Chinese with English abstract).

Wu FY, Wilde SA, Sun DY, Zhang GL. 2004. Geochronology and petrogenesis of post-orogenic Cu, Ni-bearing mafic-ultramafic intrusions in Jilin, NE China. Journal of Asian Earth Sciences, 23, 791–797. doi: 10.1016/S1367-9120(03)00114-7.

Wu FY, Zhao GC, Sun DY, Wilde SA, Yang JH. 2007. The Hulan Group: Its role in the evolution of the Central Asian Orogenic Belt of NE China. Journal of Asian Earth Sciences, 30, 542–556. doi: 10.1016/j.jseaes.2007.01.003.

Wu LR. 1963. On the metallogenic specialization of basic and ultra Basic rocks in China. Scientia Geologica Sinica, 1, 29–41 (in Chinese).

Wu Q, Sun FY, Liu JL, Tian LD, Fan XZ. 2019. Zircon U-Pb geochronology of ore-bearing olivine-pyroxenite of Changren Cu-Ni mining area in Helong, Jilin, and its geological significance. Mineral

deposits, 38(3), 620–630 (in Chinese with English abstract).

Xi AH, Cai YF, Ge YH, Sun GS, Li BL. 2008. LA-ICP-MS zircon U-Pb age of Longwang gabbro of Shanmen silver deposit in Siping City and its geological significance. Mineral Deposits, 27(1), 57–63 (in Chinese with English abstract).

Xi AH, Gu LX, Li XJ, Ye SQ, Zheng YC. 2005. Discussion on metallogenic epoch of Hongqiling Cu-Ni sulfide deposit , JilinProvince. Mineral Deposits, 24(5), 54–59 (in Chinese with English abstract).

Xi AH, Gu LX, Li XJ, Zheng YC. 2006. The magmatic sulphide Cu-Ni deposits and their earth dynamics setting in North Orogenic Belt of China: A case study of Hongqiling deposits. Acta Geologica Sinica, 80(11), 1721–1729 (in Chinese with English abstract).

Xi AH, Ren HM, Li BL, Wang YX, Shi SB. 2002. Petrology and geochemistry of the ore-bearing intrusions in Hongqiling Cu-Ni sulfide deposit, Jilin Province. Journal of Jilin University(Earth Science Edition), 32(2), 140–145 (in Chinese with English abstract).

Xi AH, Ren HM, Zhang BF, Wang YX, Zhi XJ. 2004. Characteristics on ore minerals in Hongqiling Cu-Ni sulfide deposit, Jilin Province. Journal of Jilin University(Earth Science Edition), 34(3), 338–343 (in Chinese with English abstract).

Xi AH. 2002. Geological genesis model of Hongqiling copper nickel sulfide deposit. Changchun: Jilin University, Ph. D thesis, 1–95. (in Chinese with English abstract).

Xie HQ, Zhang FQ, Miao LC, Li TS, Liu DY. 2007. Characteristics of the Piaohechuan mafic-ultramafic complex, central Jilin, Northeast China: Constrains on the nature and evolution of the northeastern North China marginal tectonic belt. Geological Bulletin of China, 26(7), 810–822.

Xing SW, Sun JG, Zhang ZJ, Ma YB, Song QH, Tang C, Sun PH, Yu C, Chai P. 2014. Studies on the Multiple-phase Metallogenesis and Prospecting Areas of Gold and Non Ferrous Metals in the Continental Margin of Northeastern China. Beijing, Geological Publishing House, 1–361 (in Chinese).

Xu ZG, Chen YC, Wang DH, Chen ZH, Li HM. 2008. The scheme of the classification of the minerogenetic units in China. Beijing, Geological Publishing House, 71–74 (in Chinese).

Xu ZH, Sun FY, Gu GW, Niu XG, Qian Y. 2022. Deep mineral exploration of magmatic Cu-Ni sulfide deposits in the Central Asian Orogenic Belt: Taking Hongqiling Cu-Ni deposits as an Example. Journal of Jilin University (Earth Science Edition), 52(5), 1649–1657 (in Chinese with English abstract).

Xu ZH. 2020. Geological-geophysical model and prediction of Mesozoic magmatic Cu-Ni sulfide deposits in the Middle East of Jilin Province. Changchun, Jilin University, Ph. D thesis, 1–230 (in Chinese with English abstract).

Xue HR. 2020. Features of the Mafic-ultramafic Rocks in Jilin Province and their Metallogenesis. Changchun, Jilin University, Ph. D thesis, 1–231 (in Chinese with English abstract).

Xue SC, Wang QF, Wang YL, Song WL, Deng J. 2022. The roles of various types of crustal contamination in the genesis of the Jinchuan magmatic Ni-Cu-PGE deposit: New mineralogical and C-S-Sr-Nd isotope constraints. Economic Geology, 118(8), 1795–1812. doi: 10.5382/econgeo.5017.

Yang XL. 2012. Research of Geophysical Methods on Deep Cu-Ni Sulfide Deposit Exploration --Case Studies on Hongqiling Cu-Ni Sulfide Deposit. Beijing, China University of Geosciences, Ph. D thesis, 1–133 (in Chinese with English abstract).

Yin GZ, Lv CD, Zhai GH, Bi P, Jia WJ, Cui J, 2019a. Geological characteristics and its guiding significance for geological prospecting of No. 7 rock-mass group in Hongqiling mining area, Jilin Province. Jilin Geology, 38(2), 9–15 (in Chinese with English abstract).

Yin GZ, Zhai GH, Jia WJ, Cui J, Bi P. 2019b. Geological characteristics of No. 1 rock mass and potential of deep copper and nickel resources in Hongqiling mining area of Jilin province. Nonferrous Metals (Mining Section), 71(2), 39–46 (in Chinese with English abstract).

Zhang GL, Wu FY. 2005. Geochronology significances of the post-orogenic mafic-ultramafic rocks in Hongqiling area of Jilin Province, NE China. Seismology and Geology, 27(4), 600–608 (in Chinese with English abstract).

Zhang LS. 2022. Study on Metallogenesis of Endogenetic Metal Deposits in Central Jilin. Changchun, Jilin University, Ph. D thesis, 1–254 (in Chinese with English abstract).

Zhang S, Ju N, Zhang GB, Zhao YD, Ren YS, Liu BS, Wang H, Guo RR, Yang Q, Sun ZM, Xu FM, Wang KY, Hao YJ. 2023. Geology and mineralization of the Duobaoshan supergiant porphyry Cu-Au-Mo-Ag deposit (2.36 Mt) in Heilongjiang Province, China: A review. China Geology, 6(1), 100–136. doi: 10.31035/cg2023006.

Zhang ZW, Li WY, Qian B, Wang YL, Li SJ, Liu CZ, Zhang JW, Yang QA, You MX, Wang ZA. 2015. Metallogenic epoch of the Xiarihamu magmatic Ni-Cu sulfide deposit in eastern Kunlun orogenic belt and its prospecting significance. Geology in China, 42(3), 438–451 (in Chinese with English abstract).

Zhang ZW, Qian B, Li WY, Wang YL, Zhang JW, You MX, Liu YL. 2017. The discovery of Early Paleozoic eclogite from the Xiarihamu magmatic Ni-Cu sulfide deposit in eastern Kunlun orogenic belt: Zircon U-Pb chronologic evidence. Geology in China, 44(4), 816–817 (in Chinese with English abstract).

Zhang ZW, Tang QY, Li CS, Wang YL, Ripley E. 2017. Sr-Nd-Os-S isotope and PGE geochemistry of the Xiarihamu magmatic sulfide deposit in the Qinghai-Tibet plateau, China. Mineralium Deposita, 52(1), 51–68. doi: 10.1007/s00126-016-0645-0.

Zhao Q, Zhang MJ. 2022. Geological characteristics of basic-ultrabasic rock copper-nickel deposit in Hami, Xinjiang. Modern Mining, 644(12), 78–81 (in Chinese with English abstract).

Zhao Y, Liu SB, Xue CJ, Li MJ. 2022. Copper isotope evidence for a Cu-rich mantle source of the world-class Jinchuan magmatic Ni-Cu deposit. American Mineralogist, 107, 673–683. doi: 10.2138/am-2021-7911.

Zhao Y, Zhai MG, Chen H, Zhang HS. 2017. Paleozoic-early Jurassic tectonic evolution of North China Craton and its adjacent orogenic belts. Geology in China, 44(1), 44–60 (in Chinese with English abstract).

Zhao ZH, Zhao X, Yin YC, Liang SS, Chen J, Li CL, Zhou JZ. 2023. Genesis of the Yidonglinchang gold deposit, Lesser Xing'an Range, China: Insights from fluid inclusions, H-O-S-Pb isotopes, and Sm-Nd and U-Pb geochronology. Ore Geology Reviews, 163, 105803. doi: 10.1016/j.oregeorev.2023.105803.

Zhi XJ. 2005. Metallogenic Law and Prospecting Assessment Cu, Ni Sulphide Deposit in Hongqiling, Jilin Province. Changchun, Jilin University, Master thesis, 1–56 (in Chinese with English abstract).

Zhou MF, Lesher CM, Yang ZX, Li JW, Sun M. 2004. Geochemistry and petrogenesis of 270 Ma Ni-Cu-(PGE) sulfide-bearing mafic intrusions in the Huangshan district, Eastern Xinjiang, Northwest China: implications for the tectonic evolution of the Central Asian orogenic belt. Chemical Geology, 209(3), 233–257. doi: 10.1016/j.chemgeo.2004.05.005.

Zhou Q, Gao S. 2008. Large nickel deposit found in the deep part of Tanghe area, Henan Province. Resources Guide, 6, 52 (in Chinese).